INFORMATION TO USERS

This manuscript has been reproduced from the microfilm master. UMI films the text directly from the original or copy submitted. Thus, some thesis and dissertation copies are in typewriter face, while others may be from any type of computer printer.

The quality of this reproduction is dependent upon the quality of the copy submitted. Broken or indistinct print, colored or poor quality illustrations and photographs, print bleedthrough, substandard margins, and improper alignment can adversely affect reproduction.

In the unlikely event that the author did not send UMI a complete manuscript and there are missing pages, these will be noted. Also, if unauthorized copyright material had to be removed, a note will indicate the deletion.

Oversize materials (e.g., maps, drawings, charts) are reproduced by sectioning the original, beginning at the upper left-hand corner and continuing from left to right in equal sections with small overlaps.

Photographs included in the original manuscript have been reproduced xerographically in this copy. Higher quality 6" x 9" black and white photographic prints are available for any photographs or illustrations appearing in this copy for an additional charge. Contact UMI directly to order.

Bell & Howell Information and Learning
300 North Zeeb Road, Ann Arbor, MI 48106-1346 USA
800-521-0600

PARTICLES EMISSION CONTROL AT GRAPHITE CATHODE IN ARC ION PLATING DEPOSITION

By

MUNTHER ISSA KANDAH

Department of the Chemical Engineering

McGill University, Montreal

Under the supervision of Dr. J.-L. Meunier

March 1997

A thesis submitted to the Faculty of Graduate Studies and Research in partial fulfillment of the requirements of the degree of Doctor of Philosophy

To my little birds :

GEORGE & TAMARA

ABSTRACT

In this work, the dependence of the vacuum arc spot velocity on physical and electrical properties of different graphite cathode materials is investigated in the presence of a variable magnetic field. A pulsed arc system is used to perform preliminary experiments on the arc mobility for the different types of graphite for the selection of proper material morphology and the design of a continuous vacuum arc system. The characteristics of arc mobility, erosion rate, and carbon ion flux emitted from the continuous carbon source are then evaluated in view of particle-free diamond-like protective coatings. Results show that the arc spot velocity on graphite cathodes is larger on cathodes having larger grain size, lower electrical resistivity and higher apparent density. The spot velocity is also lower for cathodes having larger pore sizes and total porosity. The arc spot velocity is also found to be increased by increasing the magnetic field intensity over the surface of any graphite type. Reduced residence time of the spot on a given site of the cathode resulting from arc velocity increase should lead to a reduction in the heat load input in the cathode spot. This correlates with results on the number of emitted particles, the film thickness and roughness, and the erosion rate that are found to decrease, while the ion flux emission is increased. Diamond-like carbon (DLC) films free of particles are produced in a continuous arc ion plating (AIP) system. The ion energy in the continuous AIP system is found to vary with the graphite surface properties and the intensity of a plasma confining magnetic field in front of the cathode. The ion energies measured vary between 39.8 eV to 62.6 eV.

RÉSUME

Dans ce travail, le dépendance de la vitesse du spot cathodique d'un arc électrique dans le vide sur différents types de graphite est étudiée en présence d'un champ magnétique variable et en fonction des propriétés physiques et électriques du matériau de cathode. Des études préliminaires sur la mobilité de l'arc sont faites sur un système à arc pulsé pour fin de sélection du matériau et le design d'une source ionique continue à arc dans le vide. Les caractéristiques de mobilité de l'arc, du taux d'érosion et du flux d'ions de carbone émis de la source continue sont ensuite mesurées en vue de la déposition de couches protectrices de carbone adamantin (diamond-like carbon (DLC)) ne contenant pas de particules de graphite. Les résultats montrent que la vitesse du spot cathodique sur des cathodes de graphite est plus élevée sur les cathodes à plus grande dimension de grains, à plus basse résistivité électrique et à densité apparente plus élevée. La vitesse du spot est également plus faible pour les cathodes avec des dimensions de pores et porosité totale plus élevées. La vitesse du spot augmente également lorsque l'on augmente l'intensité du champ magnétique au dessus de la surface de tous les types de graphite. Une diminution du temps de résidence du spot sur un site donné de la cathode résultant d'une augmentation de la vitesse de l'arc conduit en principe à une réduction du flux de chaleur dans le spot cathodique. Ceci est en accord avec les résultats obtenus sur la quantité des particules émises, l'épaisseur et la rugosité des films, et le taux d'érosion qui décroient, alors que le flux ionique émis augmente. Des films de carbone adamantin (DLC) ne contenant pas de particules sont produits dans le système de déposition par pulvérisation cathodique (arc ion plating (AIP)) développé. L'énergie des ions dans ce système varie

avec les propriétés de surface du graphite utilisé et l'intensité du champ magnétique de confinement du plasma devant la cathode. Les énergies ioniques mesurées varient entre 39.8 eV et 62.6 eV.

ACKNOWLEDGMENT

I would like to express my gratitude to my research supervisor Professor J.-L. Meunier, for his constant and unconditional support, encouragement and guidance during the course of this work.

I wish to thank Professor R. Munz for his leadership to the plasma group where I have received a lot of confidence throughout the valuable discussions and presentations and to Professor Berk for his cooperation with the plasma group.

My sincere thanks to the plasma members :

Francisco Moura, Nicolas Desaulniers Soucy, Jan Kwak, George Kim, Muftah El-Naas, Tony Addona, Antonio Carlos da Cruz, Sylvain Coulombe, Jorg Oberste Berghous, Patrice Nadeau, Hongsun Seon, Julie Filion and Theodora Alexakis, for the memorable time we spent together.

A special thanks to the Chemical Engineering Department staff :

Mr. A. Gagnon, Mr. L. Cusmich, Mr. W. Greenland, Mr. C. Dolan, Mr. ED. Siliauskas, Mr. Jean Dumont, Mr. Michael Harrigan, Ms. Pat Fong, Ms. Joanne Terrasi and Ms. Anne Prihoda.

I would like to thank Mr. Nabil Habib for his valuable and memorable friendship.

The financial support of the Jordan University of Science and Technology (JUST), the Natural Science and Engineering Research Council of Canada (NSERC) and the Fonds pour la Formation des Chercheurs et l'Aide à la Recherche (FCAR) in sponsoring this research are gratefully acknowledged.

My great thanks to my wife Samar, my son George and my daughter Tamara, for their love, understanding and patience when it was needed most.

Finally I wish my deeply thanks to my parents, my brothers Raouf, Jehad, Nidal and my sister Rema for their encouragement and moral support.

TABLE OF CONTENTS

FIGURE CAPTIONS

TABLE CAPTIONS

GENERAL INTRODUCTION

In the past decade, there has been increasing interest in the deposition of a special form of carbon films which are hard, dense, electrically insulating and optically transparent. These films have been called "diamond-like" and have been obtained by low energy ion-beam deposition (Aisenberg & Chabot 1971 and 1973), ion beam sputtering (Weissmantel 1981 and Banks & Rutledge 1982), rf plasma-assisted chemical vapor deposition (Grill et al 1991), dual ion beam (Cuomo et al 1991) and ion plating techniques (Coll et al 1992). The common feature to these techniques is the high ion energy bombardment which makes the deposition possible on any substrate regardless to their temperature resistance. The resultant films are low in hydrogen content, amorphous in structure, and display a high degree of sp^3 character (Tsai & Bogy 1987).

Cathodic arcs produce a highly ionized and energetic vapor which has proven useful in the production of dense and adherent coatings. On the other hand, micron-sized particles are also co-deposited in the film. For many applications the presence of these particles is unacceptable, which made the separation or elimination of these particles from the ion flux produced by cathodic arc discharge the goal of many research efforts (Aksenov et al 1978, Storer et al 1989 and McKenzie et al 1991). Almost all of the known research works dealing with the elimination of the macro-particles depend on a filtering technique of the plasma to prevent the particles from reaching the substrate. In the filtering systems, the output plasma flux, deposition rate and system efficiency are decreased. The complexity of these systems is also often considered inadequate for typical industrial environment, contrary to the normal industrial use of the AIP technique for coating such

as titanium nitride. This work involves the development of a cathodic arc source which makes use of the so-called "steered arc" magnetic control of the arc trajectory to decrease or eliminate the number of particles emitted directly at the cathode spot source. The steered arc technique has been used on metallic cathodes (e.g. Ti) to control the arc's erosion at the cathode surface. Due to the severe mobility restrictions of the spot on graphite cathodes, the steered arc technique has not been used on this material yet. Therefore, cathode surface properties and arc parameters necessary for inducing arc spot motion constitute one major objective of the present work. The emission of particles from graphite cathodes have been studied previously at McGill using a laser pulse triggering system and conditions needed to decrease their number density were given by Kandah (1993). Results obtained are used in this work to design a continuous vacuum arc source for diamond-like deposition inducing low particles content in the films. With these objectives in mind, this thesis has been divided into three parts. The first part consists of an intensive literature review on vacuum arc, macro-particles removal, carbon, graphite and diamond-like films. The second part concentrates on the pulse arc mode, in which the arc spot movement and erosion rate dependence on the cathode surface properties of eleven types of graphite are investigated. The data obtained from the pulse arc mode study is used to design the continuous arc system which is employed for the third part of this work (called continuous arc mode). The number of particles deposited on the substrate is measured as a function of arc spot velocity for different types of graphite cathodes. Also the ion flux emitted from various graphite types and reaching the substrate is measured as a function of spot velocity. A continuous arc system is built in a way that allows to avoid

the use of any filtering system. Although this work concentrates on the design and emission properties of the cathode source itself, a few structural and morphological analysis of the films were also made.

PART ONE

LITERATURE REVIEW

CHAPTER (1) : ARC ION PLATING (AIP)

1-1 : VACUUM ARC

1-1-1 : INTRODUCTION

The term "vacuum arc" is rather confusing. This term as employed here means an arc sustained by material originating from the cathode in an environment that would otherwise be a vacuum. The electrical current is conducted by a plasma of vaporized and ionized electrode material, and the arc is diffused between the electrodes (Kesaev 1965).

Vacuum Arc Deposition (VAD) technique belongs to the ion plating family (hence the term now preferentially adopted of Arc-Ion Plating (AIP)) of high energy deposition processes (also called, Cathodic Arc Plasma Depositions (CAPD) and Cathodic Pulverization). It is a physical vapor ion plating technique which uses a high current, low voltage electrical discharge to generate vapor emission from the cathode.

There is general agreement, however, that vacuum arcs are characterized by a very high current density (10^6 - 10^{12} A/m^2) passing through a small area of 10^{-8} - 10^{-4} m in diameter called the cathode spot. As a result of such high current densities, the solid cathode material is suddenly evaporated and the vapor atoms are ionized and accelerated in a heated ion cloud in front of the cathode spot (see Figure 1-1). The resulting lifetime of the cathode spot is typically 1 μs. Ionized vapor of the cathode material is deposited onto the substrate, which is normally biased negatively with respect to the chamber and anode. Tuma et al (1978) found that the cathode erosion products consist predominantly of ions and particles, the emission of neutral atomic flux from the cathode being less than 1% of the total

flux. Both the total and particle flux distributions are peaked in a direction with typically low angles to the cathode plane, whereas the ion flux distribution is peaked in the forward direction perpendicular to the cathode plane. This means that, if the substrate is placed opposite to the cathode, as the distance between the cathode and the substrate increases the number of particles deposited on the substrate is typically decreasing. There exist however a small portion of the particle flux detrimental to the coating properties emitted in a perpendicular direction to the cathode surfaces. This resulted in various methods of filtering for the removal of these particles discussed in section (1-2-1).

The substrate holder in AIP deposition is typically biased with a d.c. or a r.f. potential with different frequencies (e.g. f=3.8 MHz (Rother et al 1991) and f=10 MHz (Strel'nitskii et al 1978)). While the d.c. potential serves for ion acceleration, the r.f. power is also used to reduce charge effects during growth of any well-insulating film. The continuous arc discharge of the d.c. mode is generally operated using arc currents and voltages of about 100 A and 20-50 V, respectively. The impulse current mode is characterized by currents and voltages of approximately 10 A to a few kA (Agarwal & Holmes 1984) and from approximately 100 V to some tens of volts, respectively.

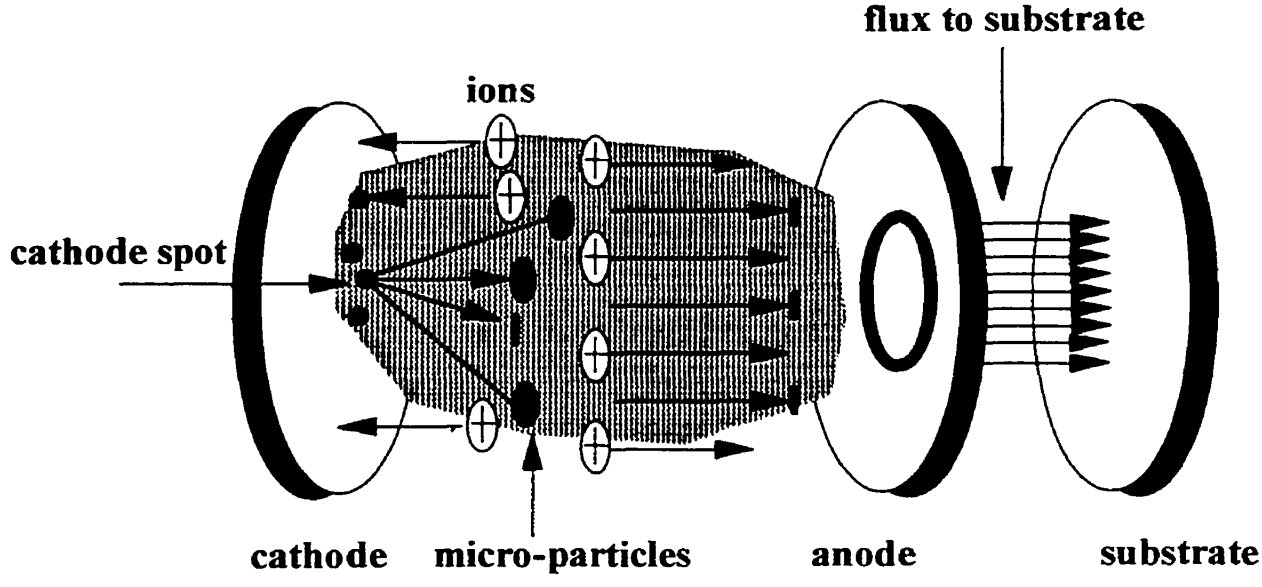

Figure (1-1) : Schematic for typical Arc Ion Plating system.

1-1-2 : WHY ARC ION PLATING (AIP) ?

Introduced by Mattox (1973), ion plating is defined as a coating process in which the substrate and growing film are continually bombarded with energetic particles prior to and/or during deposition. In this work we are using an electric arc to produce ions for plating the substrate under vacuum pressure.

A very hard, adhesive and uniform coating for wear resistance can be achieved from the uniform high-energy ion bombardment. The high-energy ions are generated at the cathode spot of the vacuum arcs. Further ion energy adjustment can be obtained by accelerating the ions through a negative biasing of the substrate.

Ion energy is a very important parameter for diamond-like films deposition in most techniques. Conventional thermal evaporation produces atoms with energies in the range 0.1 to 0.6 eV and sputtering produces atoms with energies in the range 4.0 to 10 eV. This level of deposition energy may still be too low for highly protective advance ceramic coatings. Vacuum arc process produces ions with energies in the range 10 to 100 eV depending on the cathode material (Johnson 1989).

Arc ion plating technology is so promising because it can also provide high degree of ionization of the arc-produced vapor. Conventional electron beam evaporation technique, for example, employs a high voltage beam of electrons to heat source material and achieve only a small degree of ionization between 0.1 and 0.3 % (Sanders et al 1990). In contrast, AIP approach employs a low voltage-high current discharges to ionize 10-90% of the vapor depending on the cathode material (Kimblin 1973).

Arc ion plating (AIP) technique does not rely on substrate heating but instead on high ion energy bombardment to obtain the high adhesion and dense films. Highly adhesive coatings can be deposited on substrates maintained close to room temperature. Consequently, coatings can be applied to already quenched and drawn steels without loss of hardness and distortion. In contrast, CVD technique requires high substrate temperatures in the range of 800 °C to 1100 °C to activate the chemical reaction with the associated disadvantages of loss of hardness and distortion.

The AIP technique is believed to involve low overall cost compared to the sputtering system. It has a large flexibility of operation in terms of parameteric dependency in the deposition process, for example, good quality films can be deposited throughout a relatively wide range of deposition parameters, the main one being pressure. The high efficiency of ionization and high energy of these ions, as well as the strong erosion rate of the electric arc driven source producing a very large flux of ions, contribute to the cost efficiency of these systems. The main disadvantage with using the vacuum arc ion plating technique for most industrial applications is the production of the micron-sized particles in the film. These particles do not necessarily lead to problems in view of applications and have been tolerated in many industrial applications of this technique such as in the field of cutting tools, automobile industry, decorative industry and even biological implants. The problem in fact can be relatively well controlled in the deposition of advanced ceramic films such as TiN (see for example the Ph.D. thesis of Kim 1995). The phenomena of particle emission is however much more important and difficult to control on a source such as graphite.

1-1-3 : VACUUM ARCS ON CARBON CATHODES

In vacuum the arc no longer attacks the entire cathode surface along its pathway, it moves around attacking only minute areas on the cathode surface, the so called cathode spots producing the material plasma. Most of the vapor becomes ionized in the region of high power density adjacent to the cathode spot surface (Utsumi 1971). As described before, a high degree of ionization is achieved by vacuum arc evaporation, for the case of a carbon cathode 70% of the emitted vapor was found to be ionized (Kimblin 1973). Two types of cathode spots were observed on contaminate and clean cathodes (Rakhovskii 1976, Fu 1989 and Kutzner & Miller 1989). On the contaminated cathode surfaces there is predominantly one type of cathode spots called type 1 spot. The spot in type 1 moves quickly and produces weak erosion rate. The craters left by the arc have dominantly submicron sizes. On the clean cathode surface there is predominantly another kind of cathode spot called type 2 spot. The spot in type 2 moves slower with 10 to 20 μm crater size and produces much erosion rate. Graphite cathodes typically emit electrons through thermionic emission. In such materials, large stationary spots emit electrons due to the high cathode temperature and remain quite stable in the high temperature locations. This makes the movement of the cathode spot on the graphite surface difficult. The occurrence of this stable mode of operation on graphite is in contrast to most metallic electrodes used in vacuum arc systems. Vacuum arcs devices typically work in the thermo-field (T-F) operation regime. Thermo-field emission of electrons is produced when the surface of a solid body is held at a relatively high temperature and exposed to a high electric field. The T-F emission corresponds to the transition region among thermionic emission, the

emission of electrons by a hot surface at zero electric field and field (or cold) emission of electrons which occurs by the action of a high electric field at zero temperature. In this mode of operation, the micron-size spots have short lifetime (~ 1 μs) and provide a relatively high mobility of the cathode spot attachment. The plasma parameters in the cathode spot area, and particularly the high plasma pressure (Jüttner 1985) provide the basis for the strongly ionized and high intensity ion beam emitted from this zone. A refractory cathode material such as graphite that shows the possibility of attaining the high surface temperature needed for thermionic emission may preferentially operate in this more stable regime. Such a mode of operation does not lead to the high pressures-high ion flux associated to the thermo-field operation regime. A decreased mobility of the spot induced by increased stability at high surface temperature should also contribute to higher micro-particles emission. Metallic refractory materials such as tungsten can also operate in the thermionic emission regime. This is in fact their typical mode of operation in devices used at atmospheric pressure. In vacuum however, these materials do not show the mobility problems associated with graphite electrodes. One objective of this thesis is to show that arc mobility restrictions on graphite are strongly linked to the actual surface characteristics of the highly varying graphite materials encountered.

As the cathode spots represent an intense electrical charge flow, their motion across the cathode may be stimulated by external magnetic fields providing a component parallel to the erosion surface. Such stimulation takes a particular importance if the mobility of the arc spot is considerably restricted as will appear, for example, in case of a porous cathode material such as graphite. Forcing an arc movement on graphite, as for

other refractory cathodes, should be a way to maintain the thermo-field operation regime on cold cathode surface rather than going into a thermionic type of emission.

The electric arc is usually moving in the same direction as a solid conductor following the Ampere rule. In vacuum however the arc will move in the opposite direction (retrograde direction) with regards to the Lorentz force i.e., movement is in the **- I x B** direction. This movement was shown to depend entirely on cathodic effects. There is still controversy on the mechanisms responsible of this effect. The approach that seems to fit best with the experimental results is based on the metallic plasma behavior around the spot above the cathode surface (Drouet 1985). A larger density of this plasma in a given direction increases the probability of ignition of a new spot in this direction, resulting in a net movement of the arc root.

In a study of the emitted flux, Douyon de Azevedo & Meunier (1990) measured in short pulsed arc experiments a velocity of this emitted carbon ion flux in vacuum of 1.3 x 10^4 m/s, and the angular distribution of the flux was not affected by the neutral hydrogen gas pressure in the chamber. This flux decreased with distance from the cathode as $R^{-1.4}$ in vacuum and R^{-4} in the 1-10 Torr pressure range.

The current that can be carried by a single spot appears to be limited, and depends on the cathode material. For carbon the maximum current per spot was found to be around 200 A (Kimblin 1973), while for Cu it is around 100 A (Djakov & Holmes 1971). The cathode voltage drop across the space-charge region immediately adjacent to the spot has values in the range 10-30 V depending on the cathode material. For carbon, the

cathode voltage drop is approximately equal to 16 V, while for Cu it is 20 V (Davis & Miller 1969).

McKenzie (1996) presented a comparison between the energy distribution of ions emitted from graphite cathodic arc and the distributions produced by sputtering and laser ablation. In the laser ablation, the graphite cathode is impinging by a varied laser pulse energy which affected the energy distribution of ions. The energy distribution of ions has been measured at a pulse energy of 3 J/cm^2 and has a most probable energy value of 20 eV (Cuomo et al 1991) very similar to the natural energy of the cathodic arc beam. On the other hand, sputtering of graphite cathode by inert gas ions using an ion gun at vacuum pressure, produces an average ions energy distribution of 5 eV.

1-2 : MACRO-PARTICLES

The emission of macro-particles by cathodic arcs is of great significance in the deposition of thin films, because these macro-particles get incorporated in the deposited film. It is the presence of these macro-particles in deposited films that has inhibited the more widespread applications of the physical vapour deposition (PVD) arc ion plating technique. The role of the particles should not be overrated in the case of machining and cutting tools since arc coated tools attain a very long life even if particles are present. Adhesion, stoichiometry, coating thickness, coating thickness distribution and stress condition are more important coating features which govern the performance of coated tools.

Utsumi & English (1975) investigated the macro-particles component of the emission from Au, Pd and Mg arcs. They determined that for arc current in the range of 2-6 A, macro-

droplets size ranged from a few hundred angstroms to several microns in diameter. It was noted that the percentage of the volume transported by macro-droplets for Mg, Au and Pd was found to be 80%, 50% and 10%, respectively, that is, the percentage decreased with an increasing melting point temperature of the cathode material. At higher currents similar to those used in AIP deposition systems (80-100 A), higher pressures of reactive gases reduce the number of macro-particles in reactive deposition processes because, it is believed, reaction on the cathode surface forms a compound surface film. The presence of such a film, TiN for example, on the surface of the target leads to reduced melting. Ti melts at 1600 °C while TiN melts at 2030 °C (Johnson 1989).

The composition of cathode mass loss was analyzed by Daalder (1976) for cadmium, copper and molybdenum vacuum arcs. An investigation is made of the quantitative contribution of particles and ions to the total cathode mass loss and the parameters by which these components are governed. Nearly the entire particle mass is expelled in a narrow region having an angle of 10° - 30° to the cathode surface. He also observed the shape and density of the deposited particles from copper cathodes by analysis with a scanning electron microscope (SEM). The particles number as a function of particles size were counted from SEM photographs. The individual volume of the deposited particles was determined by a microscope (for surface examination) whose construction made it possible to measure dimensions both in the plane of and perpendicular to a target disc. Large sized particles are dominantly represented in the mass flux having a small angle with the cathode plane, whereas for larger angles the smaller sized particles are representative. Figure 1-2 shows the angular distribution of particle mass flow from the cathode of a copper arc.

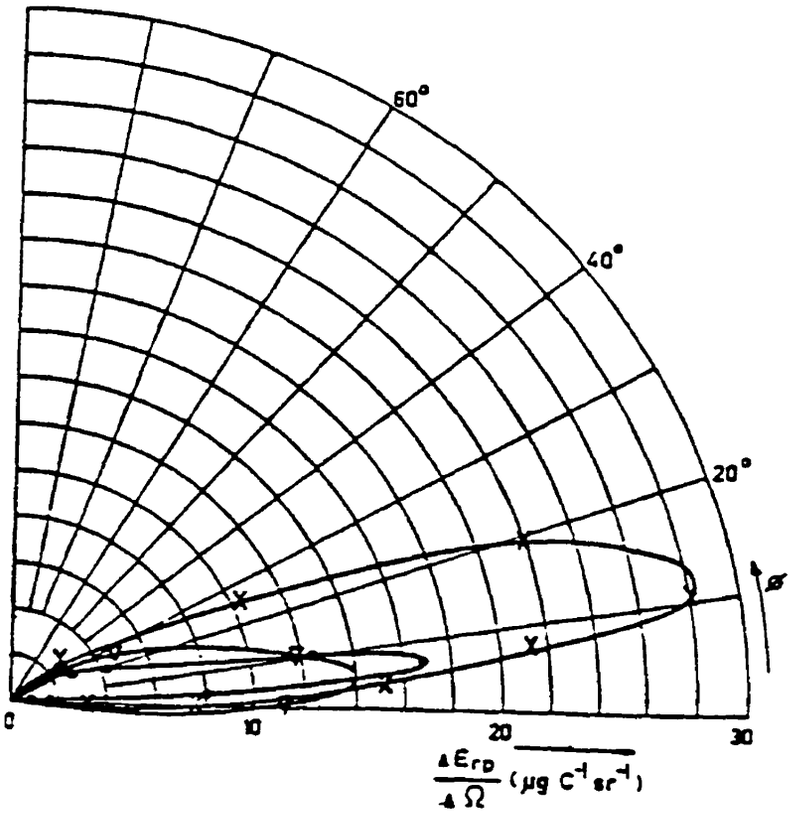

Figure (1-2) : Angular distribution of particle mass emission in a vacuum arc on a 25 mm diameter copper cathode. The angle is with respect to the cathode plane and taken from the cathode centre (Daalder 1976).

Figure (1-3a) shows the micro-spheres that appear in the film in exploratory deposition tests performed by Douyon de Azevedo (1990). Large plates with uniform appearance were also formed with indications from Raman and Auger spectroscopy of diamond-like structure. These plates show cracking along preferential directions and the incorporation of micro-spheres. The cracking and the poor adhesion of the film were

probably due to a thickness which was too large (several microns) to sustain the strong internal stresses. The film thickness reported was 4.48 μm, which is somewhat larger than maximum diamond-like film thickness of around 1 μm to maintain film integrity (Bhushan et al 1992 and Palshin et al 1995). Figure (1-3b) is a close-up of Figure (1-3a) showing a large quantity of carbon spheres imbedded in the deposit. This problem had to be addressed before any good quality films can be produced using a vacuum arc technique. The problem of particles generation at the cathode of vacuum arcs is in fact not only related to graphite cathodes. Metal cathodes will also induce this same phenomena. Important reduction or elimination of particle emission was however achieved on metallic electrodes using steered arcs and surface contamination effects in advanced ceramic deposition such as TiN (Kim 1995). Figure (1-3b) shows also a surface structure of the particles resembling that of the "cauliflower" type of CVD crystalline diamond films deposition studies. Such cauliflower appearance results in CVD diamond growth systems from an excess of diamond micro-crystal growth. They are produced when the ratio of carbon to atomic hydrogen is too high. The similarity between the surface morphology of the arc produced particles in Figure 1-3 and those of cauliflower type of diamond films led to believe that the particles may possibly have this characteristics morphology of micro-crystalline diamond. Kandah (1993) used Raman and Auger electron spectroscopy (AES) to investigate the structure of the micron-sized particles emitted from the graphite cathodes at different operating conditions. He found that all the particles have the same structure as the cathode (graphite). As in other vacuum arc systems, the most probable origin of these particles should be the cathode spot region.

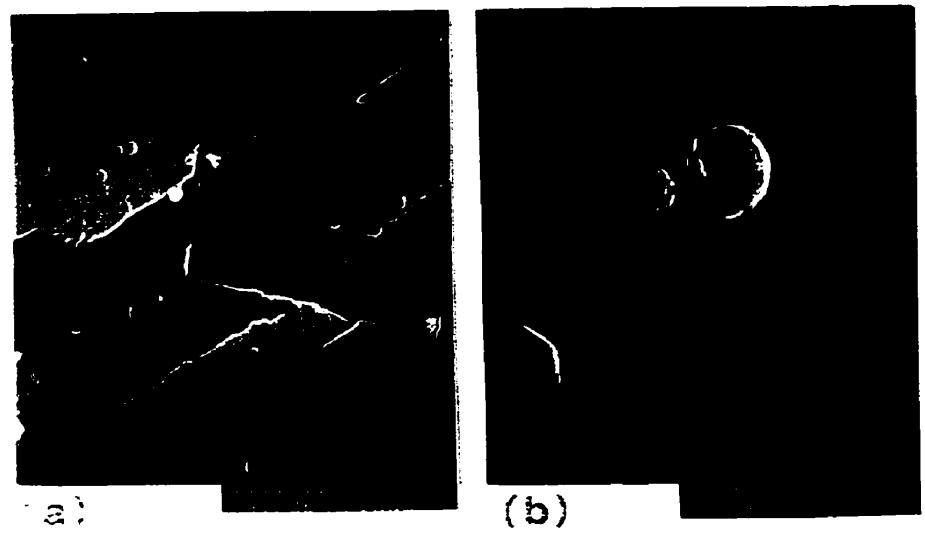

Figure (1-3) : a) SEM recording of a deposit made on tungsten in vacuum (P = 10^{-2} Pa) with T = 470 °C & V_s = -300 V.

b) Close-up of (a) showing the structure of spheres imbedded in deposit (Douyon de Azevedo 1990).

1-2-1 : REMOVAL OF MACRO-PARTICLES

Removal of macro-particles from the plasma flux ensures the elimination of defects in the coating such as punctures, outgrowths, and islets of reduced micro-hardness. Such defects in the diamond-like structure usually develop as a result of bombardment by macro-particles. Removal of low-energy neutral atoms from the plasma flux eliminates the need for the significant increase of the ion-component energy level above the energy threshold required for formation of the diamond structure. Thus when the diamond-like structure is produced the probability of exceeding the energy threshold for defect formation is reduced, improving the quality and purity of the surface and increasing micro-hardness and resistivity (Aksenov et al 1980).

The formation of diamond-like carbon film from the plasma stream of a vacuum arc after filtering by a curved magnetic solenoid was first reported by Soviet workers (Aksenov et al 1978). They employed a method for eliminating macro-particles using a plasma optic system to deflect the path of the particles in the emission flux as shown in Figure 1-4. The plasma optic comprised of a curved metal tube having a longitudinal magnetic field of several hundred oersteds (1 oersted = 10^{-4} Tesla) and a radial electric field of tens of volts. It was demonstrated, by studying the quality of the deposited films, that the ions could be successfully separated from the macro-particles and that particles-free coatings could be produced. Measurements of the radial ion current density profile at the exit of the plasma optic system indicated at a high degree of ions focusing along the axis of the system. Neutral atoms and macro-particles, their paths unaffected by the magnetic and electric fields, followed linear paths and were collected on the inner surface of the curved duct.

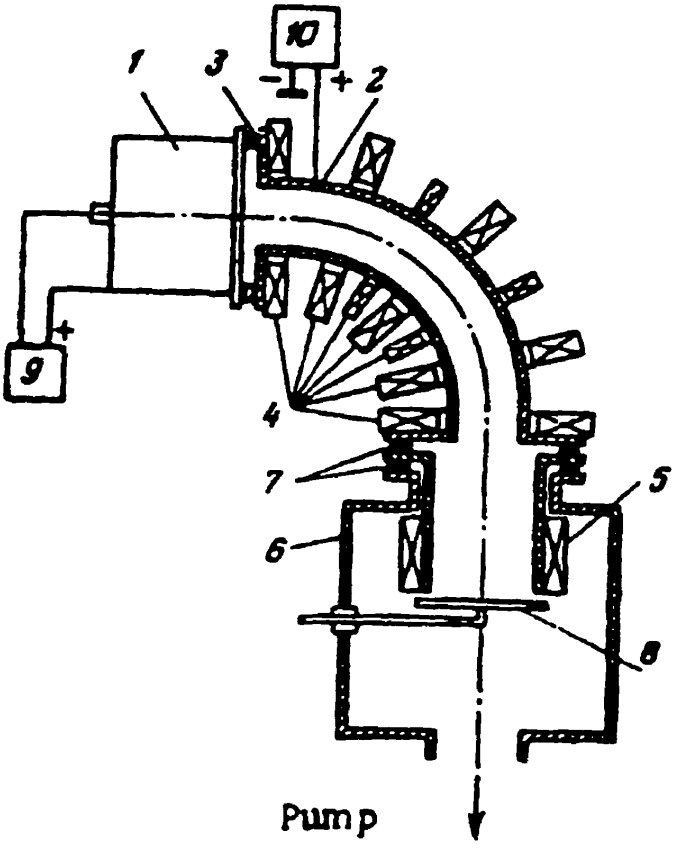

Figure (1-4) : Curvilinear separating system : 1) Arc plasma source; 2) Plasma duct; 3,7) Insulators; 4,5) Magnet coils; 6) Vacuum chamber; 8) Collector; 9) Rectifier; 10) Bias voltage for the plasma duct (Aksenov et al 1978).

Namba et al (1989) used another filtering technique to avoid the co-deposition of these particles. They applied a magnetic field on the top of the ion source to bend the flow of the ions, then the deflected ions were deposited on the substrate.

Falabella & Sanders (1992) have developed two macro-particle filtered cathodic-arc sources for use in high rate coating metals, and reactivily produced oxides and nitrides. Although the two sources are designed with the same overall constraints the two differ significantly in geometry as shown in Figure 1-5. In the Dome cathodic-arc source (Figure 1-5a) ions leave cathode target radially, and then are turned by the combination of magnetic and electric fields. In the Knee cathodic-arc source (Figure 1-5b) ions leave the cathode and travel through a 45° bend to separate macro-particles. Electrons flowing to the ring anode in the chamber produce the electrostatic field that guides the ions. Both techniques however relay on electrostatic fields produced by the flow of magnetically constrained electrons through the filter to guide the ions from cathode to substrate to be coated. Although neither of these two sources have direct line-of-sight from cathode to substrate, a large number of particles were found on the first substrates coated with these sources. They investigated the reason and found that the macro-particles are bouncing off the walls. They have in fact observed larger, luminous particles that occasionally get emitted from a carbon arc target bouncing off the walls toward the substrate. Baffles were installed to protect the substrates from macro-particles bouncing off the chamber walls.

Lossy et al (1992) used a linear magnetic filter to separate macro-particles and non-ionized carbon atoms from the beam and prevent them from reaching the substrate (see Figure 1-6).

A)

B)

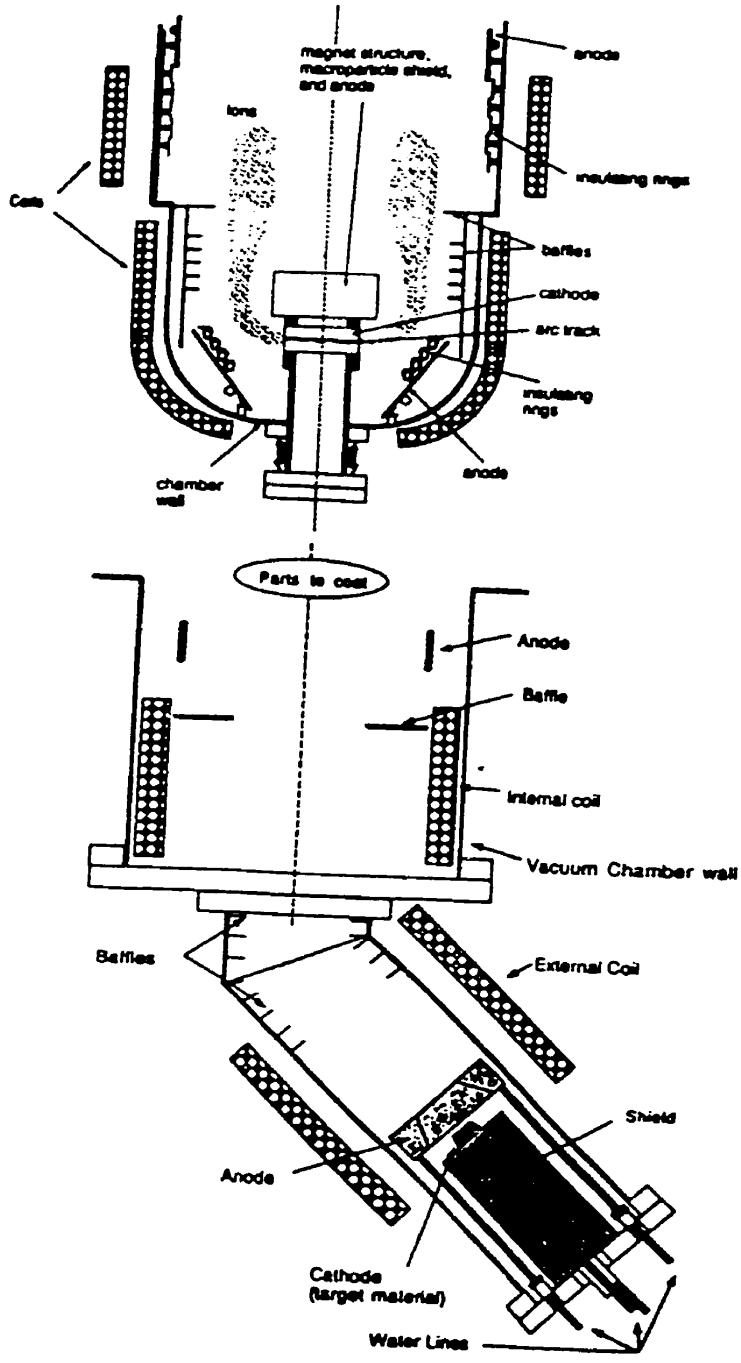

Figure (1-5) : Schematic diagram of the a) Dome cathodic-arc source; b) Knee cathodic-arc source (Falabella & Sanders 1992).

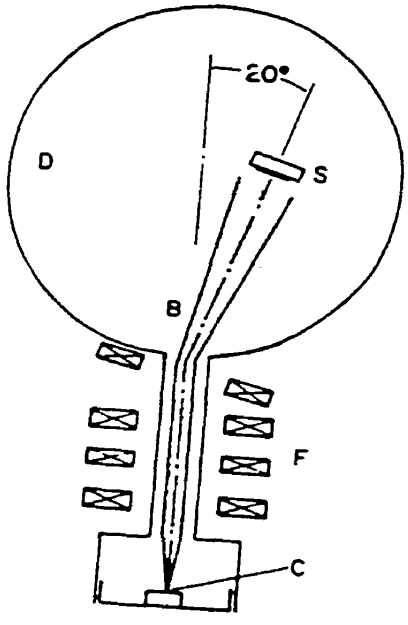

Figure (1-6) : Schematic of the linear filtered vacuum arc with cathode (C); filter magnets (F); plasma beam (B); deposition chamber (D) and substrate (S) (Lossy et al 1992).

In comparison to curved magnetic filters, the linear filter is a much simpler design, which requires a lower magnetic field and no biasing of the filter tube. The arc beam extends into a 100 mm diameter filter tube, in which the beam is guided by magnetic field lines. The magnetic field along the axis of the tube is 6 mT, which is 10% of field required for a curved magnetic filter. At the end of the filter tube, the magnetic field deflects the plasma beam off the original axis by 20°.

Kandah & Meunier (1995) have studied the generation mechanism of the emitted micron-sized particles from graphite cathodes in short pulsed experiments (0.5 ms to 14 ms). They measured the size and number of the particles deposited on the substrate as a function of arc time, arc current, charge passing through the cathode and heat load input to the cathode spot with cathode-substrate distance of 13 cm. Figure 1-7 shows that the particle production is mainly due to heating effect of the cathode spot on the graphite surface. In other word, the number of the macro-particles can hence be decreased by lowering the heat load in the cathode spot volume through a control of the arc current level and/or arc residence time on a given site. This is an important result indicating that a good control of the thermal flux in the cathode spot area is essential if one aims at a low particle content in the films. They expected that rotating the arc at the cathode surface in order to decrease the heat load into the cathode spot may decrease the number of particles emitted from the cathode.

This approach implies moving the arc in a way similar to the continuous arc sources on metallic electrodes. Some preliminary experiments were done on a graphite cathode using a continuous system developed by Kim (1995) by replacing the metallic cathode (Titanium) by a graphite cathode and using the same magnetic field intensity. The arc spot was rotating on the metallic surface uniformly, while for graphite cathode the arc spot moved for 1 cm and stayed there for an extended period of time (Figure 1-8).

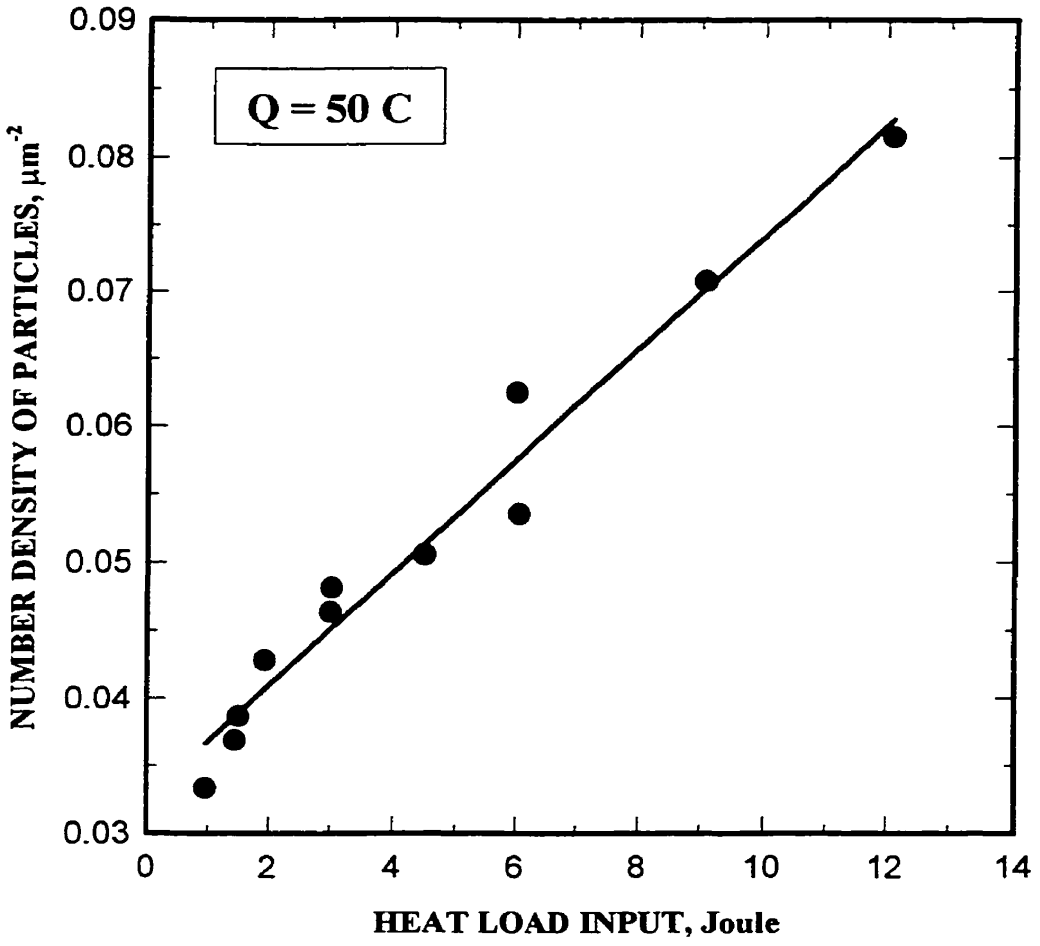

Figure (1-7) : Number density of particles as a function of heat load input to the cathode spot on silicon substrate at 13 cm between cathode and substrate (Kandah & Meunier 1995).

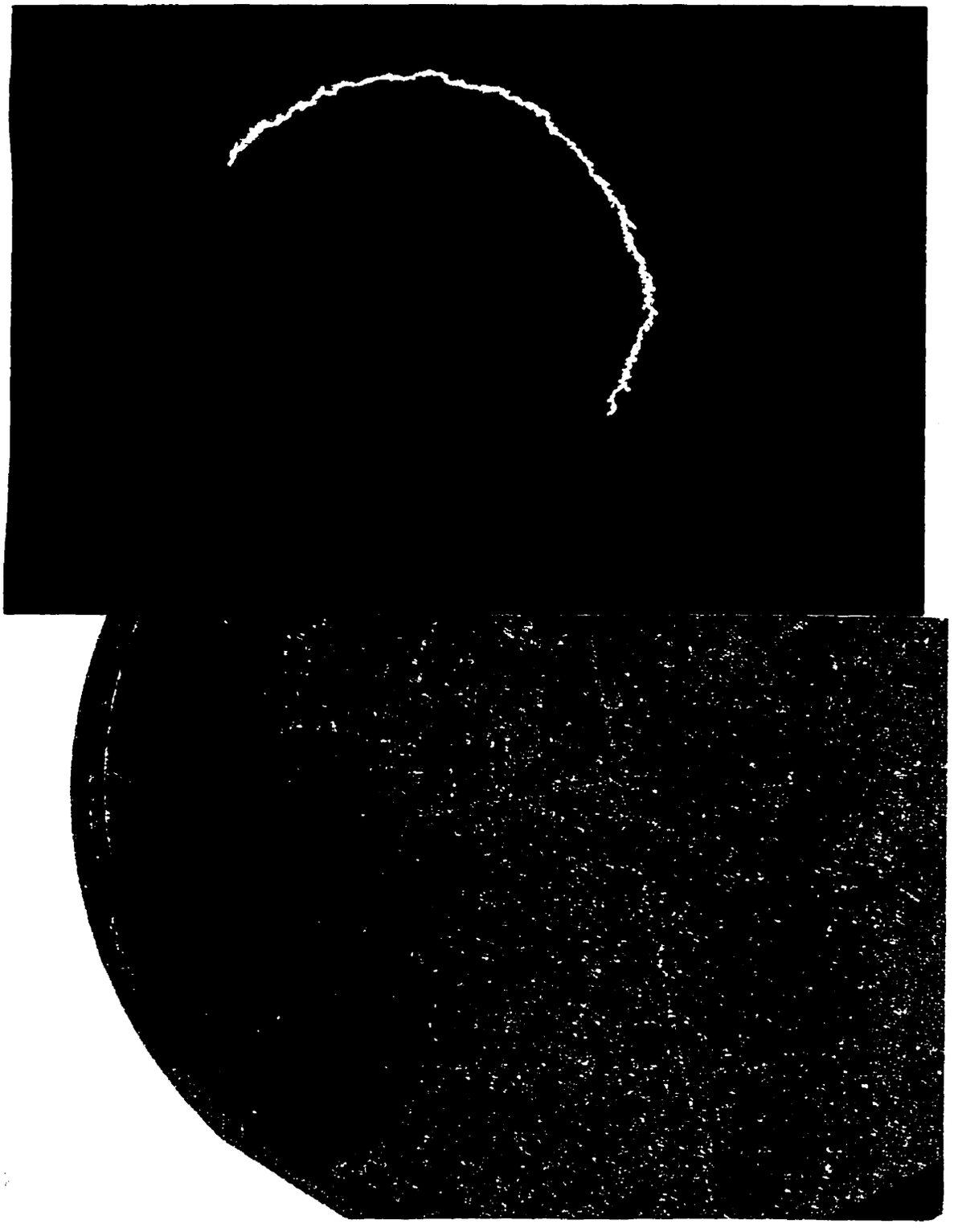

Figure (1-8) : Top: Arc spot trace on Titanium cathode (B=200 Gauss or 0.02 Tesla).
Bottom: Arc spot trace on Speer graphite cathode (B=200 Gauss).

Another experiment was performed using the continuous system developed in section 5-2 where the radial magnetic field component on the graphite surface was equal to zero (i.e., random or non-steered arc without an external magnetic field). The arc spot stayed at the ignition point all the time and created a deep crater as shown in Figure 1-9. The associated increase in local surface temperature most probably assured a stable arcing position. The random arc on metallic electrode surface such as Aluminum-coated glass plate in vacuum (Anders & Jüttner 1991), for example, shows different behavior (Figure 1-10). This indicates that much higher magnetic field intensities may be needed to move the arc spot on the graphite cathode compared to other metallic electrodes. This phenomena is the basis of one main objective of this research.

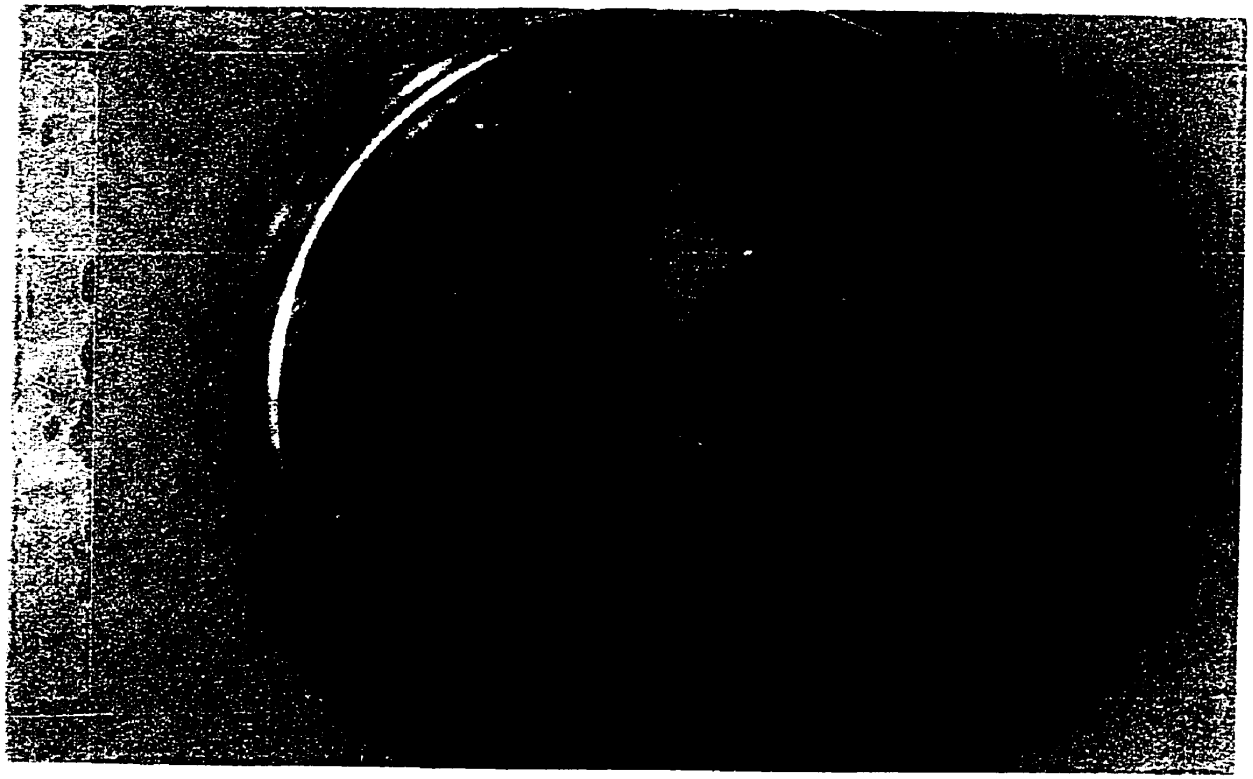

Figure (1-9) : Random arc trace over graphite surface (no magnets behind the cathode).

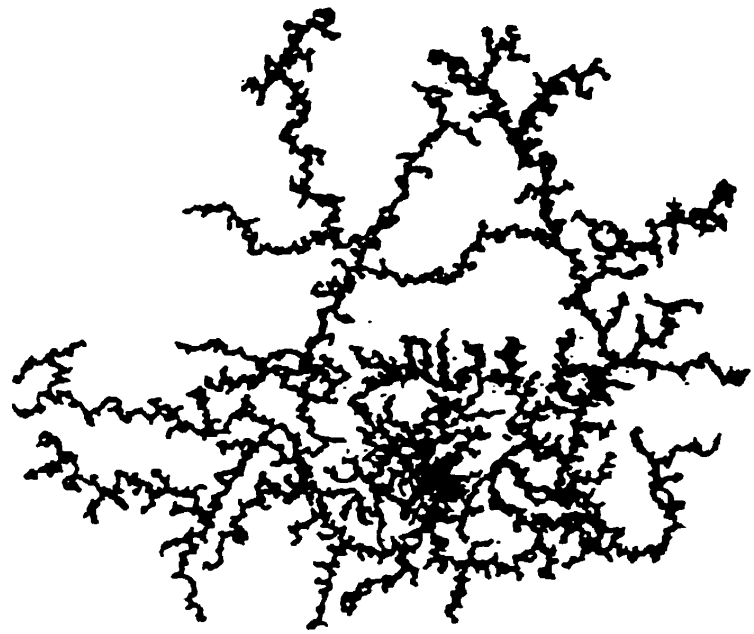

Figure (1-10) : Arc spot trace on an aluminium-coated glass plate in vacuum, I = 50 A, duration 2 ms (without an external magnetic field) (Anders & Jüttner 1991).

Although filtering systems have proved to be very efficient in preventing the macro-particles from reaching the substrate, they have not been widely used in industry due to several disadvantages. In AIP system, the number of cathodes and their arrangement can be varied in such a way as to create uniform coating conditions throughout the chamber and to coat complex shapes (Figure 1-11). The uniformity of the large coating zone is a predominant feature of the Arc Ion Plating process. The filtering system, on the other hand, has limited plasma transport efficiency and tends to collimate

the plasma leading to a restricted area of deposition. The increase in size due to the addition of the filtering tube to the main reactor and the complexity of the magnetic coils configuration around the filtering tube would make it impractical for large scale industrial use. Therefore, the particle emission control at source is essential for straightforward deposition of particle-free diamond-like films using AIP technique without the use of filtering tube.

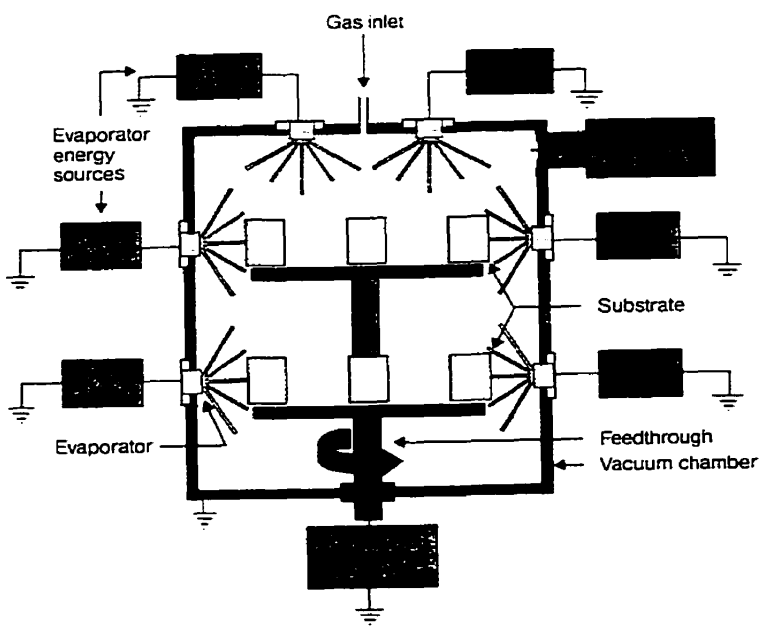

Figure (1-11) : Arc ion plating system with multiple cathodes (Mack 1990).

1-3 : OBJECTIVES

This work involves three main overall objectives :

1. Characterization of graphite material properties effect on arc spot behavior, particularly mobility.
2. Based on this characterization and previous results on particle emission mechanism, optimal conditions are to be defined and used for the design of a continuous arc source with low particle emission.
3. Flux characterization of the new source, and resulting effects on the coating with regards to macro-particle suppression.

1-3-1 : SPECIFIC OBJECTIVES :

1. Evaluate the vacuum arc velocity and magnetic field relationships for graphite materials having varying porosity, grain size, electrical resistivity and density. A review of graphite material properties and manufacturing techniques is needed to characterize the various materials.
2. Use the information above to select a graphite material for the cathodic source and design a continuous AIP system.
3. Evaluate the ion flux intensity, ion energy and the efficiency of this source for the reduction of macro-particles content in the films.

1-3-2 : METHODOLOGY :

1. Building and using a laser pulse discharge triggering system with well controlled arc discharge time length.

    a) Eleven different types of graphite cathodes will be used and the arc spot velocity measured under the influence of variable magnetic field.

    b) Determining the minimum magnetic field values needed to move the arc spot over each graphite type for the design of the continuous system.

2. Building and using a continuous vacuum arc ion plating system using selected graphite types and necessary conditions for arc mobility obtained from the pulsed discharge study.

3. Measuring the number of particles emitted from different graphite types under different operating conditions.

4. Characterization of the new source through measurement of the ion flux spatial distribution and ion energy. This requires building and using an Ion Energy Analyzer (IEA)

5. Analysis of the deposited films using several diagnostic techniques such as :

Scanning electron spectroscopy (SEM), Infra red spectroscopy (IRS) and Dektak 3 ST profilometer.

The next two chapters contain a rapid overview on carbon and diamond-like, respectively. This review clarifies the differences between different structural forms of carbon such as graphite, diamond, amorphous carbon and fullerene.

CHAPTER 2 : CARBON

2-1 : INTRODUCTION

Most of the bonding situations for carbon are described spatially in terms of three geometries: tetrahedral, trigonal, and linear as shown in Figure 2-1. Carbon compounds having four single bonds take on the approximate form of a tetrahedron, having 109.5 deg angles between bonds. The tetrahedron has a high degree of symmetry, which limits the number of isomers that exist for variously substituted carbon compounds. A carbon atom bearing one double and two single bonds may be described as trigonal, the three groups bonded to carbon take on a symmetrical planar arrangement, with angles of about 120 deg between bonds. A carbon atom with one single and one triple bond, or two double bonds, is held in linear arrangement with the two groups on opposite sides of the carbon atom. More unusual bonding situations also occur. The properties of the different phases of carbon are strongly related to the nature of the carbon bond or the electronic structure of carbon (Tsai & Bogy 1987).

Linear molecules with two identical bonds

B—A—B

Planar molecules with three identical bonds 120° apart

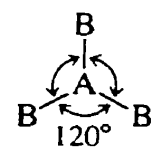

Tetrahedral molecules with four identical bonds 109.5° apart

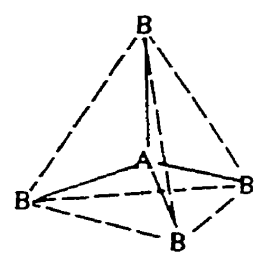

Figure (2-1) : Types of molecules and geometries; a) Linear; b) Trigonal; c) Tetrahedral.

2-2 : BASIC ELEMENTAL FORMS

Pure carbon exists as any of four allotropes, which are different crystal forms of the same element. These allotropes are diamond, graphite, amorphous carbon, and Fullerenes.

2-2-1 : DIAMOND

The diamond crystal has a sp^3 tetrahedral structure. It is a face-centered cubic with interatomic distances of 0.154 nm. Each carbon atom is bonded to four different carbon atoms and no "dangling bonds" exist (see Figure 2-2).

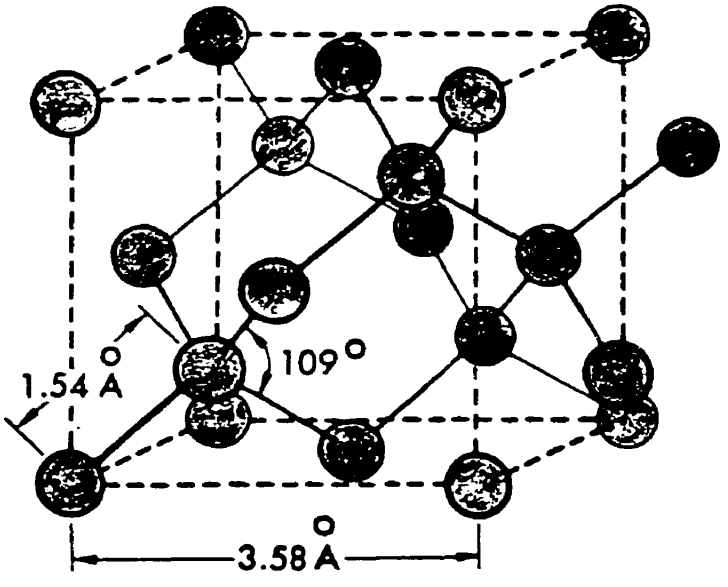

Figure (2-2) : Crystallographic structure of diamond.

Pure diamond is the hardest substance known. Although pure diamond is colorless and transparent, when contaminated with other minerals it may appear in various colors ranging from pastels to opaque black. This crystal is chemically inert but may be induced to burn in air at high temperatures. It is a very good conductor of heat and is an electrical insulator. Until 1955 the only source of diamond was natural deposits of volcanic origin.

In 1955 Robert H. Wentorf and his coworkers at the General Electric Research and Development Center produced synthetic diamond by duplicating the natural conditions of high temperatures $\cong$ 2000 °C and pressures of $\cong$ 100,000 atm. Although the first diamond made by this process looked like black sand because of the impurities present, the process has now been developed to a point such that beautiful, clear, gem-quality diamond can be produced (Zumdahl 1995). For electronic and optical applications, as well as many others, the ideal form for utilization of the unique properties of diamond is as coatings.

The high temperatures and pressures used in the GE process for making diamonds make sense if one looks at the phase diagram for carbon (Figure 2-3). Note that graphite is the most stable form of carbon under ordinary conditions of temperature and pressure. However, diamond becomes more stable than graphite at very high pressures (as one would expect from the greater density of diamond). The high temperature used in the GE process is necessary to disrupt the bonds in graphite so that diamond (the most stable form of carbon at the high pressures used in the process) can form.

This brings us to the difference between kinetics and thermodynamic stability. Under normal conditions of temperature and pressure, graphite has a lower free energy

than diamond (by $\cong 2$ kJ/mole). However, to get from diamond to graphite requires a large expenditure of energy. This is the energy of activation that determines the rate of a reaction at a particular temperature. As a result of this high activation energy, diamonds formed at the high pressures found deep in the earth's crust can be brought to the earth's surface by natural geological processes and continue to exist for millions of years. Although these diamonds are thermodynamically unstable (relative to graphite), they are kinetically stable. That is, the reaction to change diamond to graphite is favored by thermodynamics but is disfavored by kinetics, it is so slow that diamonds almost last forever. Diamond is said to be metastable (thermodynamically unstable but kinetically stable) under normal conditions of temperature and pressure. The production of diamond at such high pressure is very expensive. The phase diagram for carbon (Figure 2-3) says that diamond can not be formed at low pressures. However, researchers have found that under the right conditions diamond can be grown at low pressures. The process used is called chemical vapor deposition (CVD), in which diamond films are produced by introducing a mixture of hydrocarbon (e.g. CH_4) and Hydrogen (~ 1% CH_4) into the chamber. Energetic Carbon, Hydrogen or Argon ions (~ 10 - 1000 eV) are generated by using an excitation source (hot filament, RF, DC or microwave plasma) to create out of equilibrium conditions for a preferential growth of the diamond structure with regards to the graphite structure. Atomic hydrogen has the key role of saturating dangling bonds at the surface to prevent the formation of double bonds between the carbon atoms. Diamond films grow on substrates maintained at high temperature typically (1000 °C) to activate the chemical reaction, this temperature corresponds to a minimum solubility temperature of

carbon in the gas phase. The major advantage of CVD is that there is no need for the extraordinarily high pressures used in the traditional process for synthesizing diamonds.

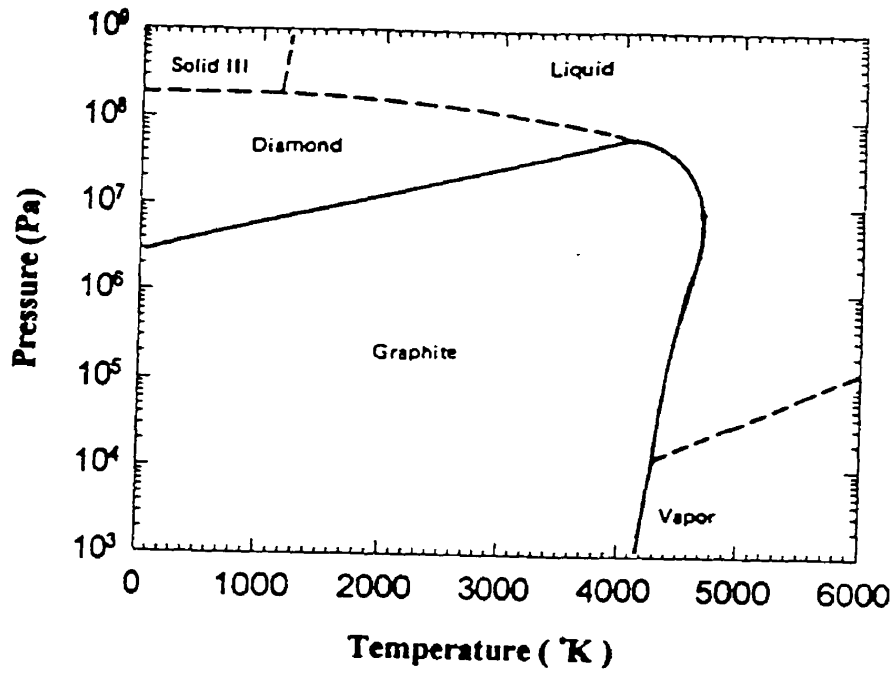

Figure (2-3) : The phase diagram of carbon (Gaskell 1981).

2-2-2 : GRAPHITE

Graphite is very different from diamond. Diamond is hard and basically colorless, and an insulator; but graphite is slippery, black, and a conductor. These differences, of course, arise from the differences in bonding in the two types of solids. In contrast to the tetrahedral arrangement of carbon atoms in diamond, graphite structure is described as layers of carbon atoms with an interatomic distance of 0.145 nm. Each carbon atom within the layers is bonded only to three carbon atoms in a trigonal planar arrangement with 120° bond angles and forming sp^2 structure (see Figure 2-4). The remaining P-type orbital forms a "dangling bond" (or a π electron bond). The layers are separated by a distance that represents a non-bonding situation. Because each atom is formally bonded to only three neighboring atoms, the remaining valence electron (one in each atom) is free to circulate within each plane of atoms, contributing to graphite's ability to conduct electricity.

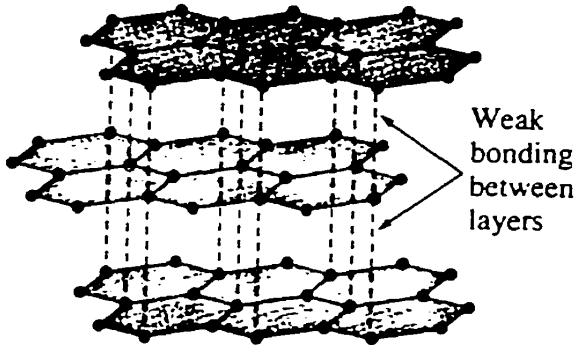

Figure (2-4) : Crystallographic structure of graphite.

One of the main uses for graphite as a lubricant results from the characteristic sliding of one layer over another within the crystal. The characteristic slipperiness of graphite can be explained by noting that graphite has very strong bonding within the layers of carbon atoms but little bonding between the layers. The valence electrons are all used to form σ and π bonds among carbons within a given layer. This arrangement allows the layers to slide past one another quite readily. It is also used as a heat-resistant material; as an electrical conductor and electrode material (in dry cells and arc furnaces for instance); and in nuclear reactors as a neutron moderator.

Manufactured graphite can be produced through different processes, therefore, different graphite cathodes are expected to show different physical, mechanical and electrical properties. Two different production processes are descried below for the graphite cathodes used in this work (i.e., polycrystalline and pyrolytic graphite).

Polycrystalline graphite is typically made by the calcination of the raw material (i.e., Petroleum coke) in large kilns to shrink it and drive out the volatile content. It is then crushed into a very fine powder and sized into different particle sizes through screens. The crushed raw material is mixed with a binder, compressed into a block, and fired at very high temperature to remove any volatile materials and to assure homogeneity. Because the coke does not melt during processing, the resultant structure is much like sand that is stuck together by a thin layer of glue. In general polycrystalline graphite has some anisotropy. The graphite cathodes used in this study however are isotropic and have uniform pore size and distribution. These were produced by **POCO GRAPHITE INC.**, USA.

Pyrolytic graphite called **PYROID** produced by **SPECIALTY MINERALS INC.**, USA, is formed in high temperature vacuum furnaces by chemical vapor deposition (CVD) from a hydrocarbon gas. This graphite is substrate nucleated in which the microstructure growth originates from the deposition surface in the form of inverted cones. A major advantage of this process is that products can be prepared in which porosity is virtually absent. **PYROID** deposition is performed on a mandrel surface, with the basal planes of the graphite structure oriented parallel to it. This type of deposit hence exhibits maximum orientation and anisotropy, with strong thermal conductivity and low electrical resistivity in directions parallel to the cathode surface corresponding to the two dimensional hexagonal structure of graphite. The opposite is true for directions perpendicular to the surface which corresponds to the Van der Waals bonds direction of graphite.

2-2-3 : AMORPHOUS CARBON

The "amorphous carbon" refers to a carbon matrix that has no crystalline long range order and includes any possible mixture of short range order components. It is less well defined than diamond or graphite. Amorphous carbon has physical and chemical properties that may vary depending on its method of manufacture and conditions to which it is later subjected. It is a deep black powder that occurs in nature as a component of coal and lignite. It may be obtained artificially from almost any organic substance by heating the substance to very high temperatures in the absence of air.

Amorphous carbon is the most reactive form of carbon. It burns relatively easily in

air, thereby serving as a fuel, and is attacked by strong oxidants. Amorphous carbon is not a finely divided graphite but appears to have some of the structural features of graphite, such as local regions of sheets and layers. Its atomic structure, however, is much more irregular. The most important uses for carbon black are as a stabilizing filler for rubber and plastics and as a black pigment in inks and paints. Charcoal and coke are used as clean-burning fuels. Certain types of "activated" charcoal are useful as absorbents of gases and of impurities from solutions.

2-2-4 : FULLERENES

In the 1980s scientists found that carbon atoms linked to form a more or less spherical molecule. A whole family of allotropes, with differing numbers of atoms, is now known to exist. The first to be identified and the most symmetrical of the family, with 60 atoms and 32 sides (20 hexagons and 12 pentagons). It was nicknamed "buckyball" and thereafter formally named Buckminsterfullerene because it resembles the geodesic domes of American architect R. Buckminster Fuller. Spherical carbon molecules as a group are called Fullerenes (Figure 2-5).

Buckminsterfullerene was first synthesized in relatively large quantities (in comparison with their original discovery using a laser impulse on a carbon target (Curl & Smalley 1988). This was done in the lab of Donald R. Huffman (University of Sussex) by vaporizing carbon from pure graphite electrodes in an atmosphere of helium gas at a pressure of 100 Torr. The soot that forms in this environment is about 5% C_{60} by mass. The scientists have also found significant quantities of another "fullerene" in this soot that

consists of C_{70} molecules. The C_{70} molecule is similar to the spherical C_{60} molecule except that the extra carbon atoms lead to an egg-shaped structure. Experiments also show that when the 60 and 70 carbon fullerenes are subjected to intense laser pulses they open their cages and combine to form huge spherical fullerenes with 400 or more carbon atoms.

Fullerenes are now being produced in marketable quantities for use by scientists. Their occurrence in carbon-containing materials on earth may not yet prove to be widespread (one site found on earth yet in Northern Ontario, Canada), and it is suggested as a fairly common interstellar molecule. Their super conducting properties and their potential for opening new areas of chemistry have made the study of the "buckyball" one of the most rapidly expanding areas of research.

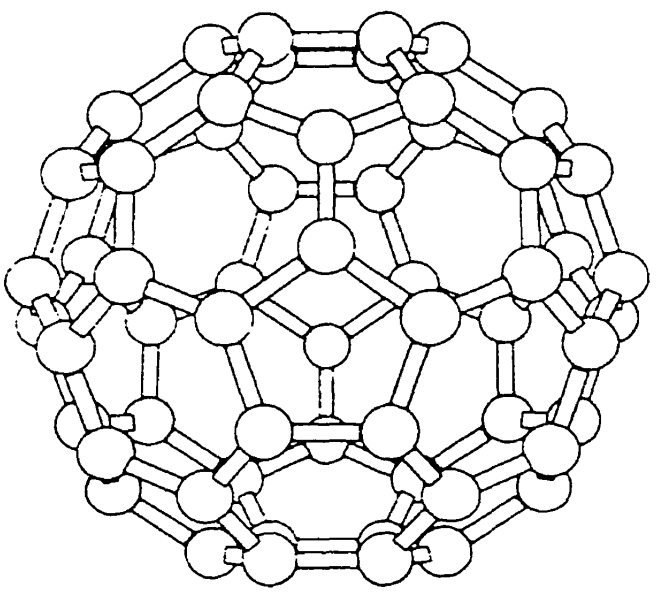

Figure (2-5) : A model of buckminsterfullerene.

CHAPTER 3 : DIAMOND-LIKE

3-1 : DIAMOND-LIKE NOMENCLATURE

Diamond-like refers to sp^3 structure being dominant with less abundant graphite (sp^2) and polymeric (sp^1) structures. Savvides (1985) suggested that the central problem in the understanding of the structure of diamond-like carbon films is the ratio of atoms of sp^3 to sp^2 coordination.

The term diamond-like covers a wide range of carbon films with hydrogen concentration from 0 to more than 70 %. Unfortunately, there has been essentially no distinction made among these materials using structural and compositional criteria. This is because diamond-like films depend on the ratio of sp^3/sp^2, bond structure and hydrogen content. Therefore, an unlimited number of films can be formed with varying physical properties, all being called diamond-like.

A variety of names have been used (Angus 1986), e.g., diamond-like films, hard carbonaceous films, hard carbon, a-C:H, a-C, and i-C. The term "diamond-like" or "diamond" coating should refer to the films that possess a true sp^3 electronic configuration (Angus 1986 and Messier et al 1987). The term "i-C" refers to films that are prepared using ions (Angus 1986). The term "a-C" refers to amorphous carbon coating without hydrogen, while "a-C:H" refers to a diamond-like coating with hydrogen where the hydrogen concentration can be variable between 10%-70% (Jansen et al 1985 and Angus 1986).

As the crystallite size falls below 0.2 μm the definitive characterization becomes more difficult and the distinction between diamond and diamond-like carbon coatings is

tenuous. The general differences between diamond and diamond-like coatings are described in Table 3-1.

Table (3-1) : Comparison Between Diamond and Diamond-Like

	DIAMOND	DIAMOND-LIKE
STRUCTURE	CRYSTALLINE	AMORPHOUS
HYDROGEN CONTENT	< 0.1%	0 - 70%
BOND TYPE	100% sp^3	66% - 98% sp^3
BONDS/ATOM	4	VARIABLE, TYPICAL 2.45

The key to the diamond-like formation is related to the energy level and the growth technique. The energy of the deposited carbon ions should be between 14.6 eV (Davies & Evans 1972) and 60 eV (Luzin 1976). At 14.6 eV the material remains as graphite, while at 20 eV the energy approaches formation of diamond. Between 20 and 60 eV the amorphous structure will be formed. Above 60 eV the material return back to the graphite form. An increase in the ion energy increases the defect density and degrades the stability of the growing diamond-like film. This effect results from the local heating of the film surface caused by the impinging energetic species (Strel'nitskii et al 1978). Hence only a certain range of energies give rise to diamond-like structure.

Diamond deposition is produced by chemical vapor deposition (CVD) technique because growth of diamond crystals results from chemical reaction effects based on hydrogen saturation of the surface. On the other hand, diamond-like films are produced by

physical vapor deposition (PVD) techniques in which the substrate is bombarded by energetic ions. PVD technique is therefore used for the production of diamond-like because the ion beam at high energy is needed to form amorphous structure at low substrate temperature, the low temperature ensuring low surface mobility of the atoms.

3-2 : EFFECT OF HYDROGEN

The mechanisms involved in the formation of diamond-like films are not well understood at this point. The role of the molecular hydrogen partial pressure in the stabilization of diamond sp^3 bonds in diamond-like films is also questionable.

With regard to structure, the hydrogen incorporated in the amorphous hydrogenated carbon (a-C:H) films may play a crucial role in the bonding configuration of the carbon atom. It is helping to stabilize tetrahedral coordination (sp^3 bonding) of the carbon atoms, which are believed by some authors to be the origin of the diamond-like properties of the films. Consequently the optical, electrical, and even mechanical properties of the a-C:H films are closely related to the hydrogen content and its form in the film (Tsai & Bogy 1987).

The hydrogenated carbon films have very high resistivity compared to unhydrogenated carbon films. It appears that unhydrogenated carbon films have a higher density than the hydrogenated carbon films, although both groups are less dense than graphite. Hardness of hydrogenated carbon films is somewhat lower than the unhydrogenated carbon films (Bhushan et al 1992).

The typical pressure in most of the diamond-like deposition systems is 10^{-4} Torr or

lower i.e., these systems are of the collisionless physical vapor deposition type. Some authors believe that diamond-like film formation is not dependent on the gas pressure (Aisenberg 1984), this remains to be proven. It is well known that atomic hydrogen has an essential role in the stabilization of real diamond surface (Savvides 1985). In diamond-like the role of hydrogen atom is not clear yet and the addition of hydrogen is not necessary, diamond-like films have been produced without any added hydrogen.

3-3 : PREVIOUS WORK ON DIAMOND-LIKE FILMS

The first diamond-like films were deposited by a beam of carbon ions produced in an Argon plasma as reported by Aisenberg & Chabot (1971) and later confirmed by Spencer et al (1976). They claimed that the carbon films produced using this technique are insulating, transparent, able to scratch glass, resistant to HCl acid for long periods of times. In addition to these properties, they have a dielectric constant between 8 and 14 (diamond is 16.5) and refraction index grater than 2.0. These carbon films are distinguished by a change from soft carbon deposits to hard films as their resistivity rises from 0.1 to 10^{12} Ω cm, their optical properties changing from those of graphite to those of a dielectric (Holland & Ojha 1979).

Berg & Andersson (1979) used a r.f. butane plasma to produce diamond-like carbon films and they found that films produced at low deposition rates were more diamond-like and highly insulating than films produced at high deposition rates. For example, films produced at a r.f. power of 50 W (500 V accelerating voltage) for 5 min. (film thickness 500 Å) were hard, had good adhesion to the glass substrate, were pale

yellow under transmitted light and showed a resistivity in the range of 10^6-10^7 Ω cm. While films produced at a r.f. power of 300 W (1200 V accelerating voltage) for 5 min. (film thickness 1000 Å) were very hard, had good adhesion, yellowish brown and showed a resistivity of about 10^2 Ω cm. On the other hand, films produced at a r.f. power of 600 W (1800 V accelerating voltage) for 2 min. (film thickness 1000 Å) were easy to remove from the substrate, brown in color and showed a very low resistivity of about 1 Ω cm.

Meyerson & Smith (1980) have studied the effect of the substrate temperature on diamond-like carbon film deposited over Mo/glass substrate using dc glow discharge decomposition of acetylene technique. They found that films produced at substrate temperature below 200 °C were transparent and grow progressively darker with the increase of the substrate temperature above 200 °C. Films grown on glass at 25 °C were faint tan and highly transparent, while those grown on glass at 350 °C were deep brown but still moderately transparent. The optical band gap was also investigated and found to be decreasing from 2.1 to 0.9 eV as the substrate temperature was increased from 25 °C to 375 °C.

Pappas et al (1992) also investigated the effect of the substrate temperature on diamond-like carbon films produced by 248 nm excimer laser vaporization of graphite targets (pulsed laser deposition). They found that films deposited at room temperature (298 K) or below (77 K) have high degree of tetrahedral coordination (sp^3 bond fraction between 70 and 85%), high optical transparency and electrically insulating. On the other hand, deposition at elevated temperature (573 K) yields a black, highly conductive and strongly absorbing material, which may be described as graphitic.

Coll et al (1992) synthesized hydrogenated and hydrogen-free carbon films using arc ion plating system called modified cathodic arc evaporator. This modified arc evaporator fitted to a rectilinear plasma optic system similar to that used by Aksenov et al (1980) to confine the arc discharge at the cathode surface. The carbon films' features were analyzed by Raman spectroscopy, Fourier transform IR spectroscopy and scanning electron microscopy. They found that very smooth DLC films with good hardness and excellent adhesion are produced on high speed steel substrates. Changing the bias voltage applied to the substrate allowed them to control the carbon ion energy easily. They claimed that few particles (maximum diameter, 500 Å or less) were observed with no adhesion failure at the film-substrate interface.

Xiong et al (1993) used a ArF (193 nm) pulsed laser ablation of graphite to deposit hydrogen-free diamond-like amorphous carbon films with a laser power density of $5x10^8$ W/cm^2. They found that the laser wavelength or photon energy plays a crucial role in controlling the properties of the pulsed-laser-deposited diamond-like carbon films.

3-4 : CHARACTERIZATION OF DLC FILMS

Several methods can be utilized to characterize diamond-like carbon films as described below :

1. Identification of Carbon Films:

A. Composition (Carbon) :

- Auger Electron Spectroscopy (AES).
- X-ray Photoelectron Spectroscopy (XPS).

- Secondary Ion Mass Spectroscopy (SIMS).

- Infra Red Spectroscopy (IRS).

B. Structure (Diamond-Like) :

- X-ray Diffraction (XRD).

- Auger Electron Spectroscopy (AES).

- Raman Spectroscopy.

- Infra Red Spectroscopy (IRS).

C. Bonding (sp^3, tetrahedral; sp^2, graphite; sp^1, polymer) :

- Raman Spectroscopy.

- Auger Electron Spectroscopy (AES).

- Electron Energy-Loss Spectroscopy (EELS).

- X-ray Photoelectron Spectroscopy (XPS).

- Infra Red Spectroscopy (IRS).

2. Defects in Diamond-Like Films :

A. Scanning Electron Microscopy (SEM) and

B. Field Emission Gun Scanning Electron Microscope (FEGSEM):

- Grain Boundaries.

- Particle Morphology.

- Secondary Nucleation.

C. Dektak 3 ST Profilometer :

- Films Roughness.

- Films Thickness.

In this work, only four of the above diagnostic tools were used due to the availability of these equipments (i.e., SEM, FEGSEM, IRS and Dektak 3 ST profilometer). The detailed description about most of these tools (how they work, advantages, limitations and what kind of data one can get and how to interpret these data) are found in Tsai & Bogy (1987). Interpretation of the data obtained by different researchers using IRS and Raman spectroscopy are described below briefly.

3-4-1 : INFRA RED SPECTROSCOPY

Infra red spectroscopy is used in general to analyze the structure of many organic and inorganic materials. For carbon films it is used mainly to analyze the C-H and C-C bonding configuration and to estimate the ratio of sp^3 to sp^2 in DLC films. The data obtained from IRS represents transmittance (or absorbance) versus energy frequency or wave number. If the IRS beam is not transmitted (or absorbed) by the sample a reflection technique can be used. The peak location identify the phase (typical wave number ν=400 - 4000 cm^{-1}). The intensity of the peaks indicate (indirectly) concentration. The identification of the absorption peaks are described in Table 3-2 according to (Dischler et al 1983, Shichang et al 1989, Zou et al 1990, Grill et al 1991 and Palshin et al 1995).

Table 3-2 : IRS Absorption Wave Numbers in DLC Films.

WAVE NUMBER (cm^{-1})	ASSIGNMENT	MODE
3300	sp^1 C-H	stretching
3060/3045	sp^2 C-H (aromatic)	stretching
3000	sp^2 C-H (olefinic)	stretching
2970/2960	sp^3 C-H_3 (asymmetric)	stretching
2930-2916	sp^3 C-H_2 (asymmetric)	stretching
2875/2870	sp^3 C-H_3 (symmetric)	stretching
2855/2850	sp^3 C-H_2 (symmetric)	stretching
1650-800	C-H	deformation

3-4-2 : RAMAN SPECTROSCOPY

Raman spectra are very sensitive to changes that disrupt the translational symmetry of the material studied, as occurs in small-dimensional crystals (Dillon et al 1984) and thus is useful for the study of disorder and crystallite formation in the i-C films. The peak location (i.e., wave number cm^{-1}) identifies the phase. The intensity ratios allow one to determine relative concentration but scattering cross section differences can complicate this. Peak width gives a qualitative indication of material quality.

The Raman spectra of both crystalline structures of carbon are well known. The first-order Raman spectrum of diamond consists of a single line at 1332 cm^{-1} (Grimsditch & Ramdas 1975). The corresponding spectrum of large single-crystal graphite also has a

single high-frequency line, the "G" line, at about 1580 cm^{-1} or 1575 cm^{-1} (Tuinstra & Koenig 1970). Polycrystalline graphite exhibits another line at 1355 cm^{-1}, sometimes called the "D" line. Figures 3-1 and 3-2 show Raman spectra of various noncrytalline carbon and typical Raman spectra for the DLC films that were deposited on two different Si interlayers., respectively.

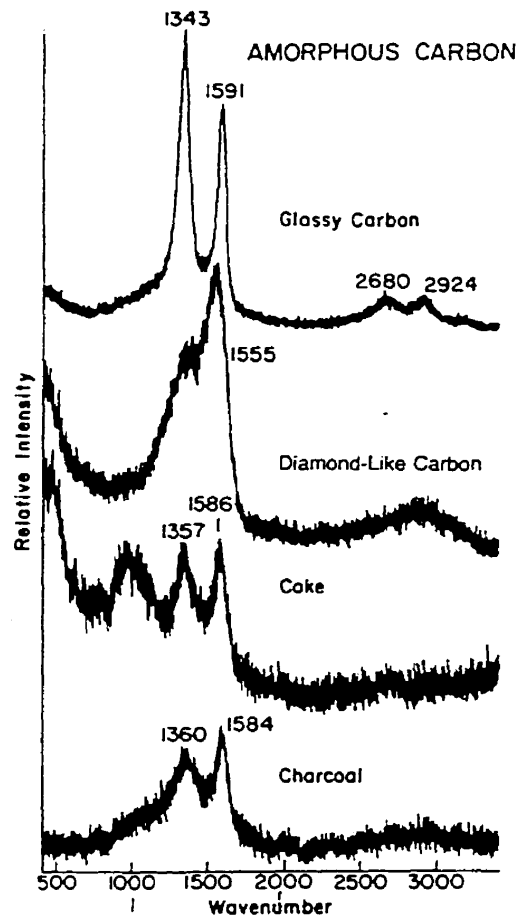

Figure (3-1) : Raman spectra of various noncrystalline, mainly graphitic carbon (Knight & White 1989)

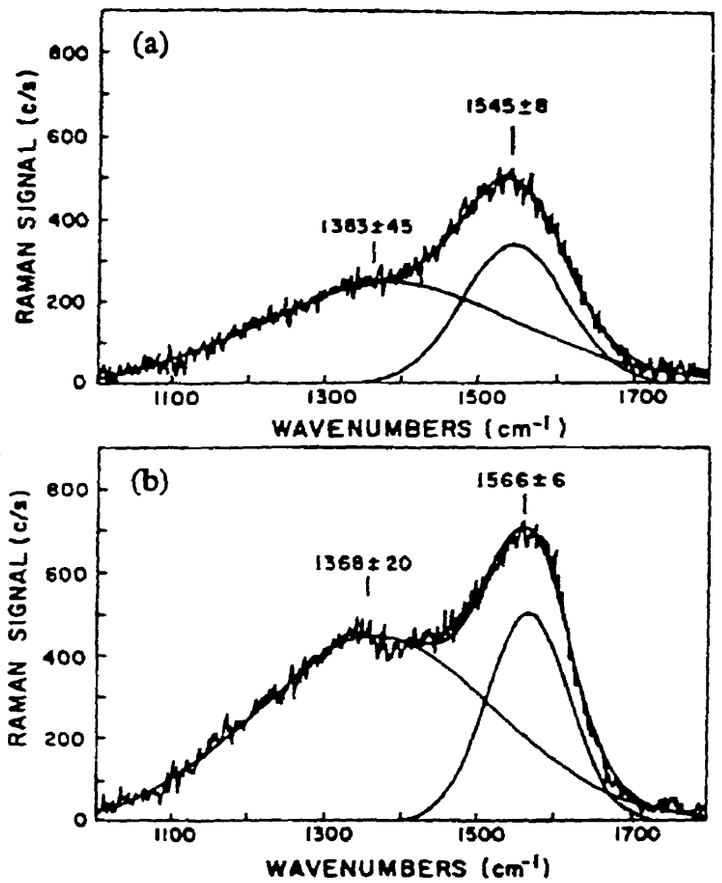

Figure (3-2) : Typical Raman spectrum of as-deposited DLC (a) Film 1 and (b) Film 2. Also shown is the Gaussian lines shape fit and analysis (Palshin et al 1995).

3-5 : APPLICATIONS

The unique characteristics of the diamond-like films and the demand of modern technologies, especially those associated with developments in the electronic industry, have attracted much attention to study these films. Diamond and diamond-like carbon films are especially attractive materials for use in extreme environments, e.g., space, nuclear reactors, and harsh chemicals. Such properties as resistance to radiation damage (due to its low Z number) and chemical inertness (caused by strong covalent bonds) are exploited for these uses. Some of the possible applications are described in Table 3-3 (Andersson 1981, Aisenberg & Stein 1982, Aisenberg 1984, Tsai & Bogy 1987 and Martinu 1990) :

Table 3-3 : Some of The Possible Applications of DLC Films.

*** optical coatings.**
*** protective thin film coatings for magnetic recording materials (e.g., computer discs) to give longer life time.**
*** heat sinks and high thermal conductivity coatings for semiconductor applications.**
*** solid state devices.**
*** moisture barriers.**
*** low friction coatings for tribological applications.**
*** protection against severe environments (sand and salt water).**
*** protective coatings compatible with body tissues for medical applications.**

Due to the high hardness of the diamond-like coating, it is recommended for wear protection applications to increase the life time of the machine parts and tools. In this respect, diamond-like coatings known as very hard, exhibit low friction coefficient and good sliding behavior, and are extremely resistant to wear. Current commercial applications of DLC include uses on infrared optics, such as germanium windows where DLC is becoming the standard antireflection coating, and on hard magnetic storage discs as a low friction, protective layer. Coatings on sliding-wear parts, surface treatment of plastics, decoration and corrosion resistance are anticipated near-term applications. In the longer-term, DLC may find uses in such exotic areas as bio-compatible implants.

PART TWO

PULSED ARC MODE

CHAPTER 4 : ARC SPOT MOVEMENT AND EROSION RATE

4-1 : INTRODUCTION

This work is aimed towards a possible control of the micron-sized particles emitted by the cathode spot. Particle emission studies on a pulsed arc system by Kandah and Meunier (1995) showed that a control of the local energy flux to a given graphite cathode site can result in significant decrease of the number, the mean size and the width of the size distributions of the emitted particles. The experimental study presented here goes further in analyzing the movement of cathode spots on various graphite materials in order to decrease the local energy input on given graphite surface emitting sites. The interaction between graphite material properties and vacuum arc spot behavior implies the choice of the graphite cathode material may be a very important issue depending on the application.

Manufactured graphite is not one specific material, but a family of materials. Each member of the family is essentially pure carbon, but varies from the other in such properties as the orientation of the crystallites, the size and the number of pore spaces, the grain size, the electrical resistivity and the density (Page 1991). Consequently, there is a corresponding variation in the physical, mechanical and electrical properties, which generate different cathode spot behaviors when subjected to a vacuum arc. Graphite electrodes are known to induce strong anchoring of the cathode spot in vacuum compared to metallic electrodes, leading to a difficult transfer from a pulsed to a continuous moving arc system (see Figures 1-8, 1-9 & 1-10).

The temperature dependence of the cathode erosion and velocities of vacuum arcs in an external magnetic field were investigated for three types of graphite (**Poco-Graphite type AXF-5Q, Papyex-Graphite and Ringsdroff-Graphite type EK-506**) by Koch et al (1984) as shown in Figures 4-1 and 4-2. Unfortunately, they do not mention the surface properties of the cathodes used in their work, only the cathodes commercial names are given. Their study showed that the velocity on **AXF-5Q** shows no dependence on temperature up to 2000 K. However on **Papyex-Graphite** cathodes the velocity increases with increasing cathode temperature above 1200 K. The measured erosion rates of **AXF-5Q** and **EK-506** show both only a very little dependence on the cathode temperature.

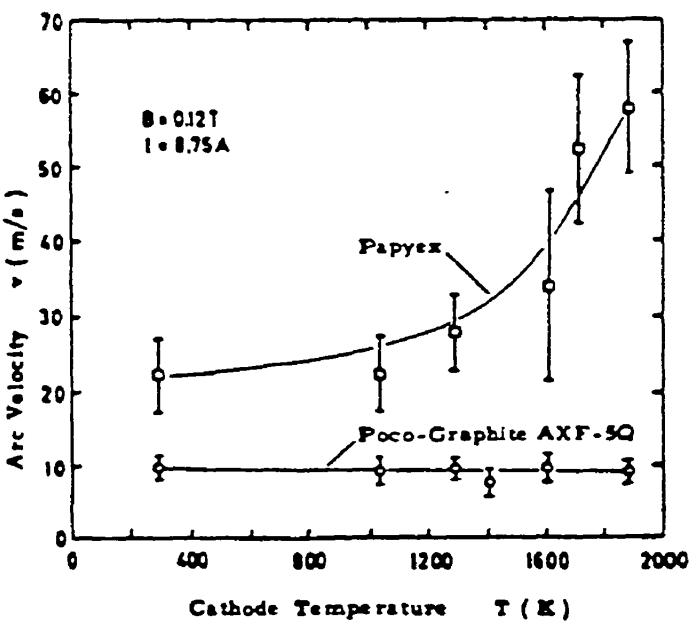

Figure (4-1) : Arc velocities on **Papyex** and Poco Graphite **AXF-5Q** cathode probes as a function of the cathode temperature (Koch et al 1984).

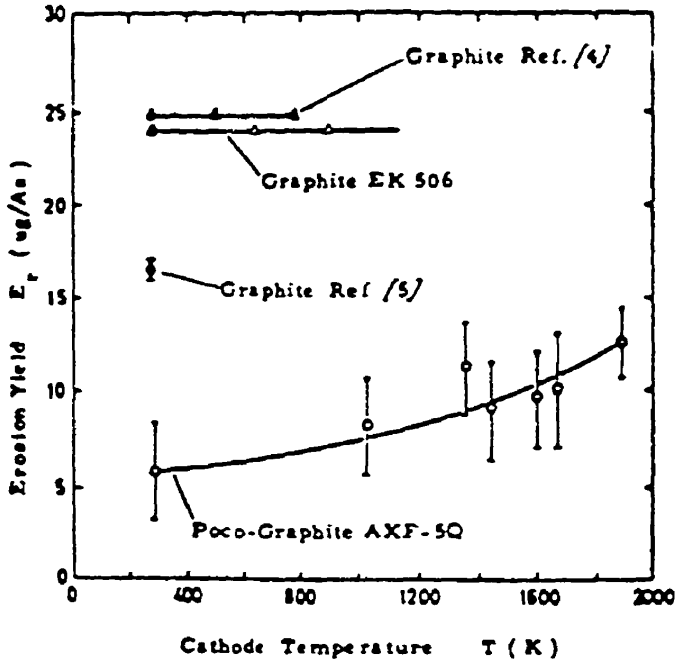

Figure (4-2) : Erosion yields of different graphite cathodes as a function of cathode temperature (Koch et al 1984).

In this work we report on the study of the movement and velocity of the cathode spot subjected to a transverse magnetic field for different graphite cathode material microstructures. The electrodes are used without any surface treatment prior to arcing and are maintained at room temperature. Also, the dependence of the erosion rate on the arc spot velocity is investigated for four different graphite cathodes under a variable transverse magnetic field.

4-2 : EXPERIMENT

The experimental setup used in this work is shown in Figure 4-3. A spherical vacuum chamber 23 cm in diameter is pumped down to a pressure of 10^{-4} Torr using mechanical and oil diffusion pumps (Figure 4-4). The graphite cathodes were made of strips (50 mm x 10 mm x 3 mm), and mounted parallel to a copper anode (50 mm x 20 mm x 5 mm) with an electrode gap of 5 mm.

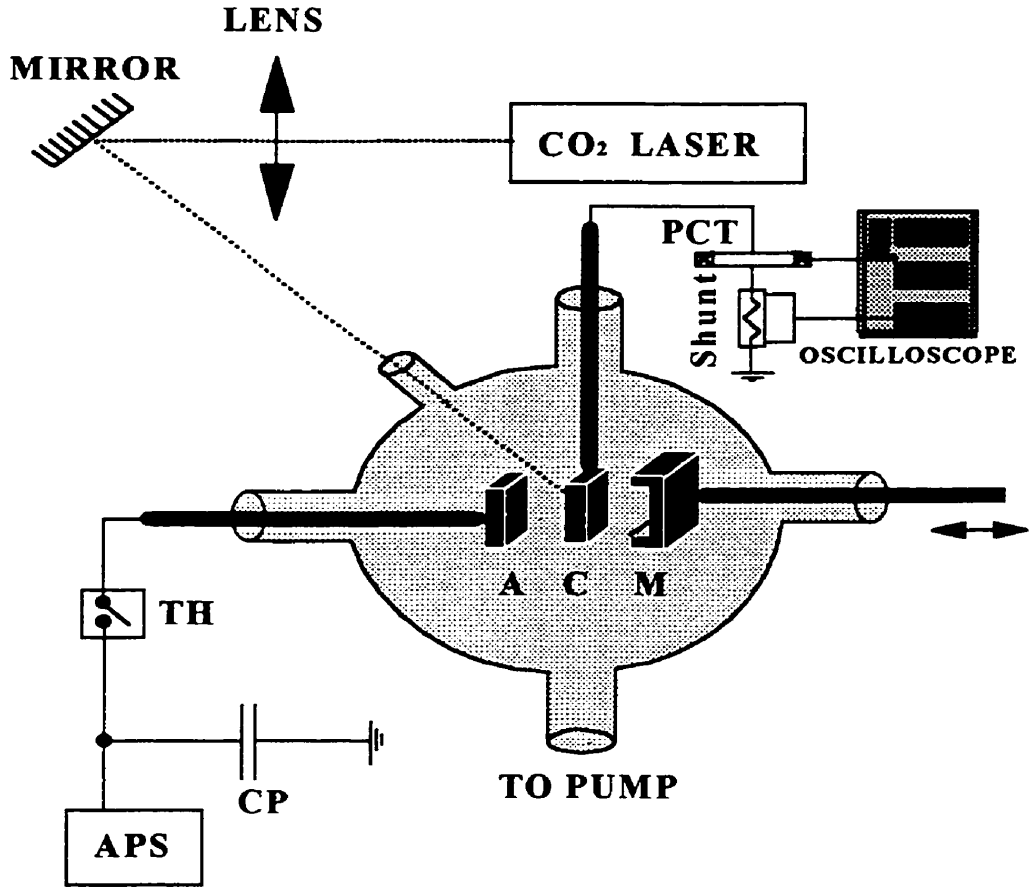

Figure (4-3) : Experimental setup, C = cathode; A = anode; M = magnets; APS = arc power supply; PCT = pearson current transformer; TH = thyristor triggering/shut-off circuit and CP = capacitor.

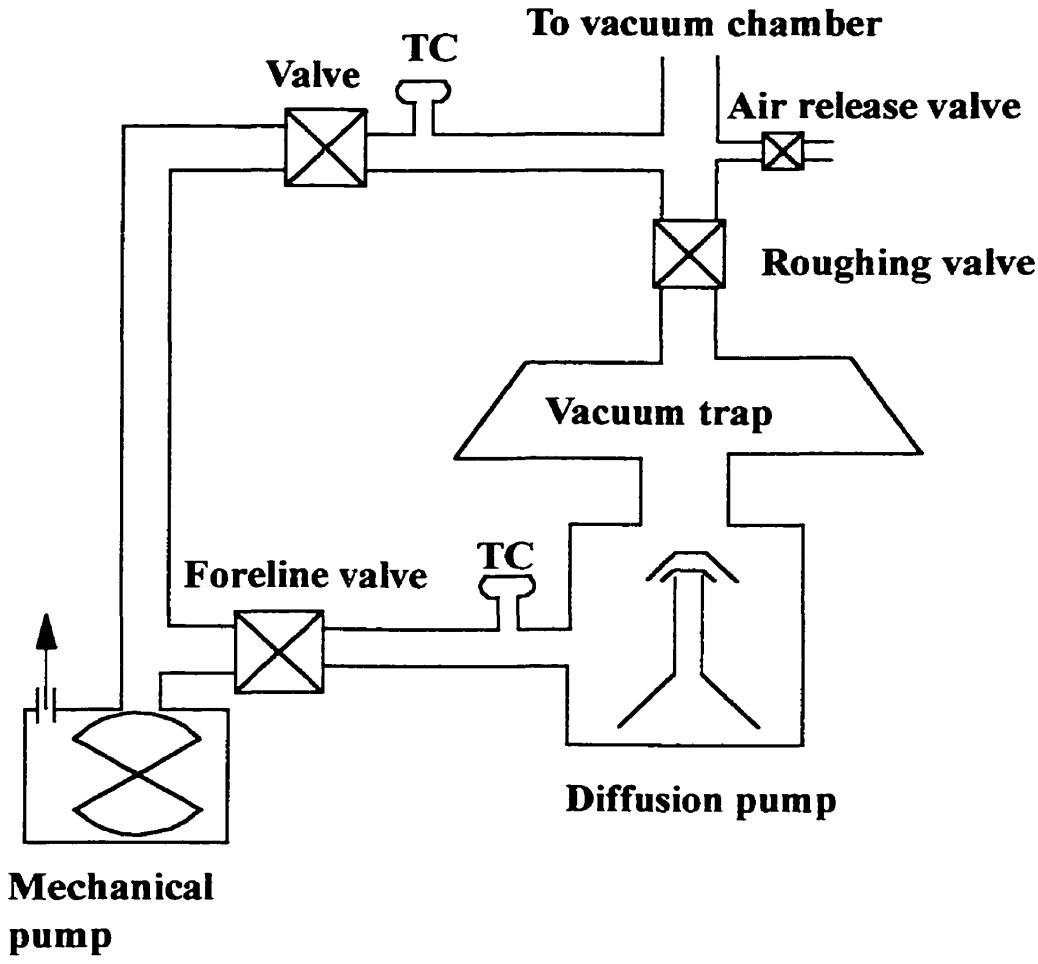

Figure (4-4) : Schematic for the vacuum pumping system; TC = Thermocouple gage.

The vacuum arc was ignited by a CO_2-TEA laser which produced a pulse of infrared radiation of maximum power of 1 MW and a duration time of 200 ns at a wavelength 10.6 μm. The laser beam was focused on the cathode surface using a NaCl window and a 25 cm focal distance ZnSe lens giving a spot size (Airy disc) of 0.5 mm. The position of the laser beam impact on the cathode corresponded to the starting point of the magnetically driven arc trace.

The arc current was generated by charging a capacitor bank of 38 mF and was varied between 60 A and 140 A. The electrical circuit (Figure 4-5) used in this work produced a constant and reproducible square current pulse. Thyristor T1 is closed at time t_i at the beginning of the current pulse, and supplies current between the electrodes from capacitor C1. At time t_f, thyristor T2 is closed to direct current to capacitor C2, hence extinguishing the arc. Power supply PS1 charges the main capacitor bank, while power supply PS2 provides the necessary negative charge to capacitor C2 to enable a zero of current between the electrodes. The voltage applied by PS1 and PS2 (HP 6448B DC power supply; 0 - 600 V & 0 - 1.5 A) are typically the same but of opposite polarity. A typical arc current pulse is shown in Figure 4-6. Triggering pulses t_i and t_f were generated by a Cordin delay generator model 453, the initial pulse t_i being simultaneously send to trigger the CO_2 laser pulse and thyristor T1. The arc duration time was measured using an oscilloscope, it was varied between 10 μs and 100 ms. The arc current was measured using a Pearson pulse current transformer No. 411 (0.1 V/A) connected to an oscilloscope type 549 Tektronix. This was useful for short arc duration times, but not useful for long arc duration times. The pulse current transformer saturates at $Q = I \times t = 0.19$ C. This

implies the current transformer does not give any signal once the 0.19 C limit is exceeded and hence we were not able to monitor the long duration times. For this reason, we were forced to use a shunt to monitor the arc current for long arc times. The shunt is in series with the circuit and shows some inductance. This produces electrical noise at the high dI/dt occurring at the on and off triggering times of the arc. The shunt, however, works very well in the constant arc current period with low dI/dt, for these reasons, both the Pearson pulse current transformer and the shunt are used to measure the arc current.

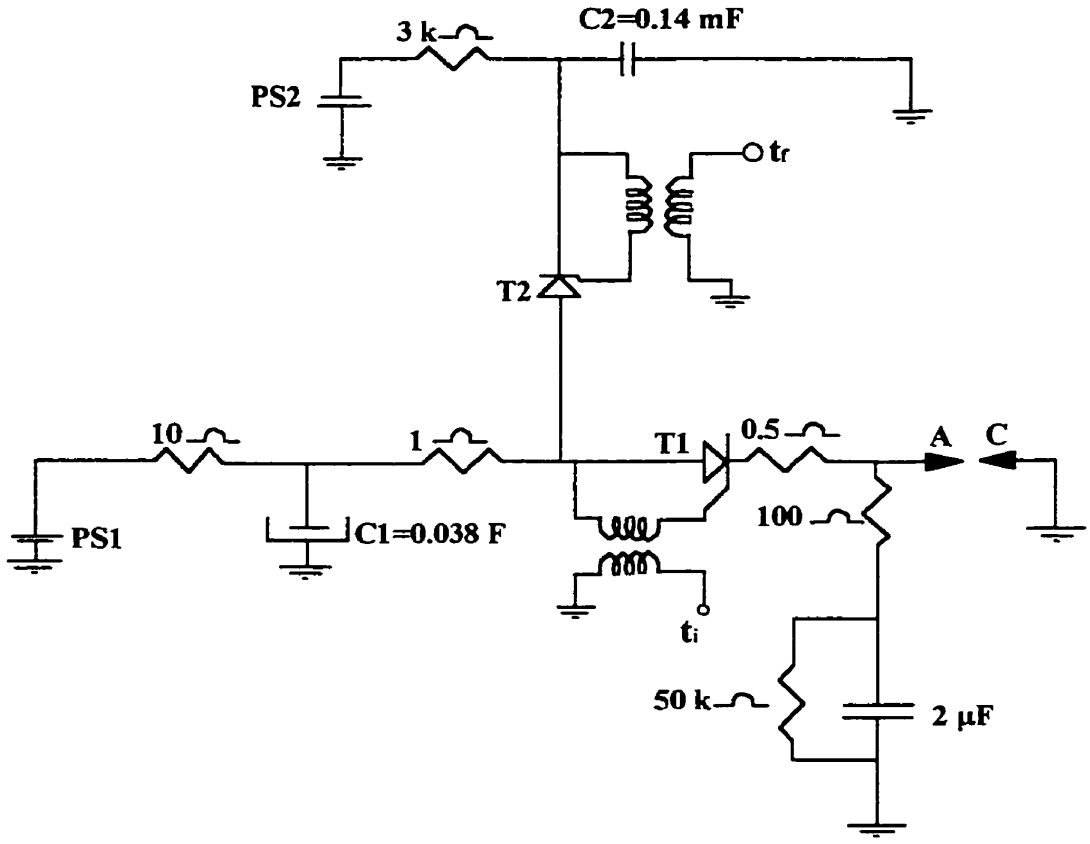

Figure (4-5) : Schematic for the electric circuit (pulse system).

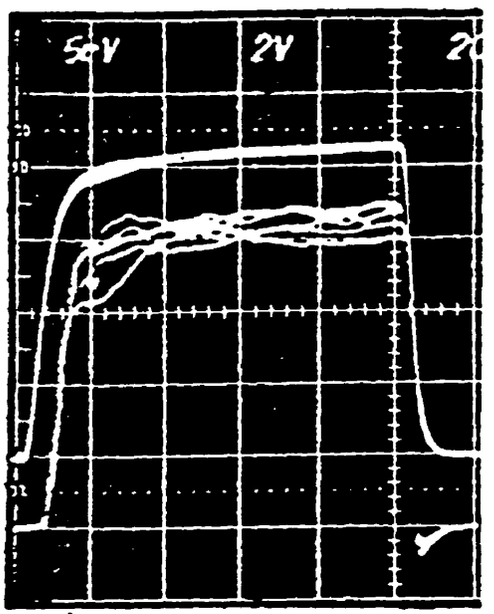

Figure (4-6) : Oscillogram showing six superposed arc current pulses (top trace; 20 A/div.), the time scale is 20 μs/div. The lower traces show typical wall current collection during the six discharges.

An external magnetic field was applied parallel to the cathode surface in order to move the arc spot on the cathode in the usual retrograde direction typical of vacuum arcs subjected to transverse magnetic fields. This ensured a relatively straight arc trace showing the typical tree-like erosion pattern. After each ignition a very clear line trace is left on the cathode surface by the arc movement which represents the arc spot path length (Figure 4-7). The mean arc spot velocity is evaluated simply by dividing this arc trace length by the

arc duration time. During the arcing, the arc current and the pressure were kept constant at 80 A and 10^{-4} Torr respectively, unless otherwise mentioned. The arcing times were adjusted to have the observable arc trace covering the full discharge time, i.e., to prevent the arc from reaching the bottom edge of the cathode.

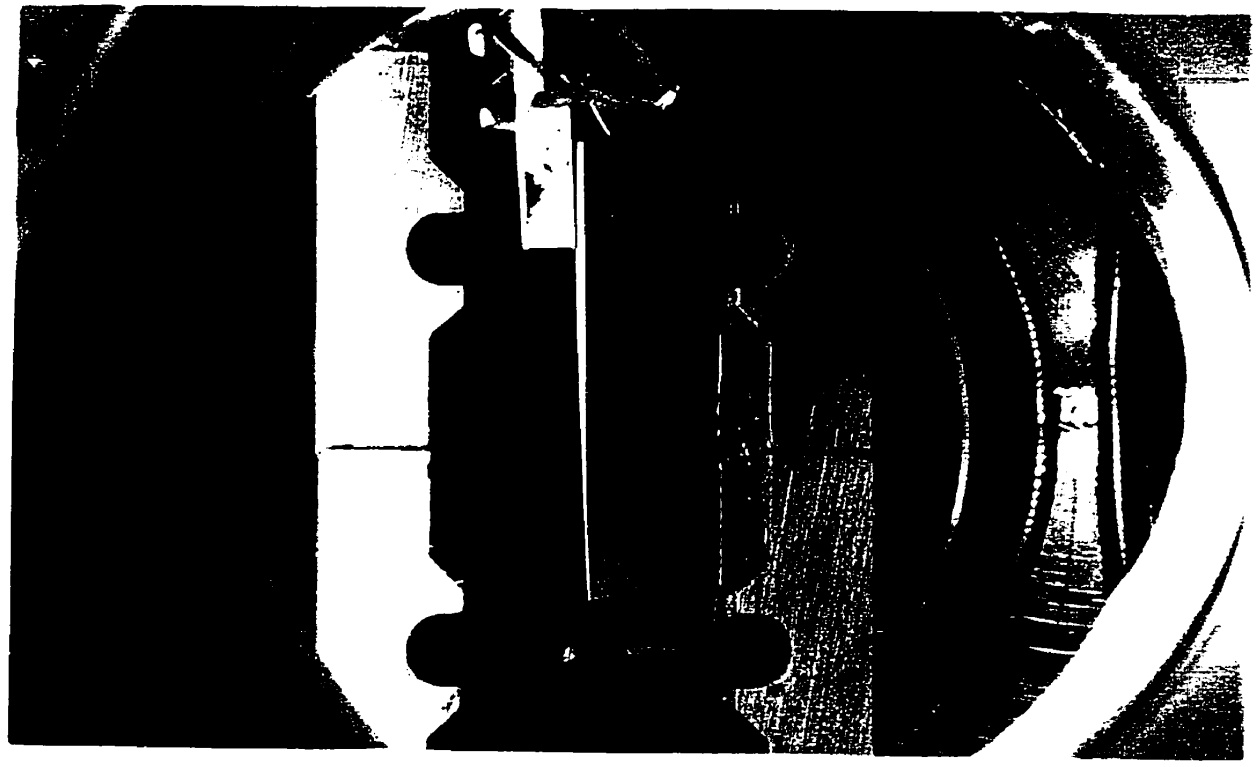

Figure (4-7) : Photograph showing the arc trace left over the graphite cathode (pulse system).

The net erosion rate values in grams per coulombs were determined by weighting the cathode before and after the arcing using a micro-balance, then dividing the weight difference by the total electric charge $Q = \int I dt$ passing through the cathode. Experiments were performed at a constant total charge of 50 C for each cathode.

Eleven different types of graphite materials were tested. Table 4-1 gives some important material properties of these cathodes. Velocity measurements were repeated three times for each type of graphite material to ensure reproducibility. Erosion rate measurements were made using a series of 2.5-5 ms individual arc pulses with a current of 70 A. The number of pulses was adjusted to yield the total electric charge of 50 C.

The cathodes used were manufactured in two different ways to obtain different microstructures (i.e., pyrolytic and polycrystalline graphite) as described in section 2-2-2. Commercial names of the different graphite structures are used in Table 4-1 and throughout this thesis. Properties are given according to the manufacturers.

Table 4-1 : Properties of Graphite Cathodes Used in This Work

CATHODE	GRAIN SIZE (μm)	PORE SIZE (μm)	DENSITY (g/cm^3)	El. RESISTIVITY (μ. ohm.cm)
PYROID	—	0	2.2	250 (||) * $3x10^5$ (⊥)
PGCS-1	15	3	1.79	1500
TM	10	1.5	1.82	1250
ZXF-5Q	1	0.2	1.8	1650
XT	20	n/a	1.71	1250
AXF-5Q	5	0.8	1.8	1400
AXZ-5Q	5	0.7	1.64	1900
AXM-5Q	5	0.8	1.74	1500
ACF-10Q	5	0.8	1.8	2500
PS	5	1.2	1.33	2900
PC	5	n/a	1.10	11500

* (||) = parallel to the cathode surface; (⊥) = perpendicular to the cathode surface.

4-3 : RESULTS

4-3-1 : EFFECT OF MAGNETIC FIELD ON CATHODE SPOT VELOCITY

Mean cathode spot velocities were measured for all cathodes as a function of the transverse magnetic field intensity. Figure 4-8 shows a large spread in the arc spot velocities between the different graphite cathode microstructures used. The applied magnetic field varied between 0.0375 T and 0.06 T. For comparison, arc spot velocities of 20 m/s are observed on titanium cathodes using magnetic field values of 0.02 T (Kim 1995). The same magnetic field applied to a graphite cathode produced by **SPEER**, having a bulk density of 1.4 g/cm^3 (Speer grade number 7716) leads to a typical mean spot velocity of only 1 cm/s and lower (see Fig. 1-8). Such low overall velocity indicates strong anchoring of the cathode spots on localized hot emission regions and a weak influence of the magnetic field on spot motion. In order for graphite to yield similar velocities as those obtained on metallic electrodes, an increase of the magnetic field intensity by at least a factor of four is needed. One can see from Figure 4-8 that the pyrolytic graphite (**PYROID**) yields much larger velocity values compared to polycrystalline graphites. Polycrystalline graphites tend to follow the order of the materials given in Table 4-1 for decreasing values of spot velocity. Very different arc spot velocities at the same magnetic field intensity can also be observed for the various types of graphite cathodes. The results of Figure 4-8 indicate that the choice of the type of graphite being used has strong effect on the arc spot behavior.

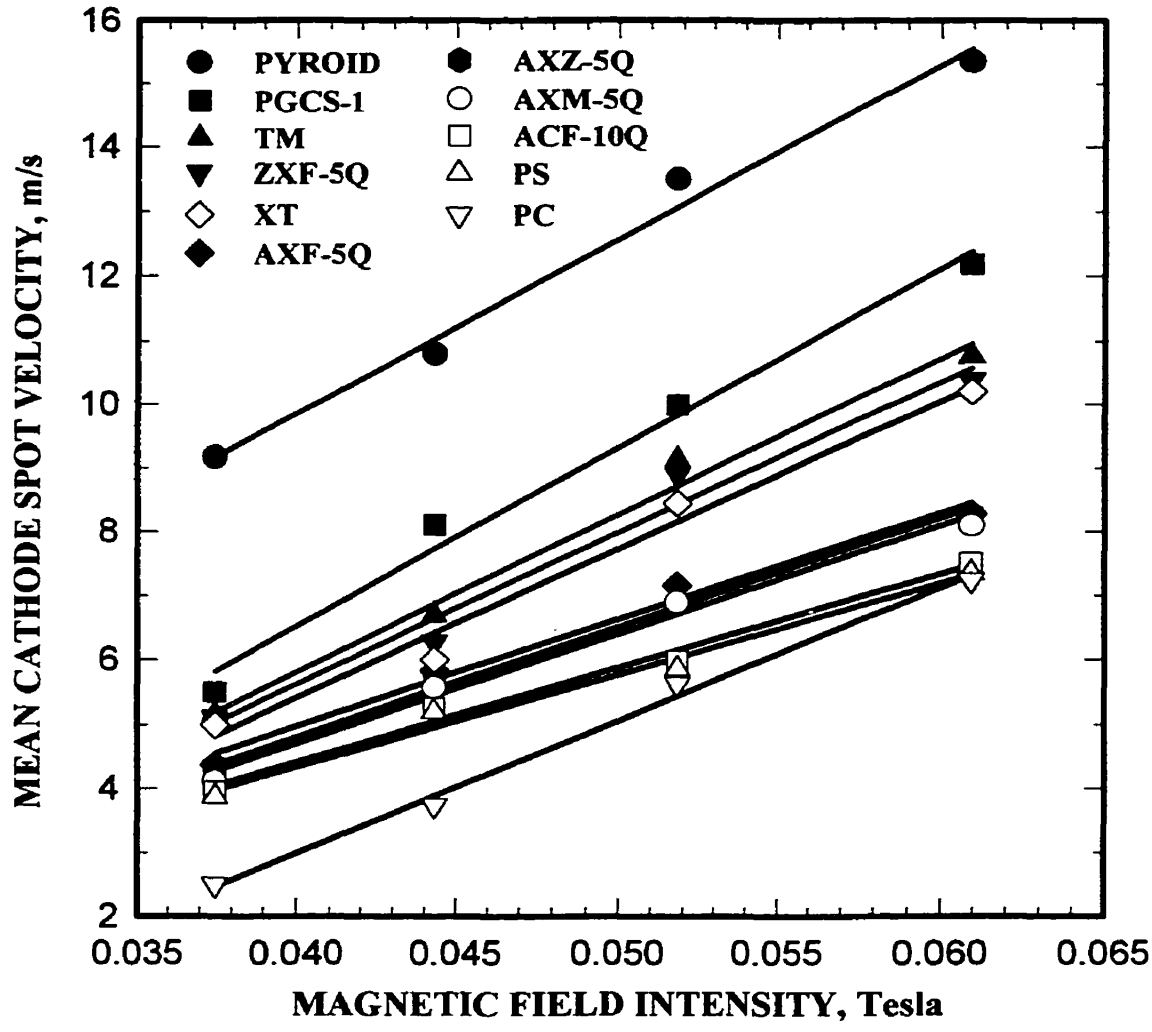

Figure (4-8) : Mean cathode spot velocity as a function of magnetic field intensity for eleven different graphite cathodes at constant arc current (80 A) and pressure (10^{-4} Torr).

4-3-2 : EFFECT OF ELECTRICAL RESISTIVITY ON ARC SPOT VELOCITY

Figure 4-9 shows the effect of the room temperature electrical resistivity of the different graphite cathodes on the arc spot velocity. Only two cathodes (**AXF-5Q** and **ACF-10Q**) showing the same grain size (5 μm), pore size (0.8 μm) and density (1.8 g/cm^3) were used in addition to the pyrolytic graphite (**PYROID**) to limit parameters to resistivity. The unfilled symbols refer to the **AXZ-5Q** cathode having the same grain size but with slightly different pore size (0.7 μm) and density (1.64 g/cm^3). The names of the graphite materials corresponding to the different electrical resistivities are given on top of the Figure. A decrease in the room temperature electrical resistivity of the graphite cathodes shows an increase in the cathode spot velocity. For pyrolytic graphite, the resistivity in the direction parallel to the atom layers (250 μΩ.cm) is lower by a factor 1000 in comparison to that in the perpendicular direction (0.3 Ω.cm). The parallel resistivity for **PYROID** is used in Figure 4-9 rather than the perpendicular resistivity. This choice was made considering the depth of the cathode spot in the material is typically very small (< 5 μm) and the ratio of cathode thickness to length in the direction towards the electrical connection is very small (typically < 0.02), the electrical connection being located at the top of the sample illustrated in Figure 4-7.

From the electrical resistivity of graphite cathodes versus their temperatures (Figure 4-10), a minimum electrical resistivity point is seen to appear with the increase in cathode temperature. This behavior might contribute to the slow arc motion at the cathode surface and its tendency to locate preferentially where the graphite resistance is the lowest.

In other words, the temperature dependence of the material resistivity might strongly influence the arc residence time on a local site, hence the overall arc velocity.

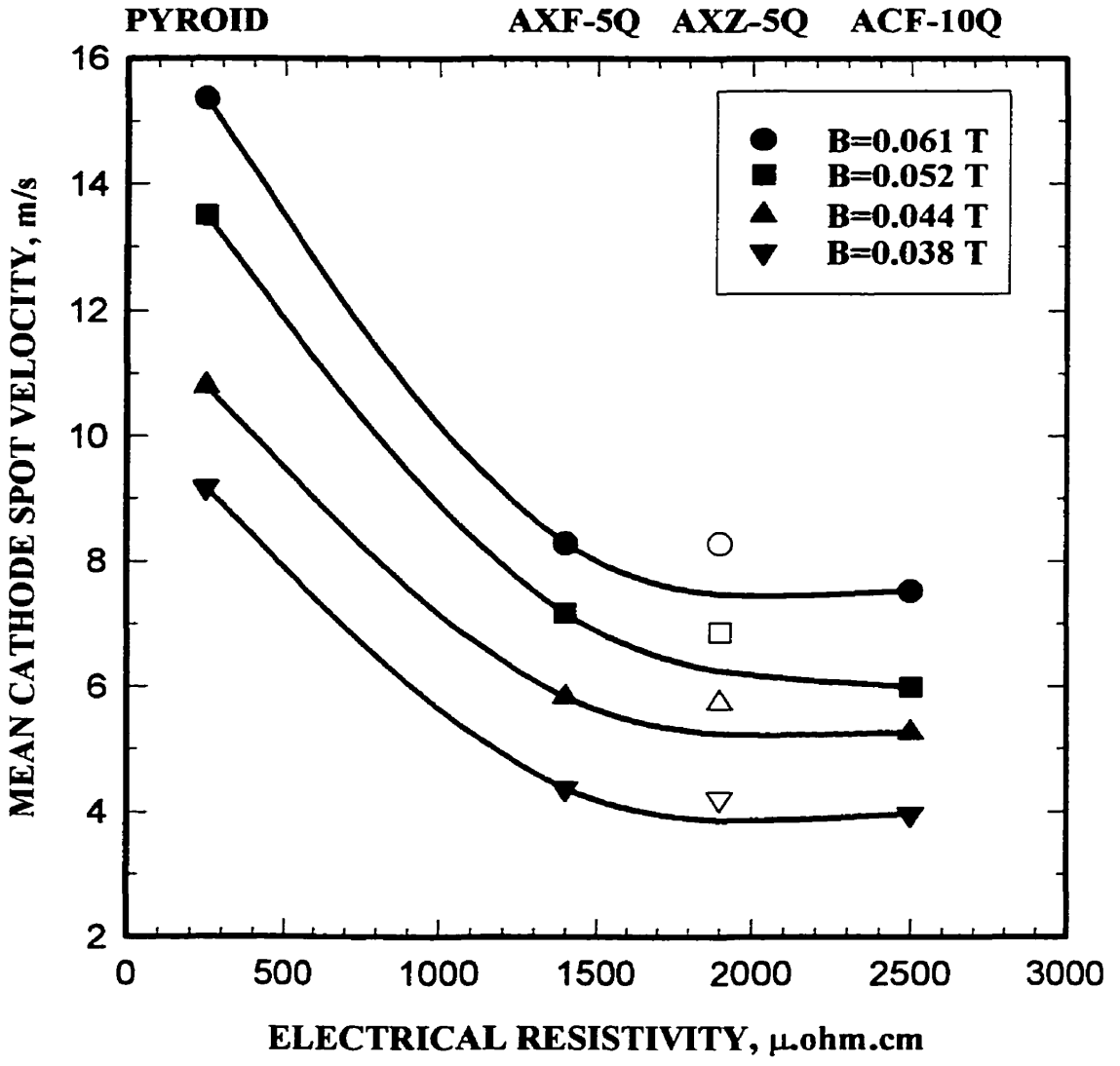

Figure (4-9) : Mean cathode spot velocity as a function of electrical resistivity for three multi-crystalline and one pyrolytic graphite cathodes.

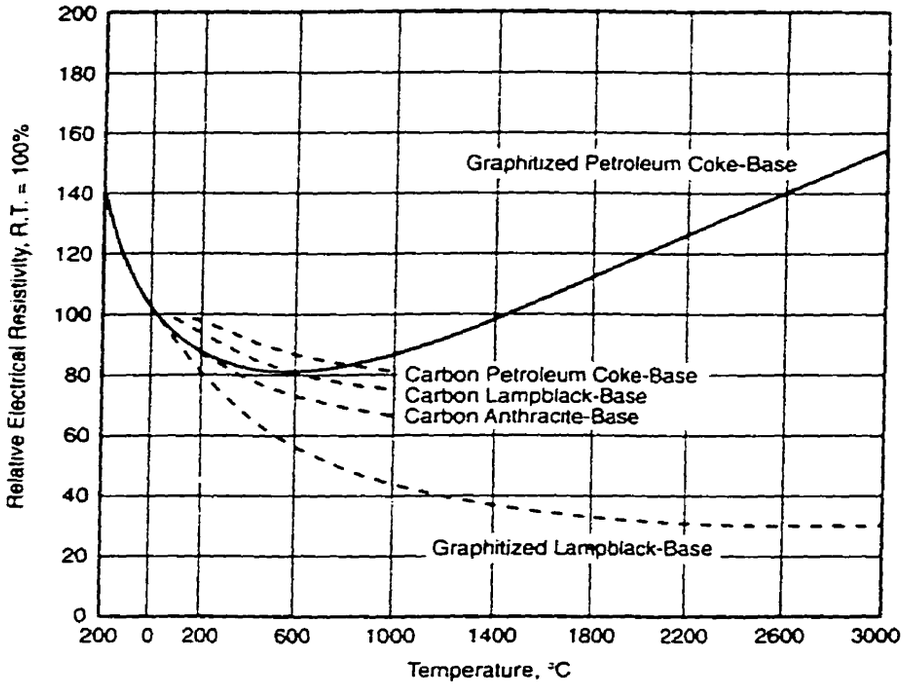

Normal Resistivity at Room Temperature	Ohm-cm
Carbon Anthracite-Base	0.0038
Carbon Petroleum Coke-Base	0.0038
Carbon Lampblack-Base	0.0051
Graphitized Petroleum Coke-Base	0.00091
Graphitized Lampblack-Base	0.0047

Figure (4-10) : Electrical resistivity of graphite cathodes versus temperature (Page 1991).

4-3-3 : EFFECT OF PORE SIZE ON CATHODE SPOT VELOCITY

The effect of cathode pore size on arc movement is investigated using three polycrystalline graphite cathodes (**AXZ-5Q, AXM-5Q** and **PS**) having the same grain size (5 μm) and pyrolytic graphite (**PYROID**) with no porosity. Figure 4-11 shows a decrease in the arc spot velocity with increasing pore size at constant grain size. Although the grain size is the same for the three polycrystalline materials, their density is changing slightly from 1.64 g/cm^3 (**AXZ-5Q**) to 1.74 g/cm^3 (**AXM-5Q**) and 1.33 g/cm^3 (**PS**).

4-3-4 : EFFECT OF GRAIN SIZE ON CATHODE SPOT VELOCITY

The dependence of the cathode spot velocity on the graphite material grain size in the presence of an external magnetic field is investigated for four different graphite cathodes (**PGCS-1**, **TM**, **PS** and **ZXF-5Q**), each having different grain and pore sizes. Figure 4-12 shows increasing arc spot mobility with an increase in the grain size. Materials in this Figure also have a correspondingly small increase in the pore size. They however can be separated in two distinct groups, one with very small pores (white symbols with 0.2 μm pores) and the other with large pores (black symbols with pores diameters between 1.2 and 3 μm). This seems to indicate that the influence of grain size on velocity may be somewhat smaller than porosity effects.

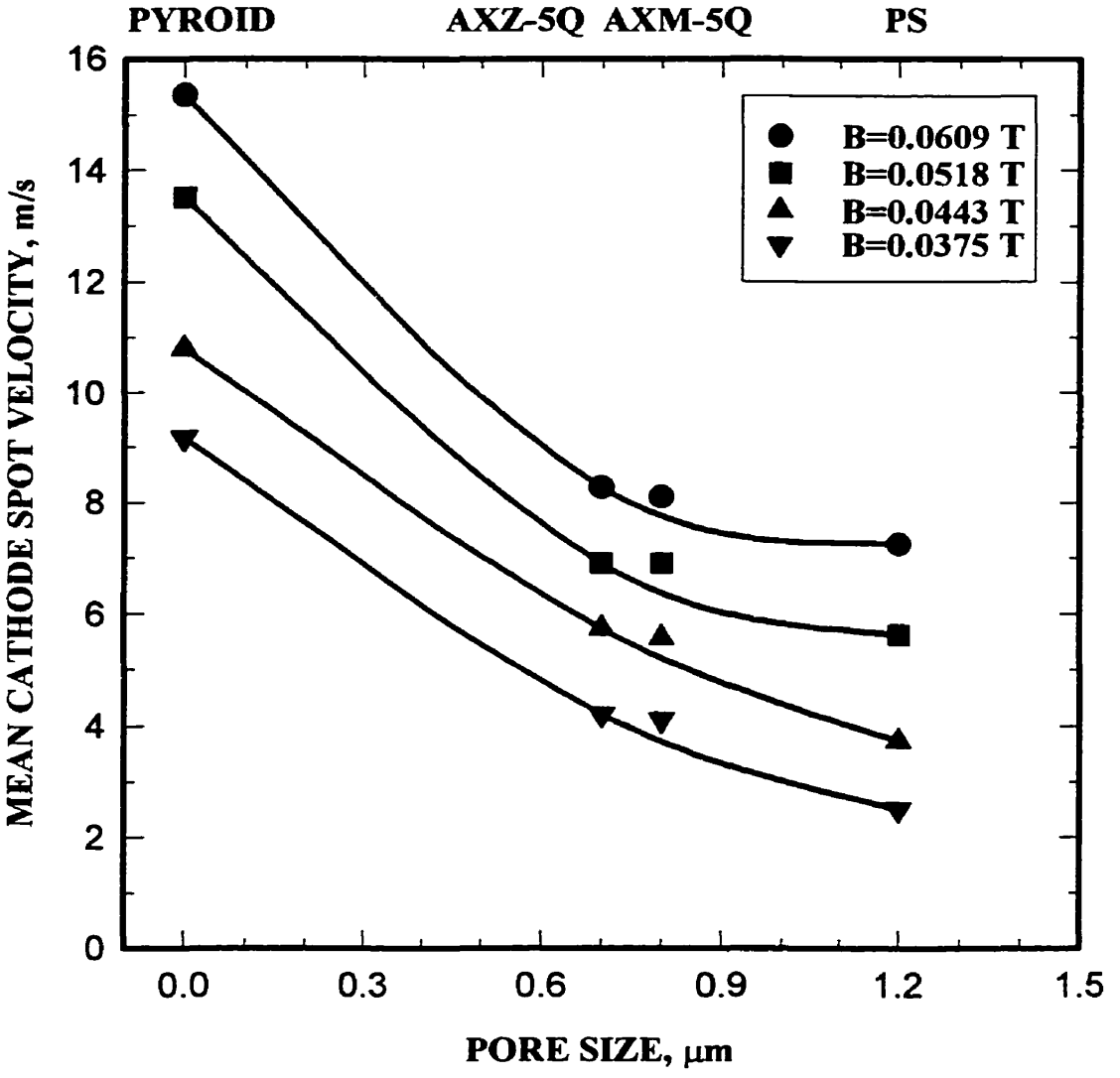

Figure (4-11) : Mean cathode spot velocity as a function of pore size for three different poly-crystalline graphites having the same grain size and one pyrolytic graphite.

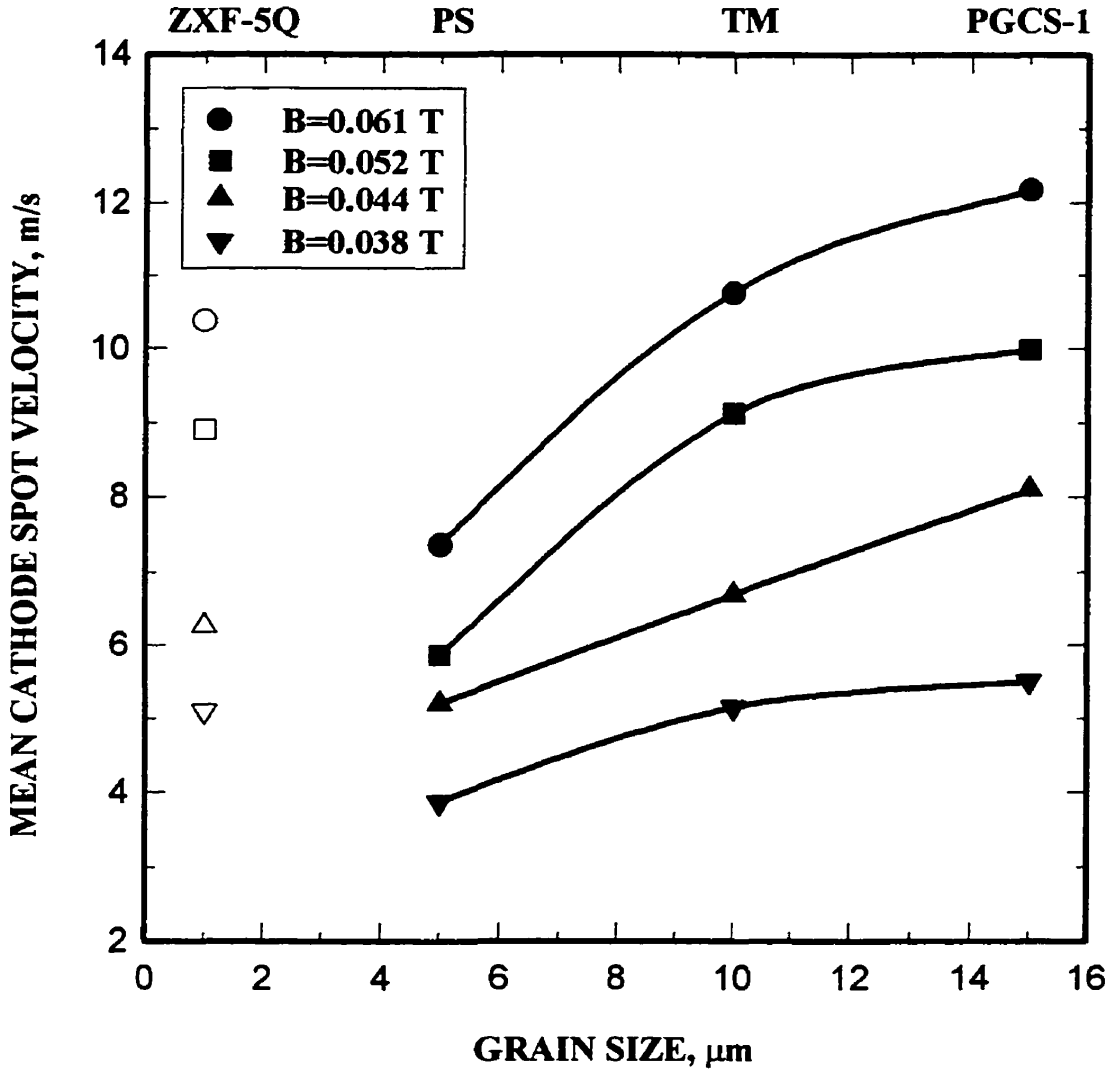

Figure (4-12) : Mean cathode spot velocity as a function of grain size for four different graphite cathodes having different grain and pore sizes.

4-3-5 : EFFECT OF DENSITY ON CATHODE SPOT VELOCITY

The cathode spot velocity can also be plotted as a function of the cathode material density keeping constant the grain and the pore sizes of the materials. Figure 4-13 shows that an increase in the apparent density, hence a decrease in the total porosity at constant grain and pore sizes, leads to an increase in the spot velocity. The unfilled symbols represent **AXZ-5Q** cathodes for which the pore size is lower than that of **AXM-5Q** or **AXF-5Q**. The effect of density on the cathode spot velocity for the polycrystalline graphite cathodes shown in Figure 4-13 is very small, these cathodes were the only ones available having constant pore and grain sizes.

4-3-6 : ARC CURRENT

Figure 4-14 shows the effect of the arc current on the cathode spot movement for two different graphite cathodes (polycrystalline **PGCS-1** and pyrolytic **PYROID**). The increase in the arc current from 60 A to 140 A led to an increase in the cathode spot velocity from 12.5 m/s to 27.4 m/s on the **PYROID** graphite and from 9.8 m/s to 20 m/s on the **PGCS-1** graphite. Figure 4-15 shows examples of four traces left on the cathode after a single arc discharge. One can see a single arc spot trace on **PYROID** at 110 A splitting into three arc spots traces at 160 A. Similarly, the **ZXF-5Q** graphite shows only one to two arc spots at an even higher current of 200 A. Hence, Figure 4-15 indicates that for a constant arc current the number of spots observed for different graphite cathode materials is not necessarily constant. The graphite materials properties therefore also influence the maximum current per spot and spot splitting. Care should thus be taken

when using the available literature data of the maximum current per spot established for carbon of unknown grade at 200 A by Kimblin (1973). This value in fact depends on the properties of the carbon used.

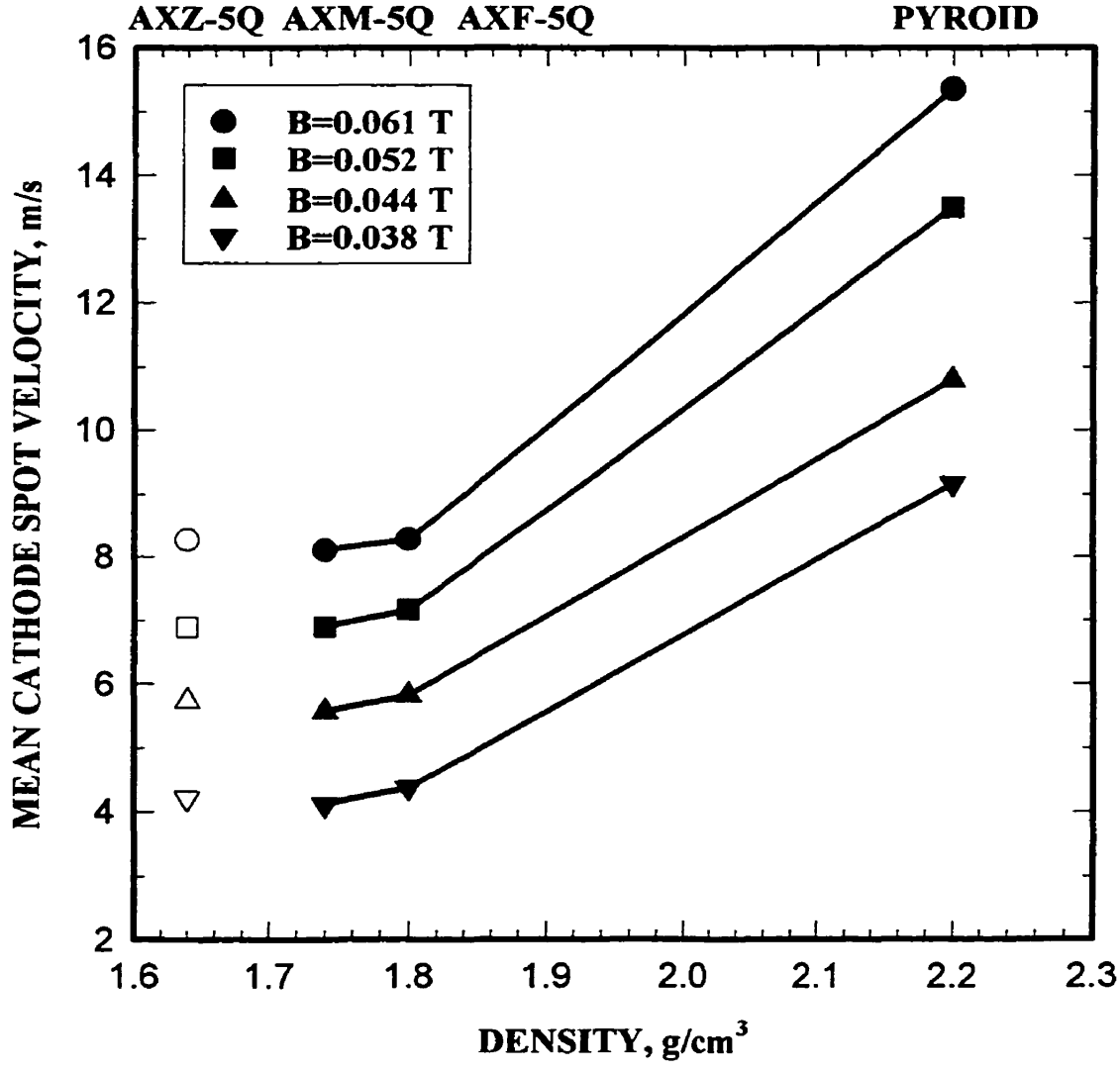

Figure (4-13) : Mean cathode spot velocity as a function of density for three different poly-crystalline graphite cathodes and one pyrolytic cathode.

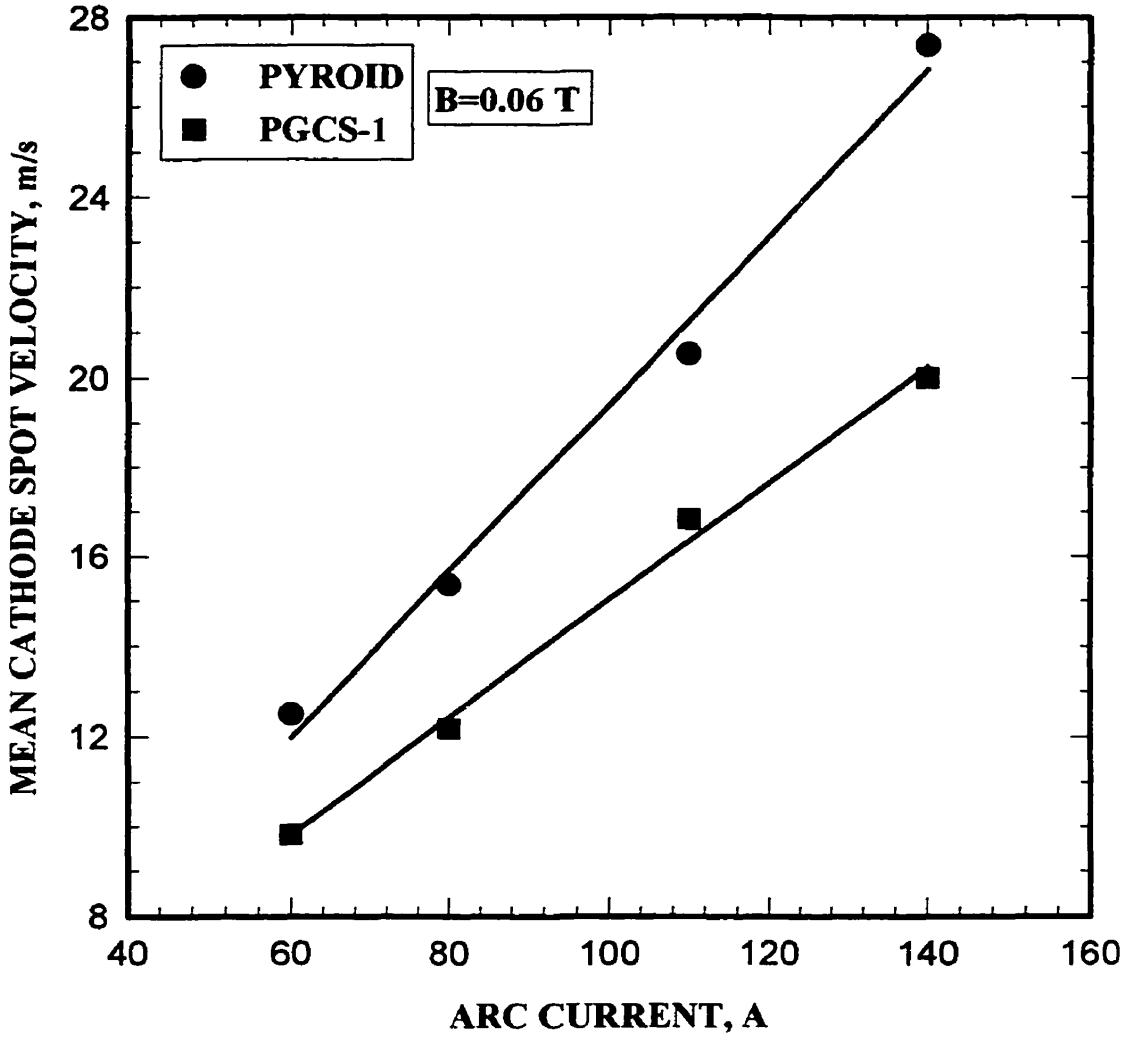

Figure (4-14) : Mean cathode spot velocity as a function of arc current for two different graphite cathodes at constant magnetic field intensity.

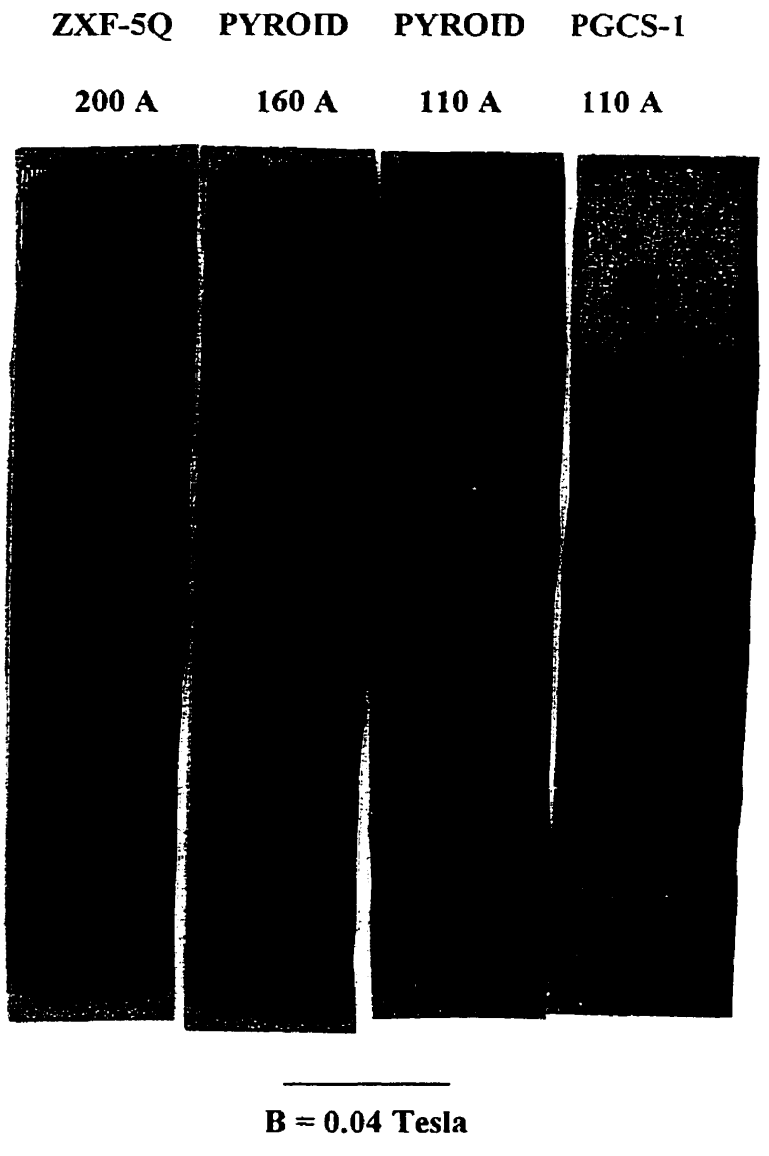

Figure (4-15) : Photographs of the arc traces on four cathodes showing the effect of the arc current on the number of spots at constant magnetic field and pressure (10^{-4} Torr). Arc duration was constant at 1.9 ms.

4-3-7 : EFFECT OF CATHODE SPOT VELOCITY ON EROSION RATE

Figure (4-16a) shows that for all the graphite cathodes used, increasing the magnetic field intensity leads to an increase in the arc spot velocity, and a decrease in the net cathode erosion rate. This was to be expected, an increase in the arc spot velocity results in a decrease in the residence time of the spot on a given site of the cathode, hence a decrease of the localized heating of the surface. Such a decrease in the local heat load in the cathode spot zone was shown to reduce the amount and size of the particles flux emitted by the spot (Kandah & Meunier 1995). Cathode spot velocity is considered here as one main controlling parameter defining the residence time of the arc spot on a given site and the net heat load on that site. Figure (4-16b) shows the same data as in Figure (4-16a) viewed using the spot velocity as the independent controlling parameter. Similar trends of erosion rate with velocity are observed for the four materials. One can see again in Figure 4-16 that various graphite cathodes lead to different erosion rate values whatever the spot velocity. Another way of looking at these results is to consider the evolution in erosion rate and spot velocity of the various materials taken at a constant magnetic field value. For clarity, Figure 4-17 simply reproduces the values of Figure (4-16a) for a constant magnetic field intensity of 0.04 T. This reveals the very surprising and interesting result that cathodes having higher spot velocities due to their surface characteristics also give rise to the highest erosion rate. The materials in Figures 4-16 and 4-17 follow the order of the list in Table 4-1. Materials showing the highest erosion rate and spot velocity have the lowest electrical resistivity and pore sizes, and also the largest density. The behavior indicated by Figure 4-17 may lead to very interesting and important

consequences in view of deposition applications. An increase of the arc velocity through a judicious choice of the graphite material surface characteristics should result in a trend similar to that of reducing the local heat load : a net reduction of the macro-particles emission. Figure 4-17, however, indicates that the total erosion rate is in fact higher for cathodes showing higher arc spot velocity. This indicates that the other erosion rate component (i.e., ions) may be expected to increase.

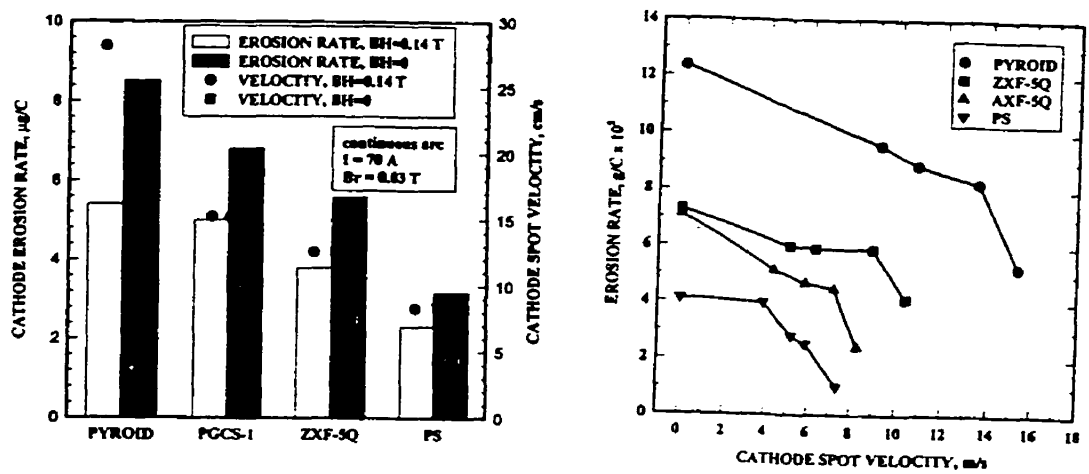

(a) (b)

Figure (4-16) : a) Erosion rate (columns, left axis) and spot velocity (dots, right axis) of four graphite materials under variable magnetic field intensity.

b) Data of Figure 4-16a expressed using the cathode spot velocity as a control parameter for erosion.

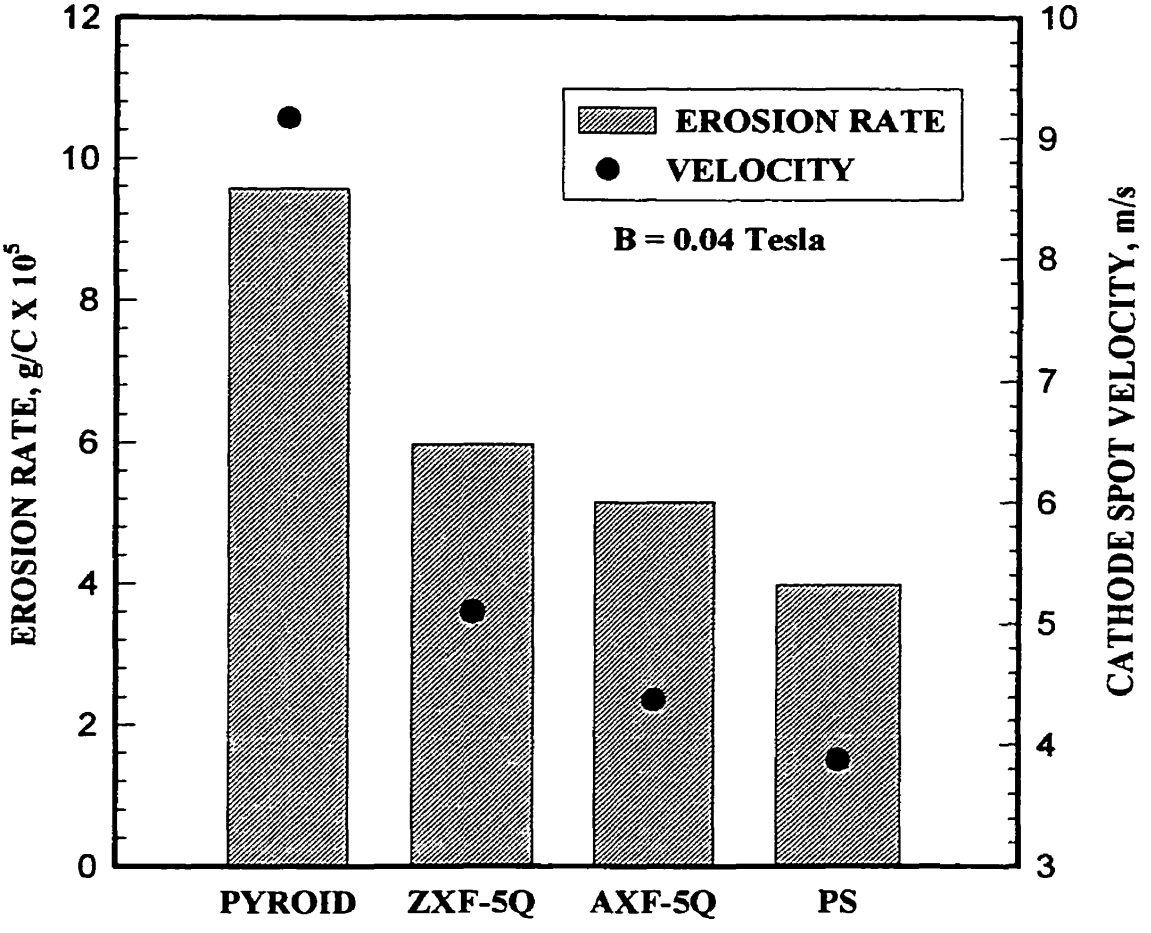

Figure (4-17) : Erosion rate and spot velocity for four types of graphite at a constant magnetic field intensity of 0.04 Tesla.

4-3-8 : CATHODE SPOT SIZE AND RIM WIDTH :

Figure (4-18) shows the morphology of some cathode spots (craters) over a graphite cathode surface after arcing with 75 A. The cathode spots have circular shapes with few micrometers in diameters surrounded by white rings, thereafter called "rims". Figure (4-19a) is a close-up of Figure (4-18) showing the crater and the rim in more details. It is not clear from the SEM study if the rims observed here are formed due to charging effects initiated by the high energy electron beam inside the SEM, or actually have a surface topography similar to the rims produced on metallic electrodes when a large quantity of liquid metal is solidified after spot extinction. In the first case however, the local properties of the graphite material in this region is the result of a very short but intense heat load as well as a high pressure during the spot lifetime. One can thus believe that properties such as electrical resistivity, local porosity and crystallinity in the rim volume were affected by the characteristics of the spot, such as residence time and local heat load. The high energy electron beam of the SEM penetrate relatively deep into the surface compared for example to the low energy beam in a field effect gun SEM (FEGSEM). One may thus speculate that the rims observed may characterize morphological changes within the material at the crater edges. As will be shown, the width of these rims vary in accordance with the local heat load on the various materials. It is known that graphite sublimes at high temperatures and low pressures. According to Ivanov et al (1984) and Jüttner (1985), the plasma pressure above the cathode spot evaluated for metallic electrodes should be of the order of 10^6 Pa with a plasma density of 10^{25} m^{-3}. From the phase diagram for carbon given in Figure (2-3), a graphite liquid phase

may be achieved at this pressure if the spot temperature is over 4600 °C (Kandah & Meunier 1995). A few analysis of the surface topography within the spot were possible using the low energy upper detector of a field emission-SEM (FEGSEM) model Hitachi S-5000 (Courtesy of Hitachi Corporation, Toronto). The geometry of the detection system in this microscope permitted imaging and high magnification study of the topography inside the cathode spot, the imaging being made at very low beam energy. Figure (4-19b) shows the surface topography is actually very different within the spot as compared to a non-arced surface. Figure (4-20a) shows a high magnification image taken inside the spot. One can clearly see a surface topography indicating that a liquid state of the graphite was attained during arcing (Figure 4-20b).

For refractory metals the rim formations are generally less pronounced and relatively smaller in size than that shown on lower melting temperature metallic electrodes (Daalder 1978). The majority of the particles emitted from the graphite cathode spots in this work show almost regular spherical shapes, indicating that the origin of these particles is the melted volume in the cathode spots. The size of the cathode spot (D) and the rim width $\frac{\Delta r1+\Delta r2}{2}$ are measured from SEM photographs for isolated spots resulting from single arcing for short arc times. The values of $\Delta r \pm 0.01$ and $D \pm 1.0$ correspond to an average over more than 10 measurements from each sample.

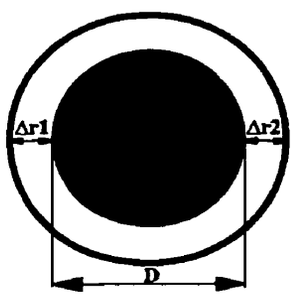

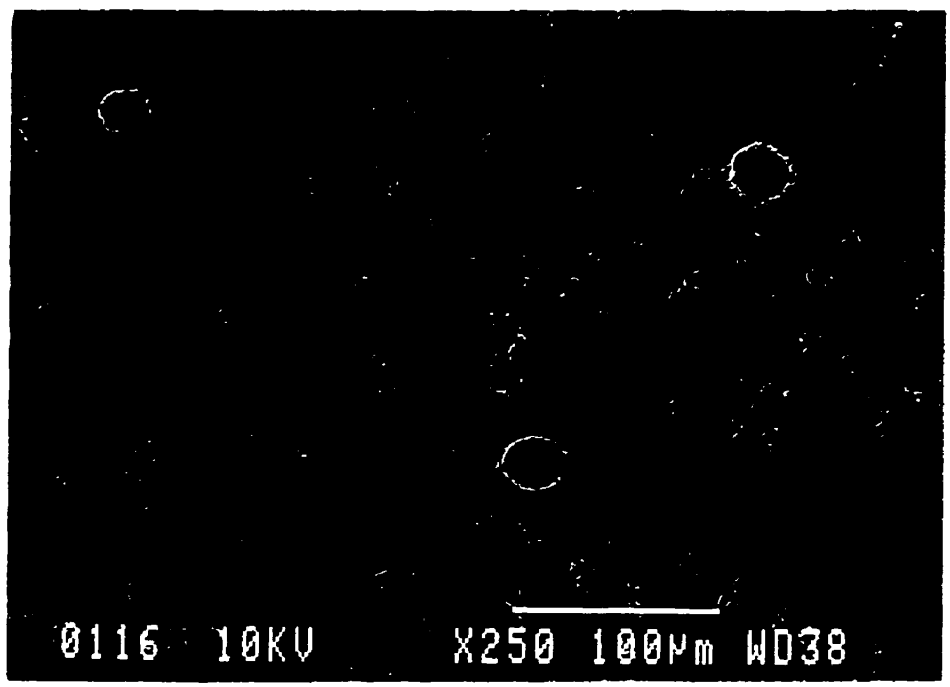

Figure (4-18) : SEM photograph showing the morphology of some cathode spots.

A)

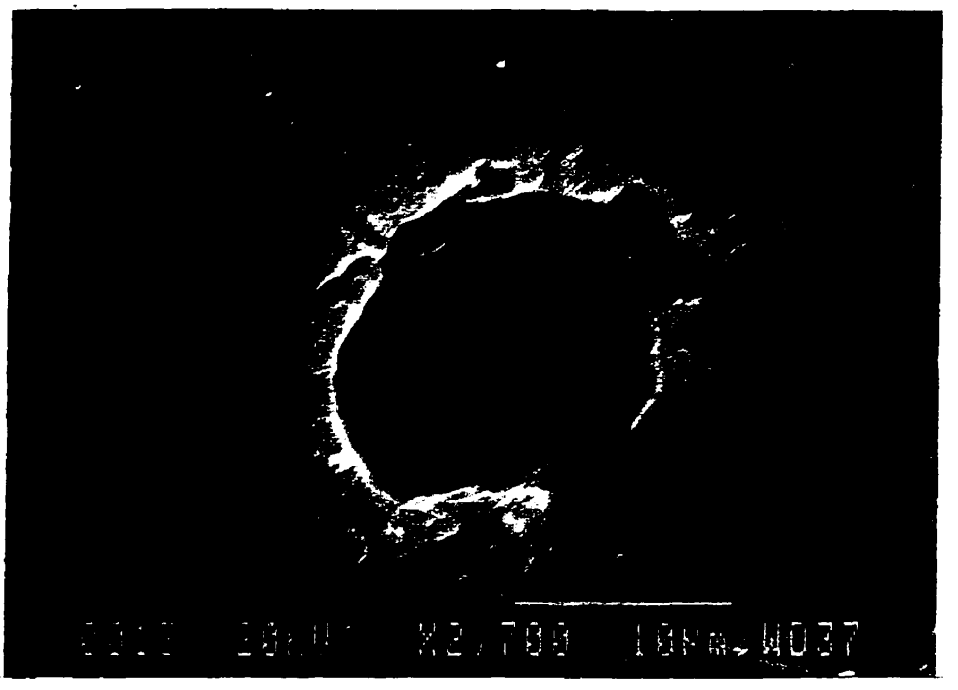

B)

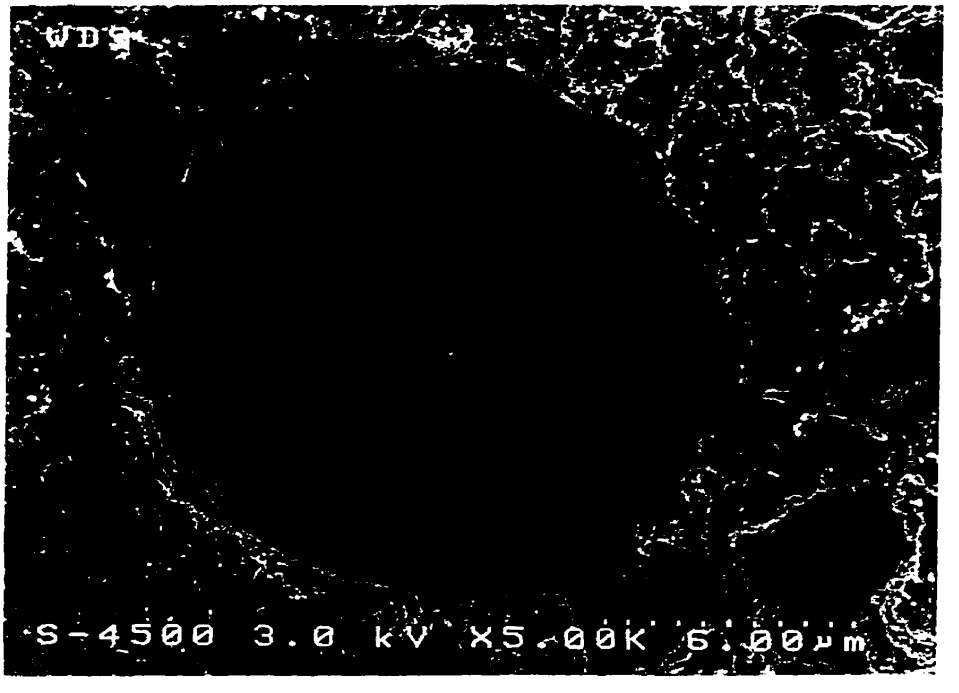

Figure (4-19) : a) Close up of Figure (4-18); b) FEGSEM photograph of a typical cathode spot crater for I = 80 A; B = 0.04 Tesla;

A)

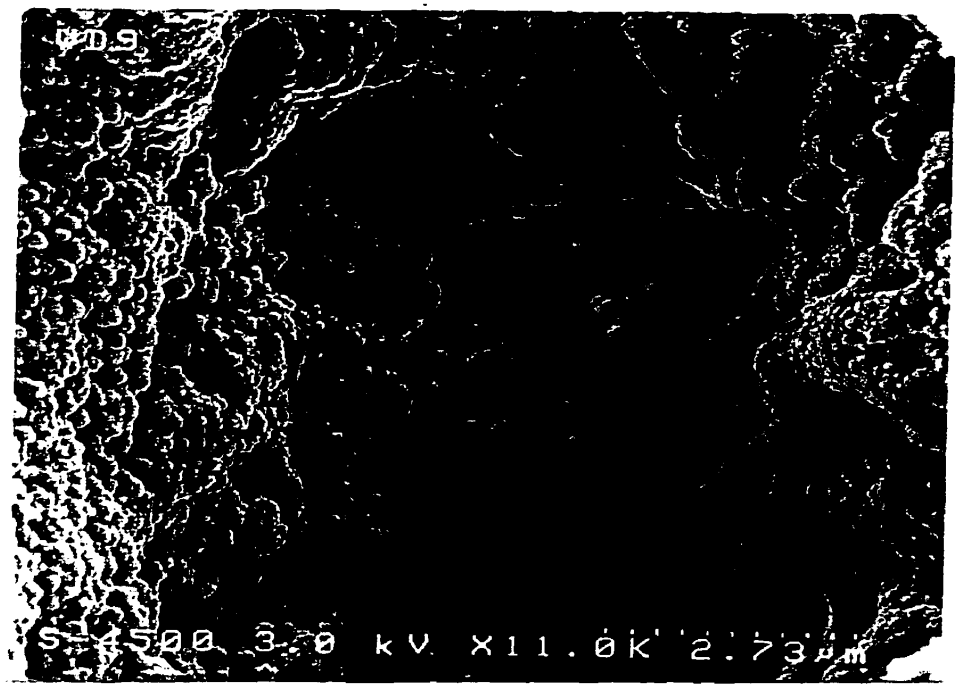

B)

Figure (4-20) : a) Close up of Figure (4-19b) using low voltage FEGSEM.

b) At higher magnification of Figure (4-19b), a region within the spot showing a melted-like structure.

Figures 4-21 and 4-22 show the size of the cathode spot and the width of the spot rim, respectively, for different materials at a magnetic field of 0.0375 T. Again, the order of the materials listed follow that of Table 4-1. Also given as a reference parameter are the cathode spot velocities for each material at this field value. These figures indicate opposite trends in the evolution of spot velocity and the size parameters for the various materials : higher velocity correlates with small spot size and small rim width. The increase in the spot velocity can be associated with the decrease of the cathode pore size for all graphite types except **PGCS-1**. In spite of the fact that **PGCS-1** has high pore size, it has a very high density, high grain size and low electrical resistivity comparing to the other graphite types which allows it to show high velocity.

4-3-9 : CATHODE MORPHOLOGY

This work shows that under similar operating conditions, different graphite material properties are expected to show various spot movement behavior. Graphite electrodes are characterized by a very different arc spot motion even at moderate magnetic field values when compared to metallic electrodes. This is shown in the photograph of Figure 4-23 giving the erosion traces over three graphite materials at zero magnetic field intensity. These traces are the result of only one arc discharge on each graphite type for constant arcing time and electric charge transferred through the cathode. Again, this stresses the importance of the graphite cathode material properties on the cathode spot characteristics for this material. One can see however that materials with low pore size

tend to generate a more important random movement of the spots, in a way similar to metallic electrodes.

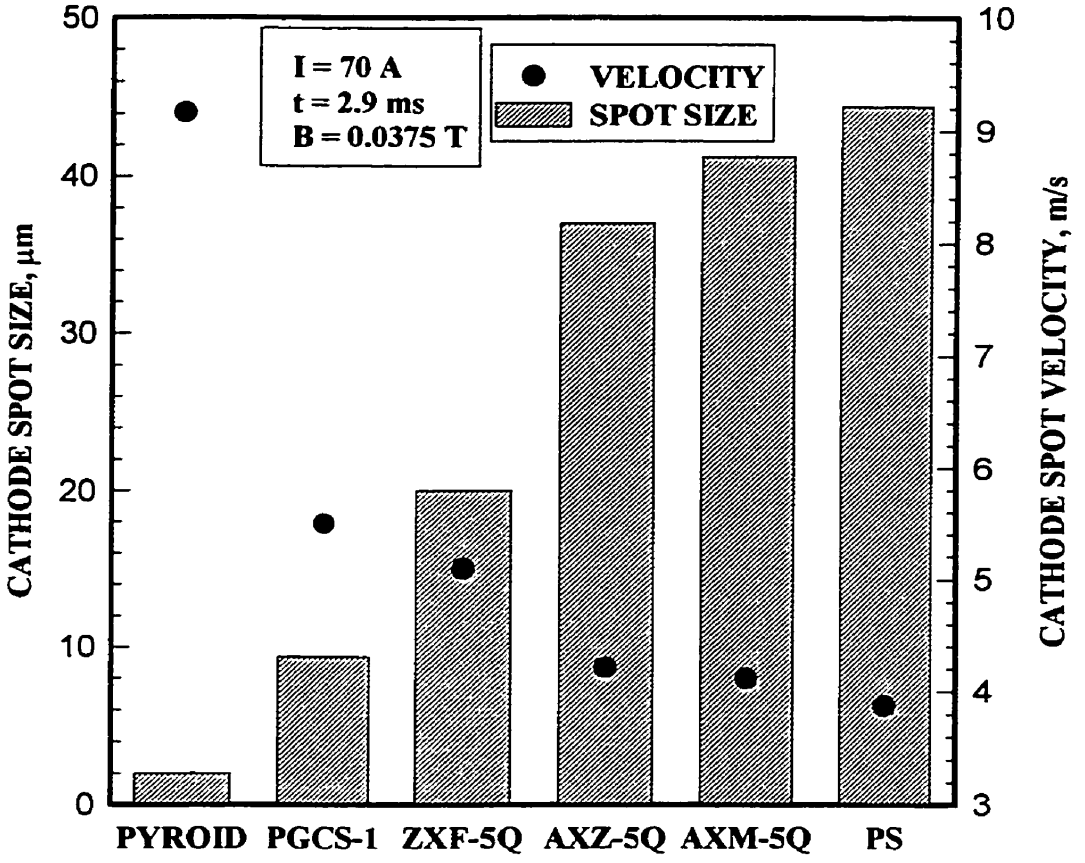

Figure (4-21) : Mean size of the cathode spots (columns, left axis), and spot velocity (dots, right axis) for six graphite materials for a constant magnetic field of 0.0375 T and arc current of 70 A. The left to right order of the materials follow that of table 4-1.

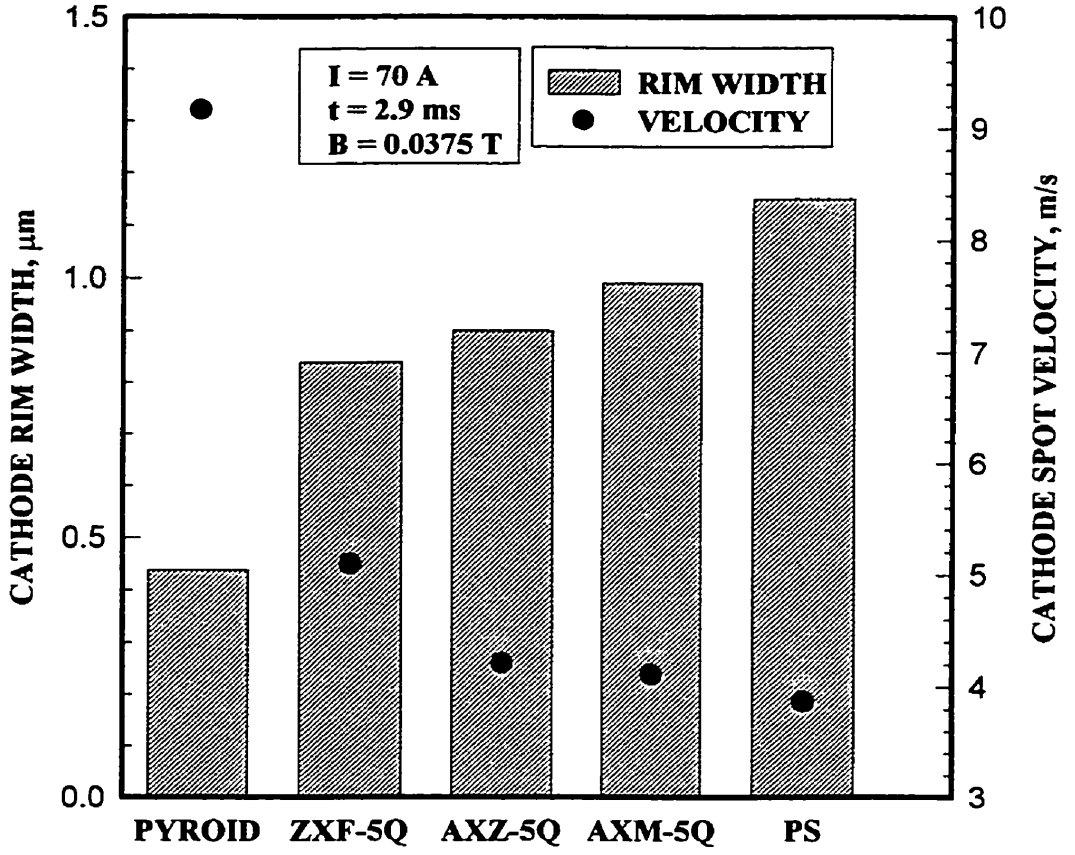

Figure (4-22) : Mean width of the cathode spot rims (columns, left axis), and spot velocity (dots, right axis) for five graphite materials for a constant magnetic field of 0.0375 T and arc current of 70 A. The left to right order of the materials follow that of table 4-1.

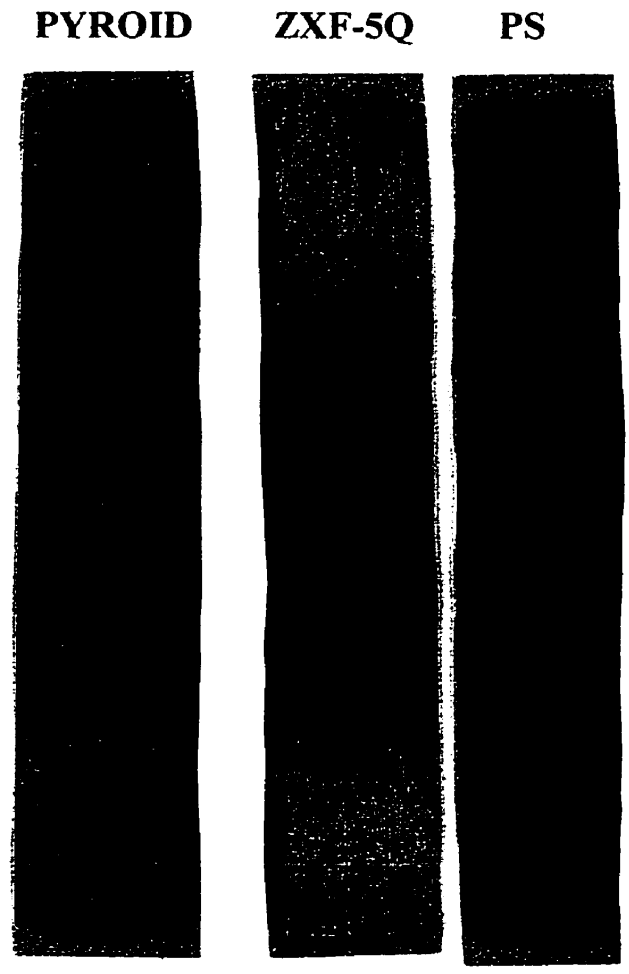

Figure (4-23) : Photographs showing the behavior of the arc spot over three different graphite types at zero magnetic field intensity.

4-4 : DISCUSSION

The erosion rate for carbon cathode measured by Kimblin (1973) is 1.7×10^{-5} gram/coulomb. This value however is shown here to depend heavily on the cathode material characteristics. In this work attention is focused on the effect of different graphite material properties on the spot behavior and the erosion rate. One can see from Figure 4-8 that arc spot velocity depends strongly on the surface properties of the different graphite cathodes. The order of the various graphite for decreasing spot velocity follows that of Table 4-1 for their structural and electrical properties. In the absence of any external disturbance on any continuous homogeneous metallic surface, an arc spot typically moves randomly over the surface of the cathode (Fang 1982 and Daalder 1983). If the arc encounters a discontinuity, such as a crack or a large pore size, one might expect a relative low arc spot velocity due to the repetitive formation of craters in a limited area. As a consequence the local energy density on the surface would be increased and a deep crater formed, reducing the motion of the spot and increasing the erosion rate. These surface effects become predominant on graphite.

Roman (1963) for example observed that an obstruction on the cathode surface stopped the arc when forced to move in the retrograde direction and delayed it when in Amperian direction. Excepted for the pyrolytic (**PYROID**) graphite used in this study, graphite materials usually show a porous structure. Typical graphite showing large pore size such as those described in the bottom half of Table 4-1 will generally yield very limited spot motion in the random, non steered arcing mode. The results of Figure 4-11 indicate porosity is a factor favoring the reduction of steered arc velocity on graphite

electrodes. Figure 4-12 indicates the same trend, larger grain sizes resulting in surface structures that are comparatively more homogeneous with less grain boundary lines per unit surface area. In fact, the pyrolytic graphite with no porosity and low electrical resistivity is distinctive in yielding arc spot velocities that are systematically higher. This material shows similarities both in velocity and arc trace structure as compared to metallic electrodes.

Two independent parameters are used here to increase the graphite arc spot velocity, the external magnetic field and the surface characteristics of the cathode material. Each is shown to have different and opposite effect on the erosion rate. This work indicates that an increase in the arc spot velocity resulting from a change in the graphite cathode surface properties leads to an increase in the total erosion rate. A decrease of the heat load input on a given site of the cathode was shown previously (Kandah & Meunier 1995) to result in a decrease of the emitted particles. Combining these two effects could eventually lead to an increase in the fraction of carbon ions emitted. Larger deposition rates in arc ion-plating systems together with lower macro-particles content per unit film thickness can thus be expected. An increase of the arc spot velocity induced by a change in the applied external magnetic field is shown here to reduce the total erosion rate. Lowering the heat load on the cathode spot should however also correspond to a decrease in the emitted particles. Measurement of the number of emitted particles and ion flux for different types of graphite cathodes as a function of arc spot velocity constitutes one objective of the third section of this work (continuous arc mode).

The nature of the thermal dependence of electrical resistivity of manufactured

graphites varies widely. In general, at low and moderate temperatures, increasing temperature decreases the resistivity, the opposite being generally true at higher temperatures (Page 1991). This typically results in a minimum value of the electrical resistivity $R_{min}(T)$ reached at some characteristic temperature of the given graphite material. One may speculate the arc spot will follow preferentially zones of lowest resistivity. In such a case, cathodes having their minimum electrical resistivity at low temperatures are expected to show higher cathode spot velocities. Larger residence times of the cathode spot on a given zone of this material would tend to increase the local temperature and resistivity above R_{min} and favor spot motion to another site. Although the R(T) data for the various graphites was not available nor measured in this work. Figure 4-9 indicates higher cathode spot velocities are observed for graphites having low electrical resistivity at room temperature. Figure 4-8 also indicates that the material having by far the highest resistivity (**PC** graphite) yields the lowest arc spot mobility and (**PYROID** graphite) having the lowest resistivity yields the highest arc spot mobility. These results correlate with the expected trend indicated above. More in depth study of the resistivity-temperature curves of the various materials and the local temperature in the arc spot region is however needed to fully verify this hypothesis.

The density of polycrystalline graphites seldom exceeds 80% of the theoretical value of 2.26 g/cm^3 due to the voids or pores. Single crystal and pyrolytic graphites, because of their highly ordered structures, have densities closely approaching the theoretical density. Keeping the other factors constant, the increase in the apparent density is reflected in the improved mechanical strength, surface homogeneity and thermal

conductivity in addition to the decrease in the electrical resistivity (Page 1991). Figure 4-13 indicates an increase in the graphite density favors arc mobility, in agreement with the trend observed with a decrease of porosity.

As the arc current delivered to the cathode is increased, a point is reached where an arc burning on a single cathode spot will split into two spots. The number of cathode spots is dependent on the arc current and the cathode material (Djakov & Holmes 1971). Different graphite cathode materials have different surface characteristics, and this study shows that each graphite cathode has its own arc current/spot limit. Three spots for example were observed on **PYROID** at 160 A and only one spot at 110 A, while **ZXF-5Q** graphite only shows one spot at 200 A. This indicates every graphite cathode material should be treated as a very specific type of electrode.

The cathode spot velocity was found to decrease with the increase in the cathode pore size. Such a decrease results in larger residence times of the cathode spot at any given site. As a result the heating flux through the cathode spot increased and more melted volume is expected due to the highly repetitive arcing. Therefore, the cathode spot size and rim width are both found to increase, as well as the number and mean size of the macro-particles emitted by the spot (Kandah & Meunier 1995). These effects cause arc instability leading to extinguishing of the arc after short arc duration times (few seconds), requiring re-ignition. Re-igniting the arc many times increases the emission of chunks (irregular graphite particles) from the cathode spots. Melting of the graphite cathode in the spot zone at high temperature (~ 4600 °C) and high pressure (10^6 Pa) has been indicated by Kandah & Meunier (1995) to be responsible for the very regular spherical shape of the

emitted macro-particles. It is shown in Figure 4-20b that melted zones of graphite are actually present in the cathode spot volume during arcing. The origin of the spherical macro-particles is hence considered to be the melted zones within the spot, the number and size of emitted particles is thus expected to increase with conditions increasing the volume of these melted zones. The macro-particles formation has been attributed to high heat flux and high pressures over the cathode spot. Several researchers (Boxman and Goldsmith 1981, Shalev et al 1986) have stated that considerable evaporation may occur from the macro-particles in flight, producing some neutral and slow singly ionized ions in addition to the emitted energetic ion flux from the spot. A better control of the macro-particle emission should hence also result in a higher percentage of the flux being in the ionized form and possibly in a shift to higher energy.

4-5 : CONCLUSIONS

The use of graphite cathodes in a continuous arc ion-plating deposition system is more problematical when compared to metallic electrodes. Eleven graphite materials having various physical and electrical properties reveal in this study different cathode spot behavior and erosion rate values. This study shows the strong variability of graphite materials with respect to arc mobility. The amount of particles emitted by graphite cathodes is directly related to the heat load input to a given site of the cathode (Kandah & Meunier 1995). Inducing high arc spot velocities on graphite in order to decrease this heat flux requires much larger magnetic field strength intensities compared to metallic cathodes, and proper selection of the graphite material characteristics. Erosion rates for

these graphite materials are ranging from $1.02x10^{-5}$ g/C to $1.24x10^{-4}$ g/C and strongly depend on the type of graphite and the arc spot velocity. Cathodes showing less surface discontinuities, e.g. higher density and smaller pore sizes, show higher spot velocities and higher erosion rates at constant magnetic field intensity. This should possibly lead also to lower particle emission from the cathode. In addition, these cathodes are expected to show a larger fraction of the total erosion rate transported by the ion flux. The trend toward higher spot velocities and erosion rates also correlates with a lower electrical resistivity of the graphite material at room temperature. For any given graphite structure however, an increase in spot velocity induced by higher magnetic field intensity results in a reduction of the erosion rate.

This work shows magnetic field intensities of 0.06 T are needed to induce arc spot velocities of 15 m/s on pyrolytic graphite at I = 80 A, polycrystalline graphite yielding lower velocities at the same field values.

Cathodes having lower pore size, total porosity and room temperature electrical resistivity were shown to yield higher cathode spot velocities. An increase in the grain size and density of the graphite material was shown to increase the cathode spot velocity. An increase in the arc current also increases the cathode spot velocity but may have the adverse consequence of increasing the number of emitted particles through a larger heat load in the cathode spot region. Finally, this study also shows that different graphite cathode material properties yield different arc current per spot limits. Cathode spot size and rim width are both found to be increasing when cathodes showing lower spot velocities are used.

PART THREE

CONTINUOUS ARC MODE

CHAPTER 5 : DIAMOND-LIKE FILMS

5-1 : INTRODUCTION

The Arc Ion Plating process (AIP) is considered as one of the most advanced process among the ion and plasma assisted vacuum coating technologies. AIP offers the ability to provide highly ionized coating atoms of the correct energy at the coating interface which allows the deposition at low substrate temperatures.

AIP process can be carried out in two modes, i.e., pulse and continuous modes. While the pulse mode presents certain advantages such as the ability to limit thermal loading on cathodes and better control to the film thickness, the continuous vacuum arc coating mode is better in coating large size parts at higher deposition rates in an industrial environment.

From the previous study (pulsed arc mode), the magnetic field intensity needed to move the arc spot on each graphite type with a certain velocity is determined. Based on that study the continuous arc ion plating system is designed.

The filtering technique is the most popular known technique (section 1-2-1) to prevent the particles from reaching the substrate, in which the charged particles are separated from the neutrals and macro-particles by a magnetic field. The approach used in this work is to control the macro-particles emission at the cathode source using the rotation of the arc spot over the cathode surface by applying a radial magnetic field parallel to the erosion surface. The arc plasma discharge is also confined and the plasma density increased at the cathode surface using a Helmholtz field configuration.

5-2 : EXPERIMENTAL SETUP

The experimental setup used in this work is illustrated in Figure 5-1, showing the main parts of the AIP system such as cathode, anode, substrate, triggering system and power supply. The details of the arc zone section are shown in Figure 5-2. The cathode is made of a graphite disc (6.35 cm in diameter and 3.175 mm thick) which is held by a water cooled brass tube. Different graphite types are used as shown in Table 4-1. Inside the brass tube and just behind the cathode, twelve (12) Samarium/Cobalt (SmCo 32) permanent magnets (1.27 cm diameter x 0.635 cm length disc each) are placed within the water cooled cavity. The permanent magnets are fixed in a certain way to provide radial magnetic field component parallel to the erosion surface of the cathode. This magnetic field component allows the arc to rotate in retrograde motion over the cathode surface uniformly. The vacuum chamber consists of a hexagonal aluminum part (25.4 cm in diameter and 10.16 cm in width) attached to two stainless steel tubes (30 cm in length, 7.62 cm inner diameter and 10.16 cm outer diameter each). The hexagonal part is isolated electrically from the cathode by a Teflon ring. Both anode and vacuum chamber are grounded. The arc is ignited with a grounded mechanical trigger as a result of brief contact with the cathode. The shaft of the trigger was made of stainless steel with a tungsten tip. A vacuum pressure of $\sim 10^{-4}$ Torr is generated inside the vacuum chamber using mechanical and oil diffusion pumps. The arc current is supplied by four Miller welding power supplies connected in series to boost the open-circuit voltage to approximately 320 V with a power rating of 80 kW. The graphite cathode is surrounded by a boron nitride passive border (grade **AX05** produced by carborundum) to prevent the

arc from leaving the cathode surface. Two coils were attached around the electrodes to constrain the arc generated plasma as shown in Figure 5-3, and increase the plasma density in front of the cathode spot. Helmholtz coils are designed to provide a constant magnetic field between the coils when the distance between the two coils equals their mean radius. The physical background and advantages of this configuration will be discussed later. A 1.5 Ω resistor was connected in series with the cathode to limit the current, stabilize the electrical circuit, and to protect the power supply in case of unstable arcs. The arc current is measured by monitoring the voltage developed across a precision shunt of 0.005 Ω, while the anode-cathode voltage drop is measured directly (see Figure 5-4). Vacuum arcs typically generate large voltage noise associated to the ignition/extinction of arc spots. Hence, the electrical circuit incorporates chokes, capacitors and current limiter devices to protect both the power supply electronics and the current/voltage measurement devices. The arc current is kept constant at 70 A in all the continuous mode experiments.

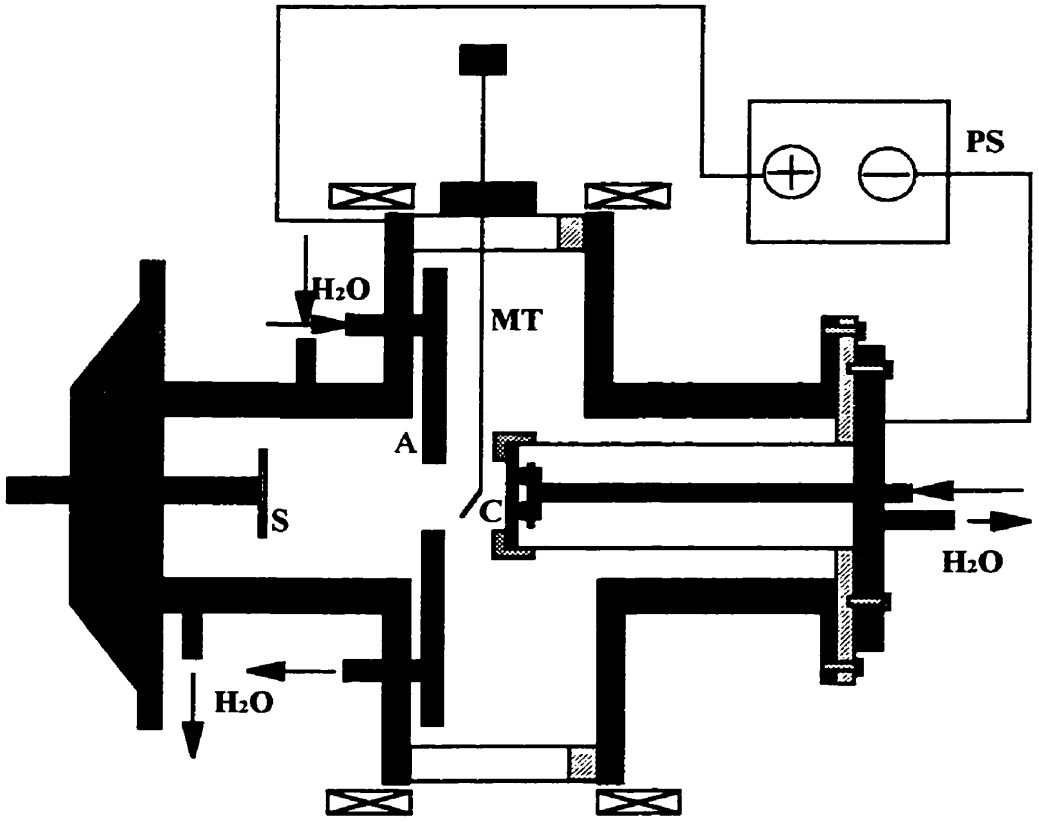

Figure (5-1) : Experimental setup for the continuous arc mode study (not to scale); C = cathode; A = anode; MT = mechanical trigger; PS = power supply and S = substrate.

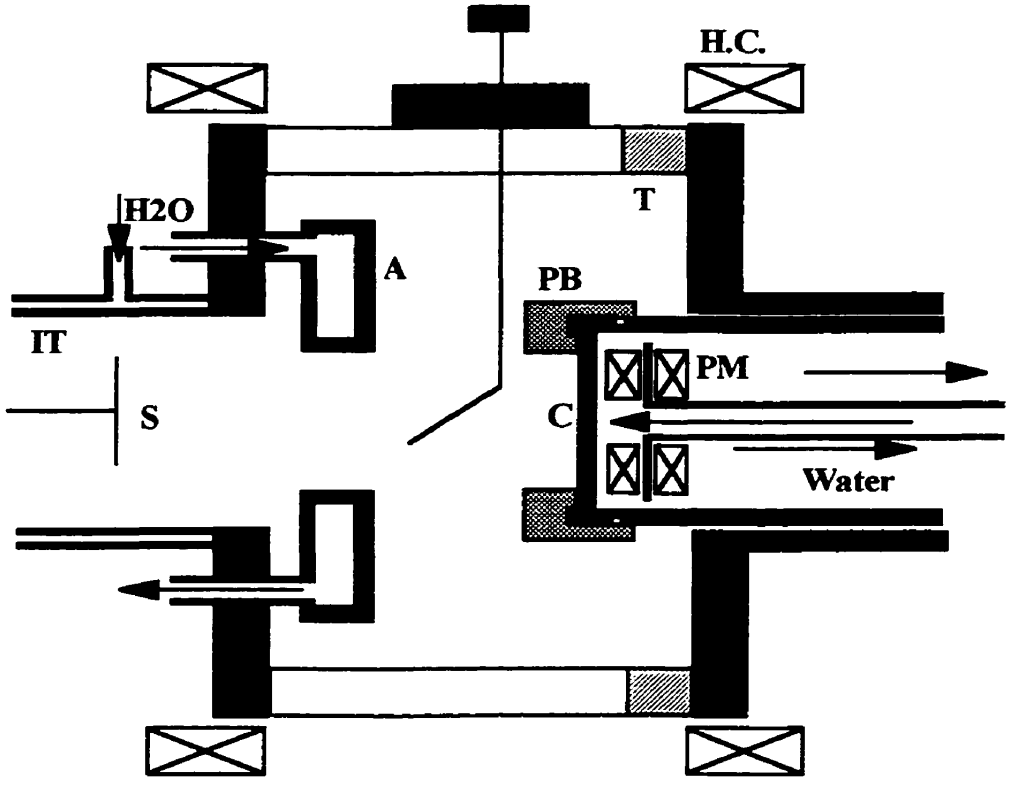

Figure (5-2) : Arc zone section in more details; IT = inner tube; PB = passive border; T = Teflon; H.C. = Helmholtz coils and PM = permanent magnets.

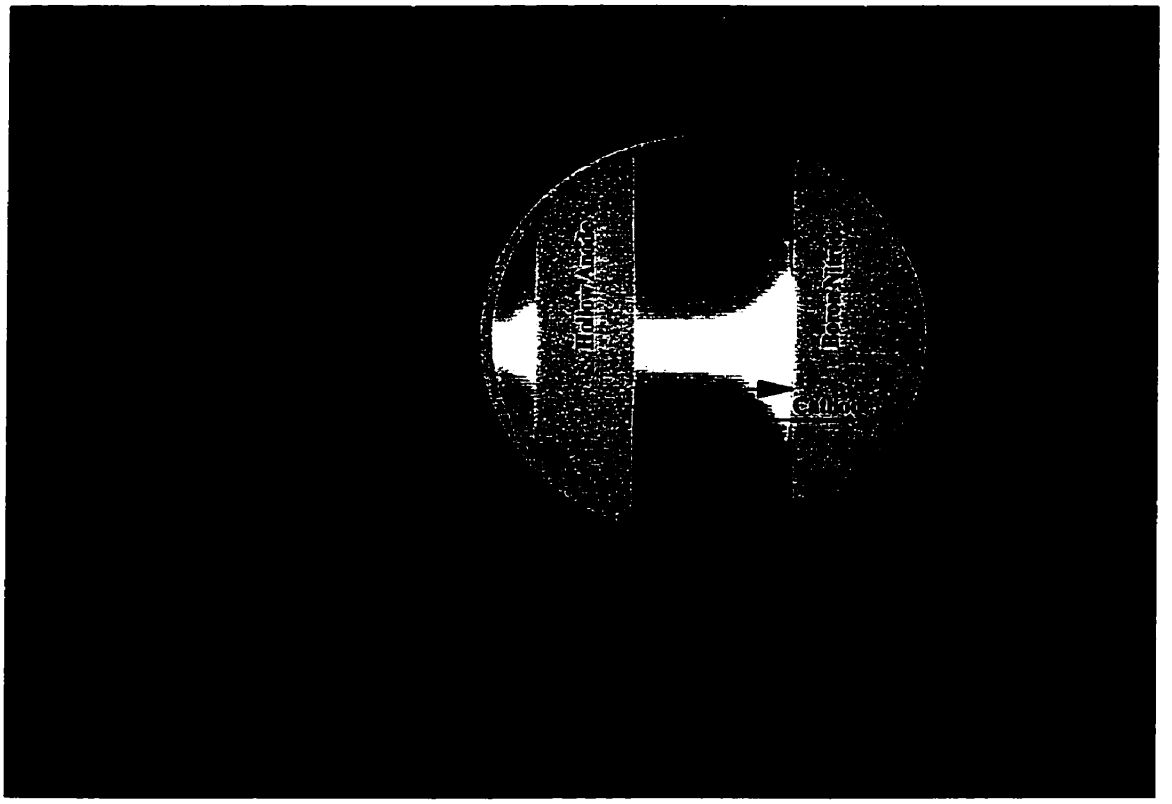

Figure (5-3) : Electric arc plasma geometry using Helmholtz coils, as seen from the side window.

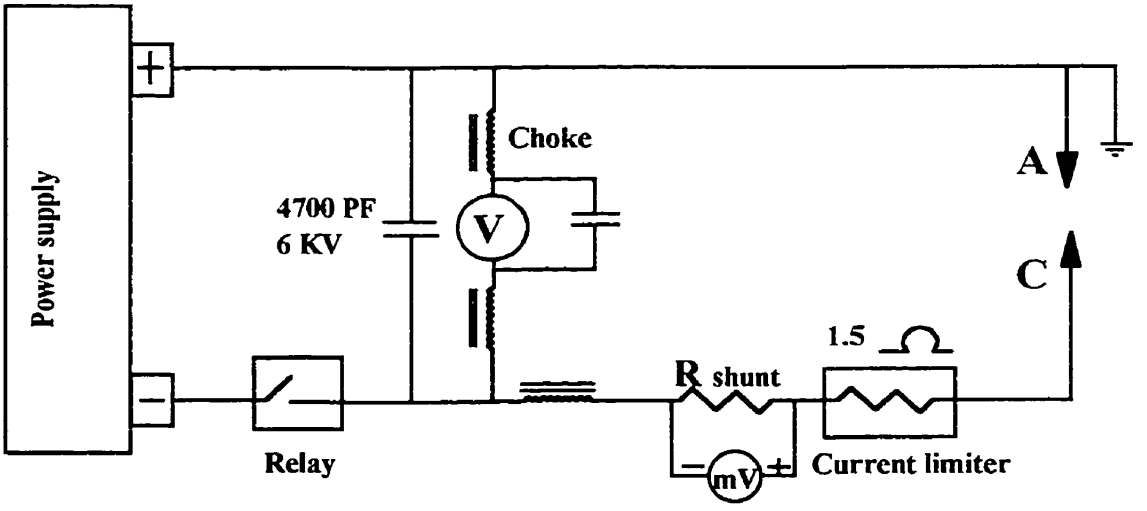

Figure (5-4) : Schematic of the electric circuit used in the continuous arc system.

Four kinds of substrates are used in this work, silicon wafers, glass used for microscopy analysis, titanium/ aluminum/ vanadium (Ti 90/ Al 6/ V 4) foil and stainless steel (Fe/ Cr 18/ Ni 8/ Mo 3) foil. The first choice was the glass substrate because of its low price. One problem associated with the use of this substrate comes from charges accumulation inside the SEM due to its high dielectric properties. Therefore, for the SEM purposes, a semiconductor substrate was chosen (i.e., silicon wafer). The last two alloys were used to study the effect of substrate types on DLC films structure, the Ti/ Al/ V alloy being similar to turbine blade alloy. A substrate shutter was used to hide the substrate for the first 10 to 15 seconds after the ignition of the arc. The reason is to protect the substrate from the large quantity of spherical particles and chunks (irregular shaped particles) emitted during the mechanical triggering sequence and the arc instability during the first 10 to 15 s (see Figure 5-5). A water cooled substrate holder (Figure 5-6) was used to keep the small substrates from overheating as a result of the strong ion flux.

The thickness of the films were measured using a Dektak 3 ST profilometer. Before and during the deposition process, part of the substrate was masked using copper tape. At the end of the deposition process, the tape was removed and the difference in the height between the covered and non-covered areas was measured as the film thickness. The roughness of the deposited film was measured using the same diagnostic tool (i.e., Dektak 3 ST profilometer).

A)

B)

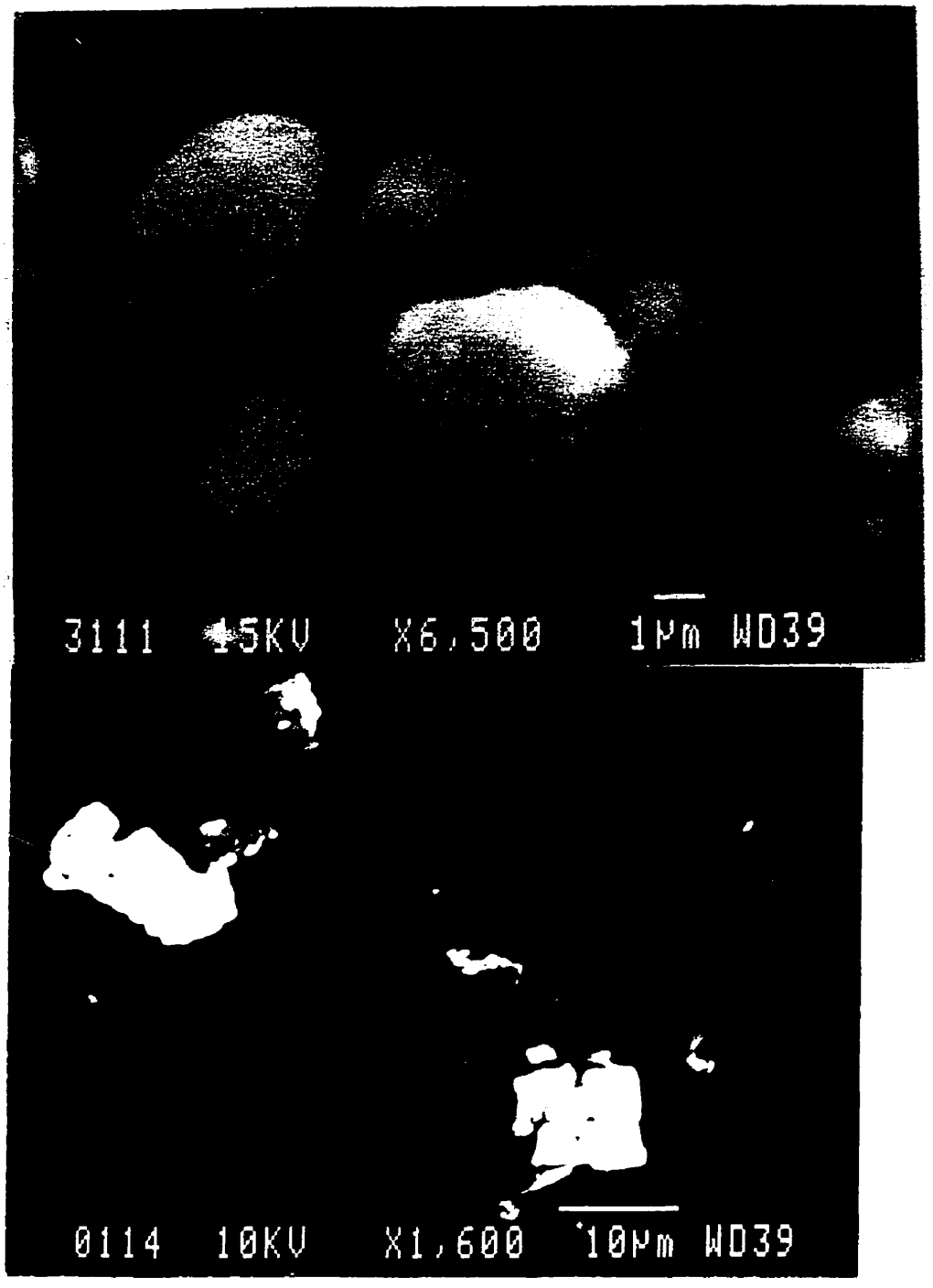

Figure (5-5) : SEM recording showing examples of macro-particles emitted during the early stage of the discharge; a) spherical particles; b) chunks (irregular shaped particles).

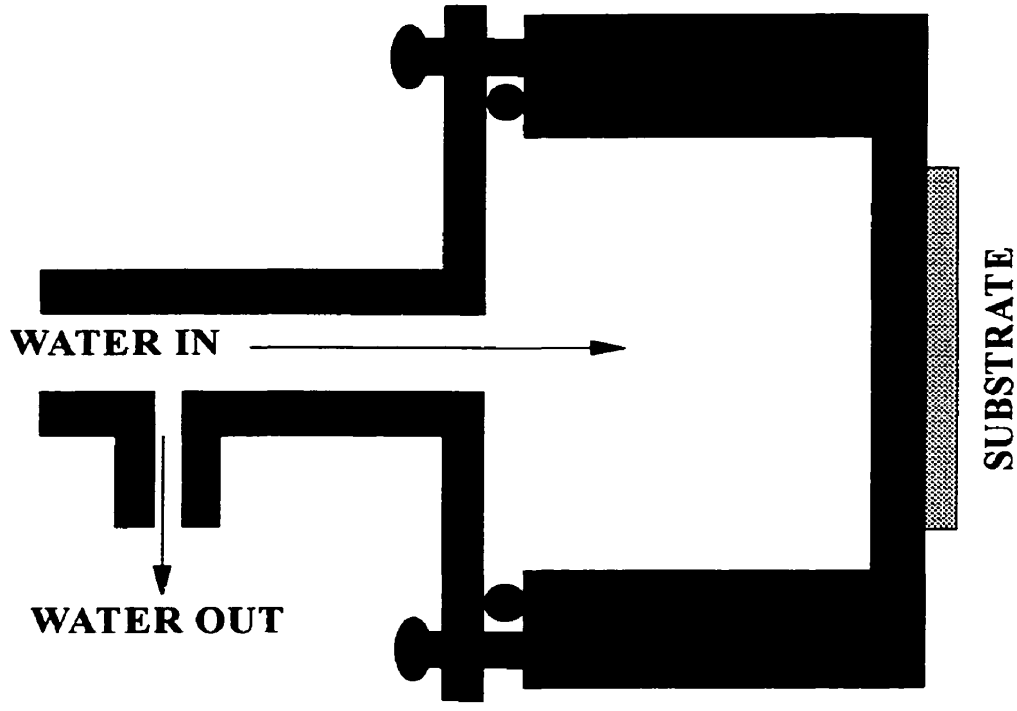

Figure (5-6) : Water cooled substrate holder.

5-3 : RESULTS

5-3-1 : MAGNETIC FIELD MEASUREMENT:

The model 912 Gaussmeter (RLF Industries Inc.) is used for the measurement of the magnetic field intensity (measuring range from 10 mG to 100 kG (10^{-7} Tesla - 10 Tesla) using Hall-effect probes). Nominal accuracy is within ± 0.5 percent.

The magnetic field intensity distribution induced by Helmholtz coils without the presence of the permanent magnets is measured along the chamber axis from cathode to any substrate position as shown in Figure 5-7. The axial magnetic field component (BH) is being constant and having its maximum intensity between the two coils. Outside the coil

edges, the magnetic field intensity starts to decrease exponentially until reaching the value of BH = 0. The radial component induced by Helmholtz field at the cathode surface is small and negligible. As shown in Figure 5-7 the cathode is located between the two coils in the constant magnetic field intensity regime. Figure 5-8 represents the magnetic field distribution induced by the permanent magnets behind the cathode. Two magnetic field components are measured, i.e., radial and axial (perpendicular) to the cathode surface Br and Ba, respectively. The radial field component of 0.044 Tesla is the maximum that we were able to achieve with this configuration due to some design restrictions. The zero axial field component occurs at distance between 2.1 - 2.3 cm from the cathode center where the corresponding radial component at this distance was equal to 0.03 Tesla. It has been shown by Kim (1995) on titanium cathodes that arc rotation occurs at this position of zero axial field.

The direction of the axial component (BH) induced by Helmholtz field is always kept opposite to the axial component induced by the permanent magnets (Ba). Therefore, using the permanent magnets without Helmholtz coils will increase the value of Ba and change the position of the zero axial component at the cathode surface.

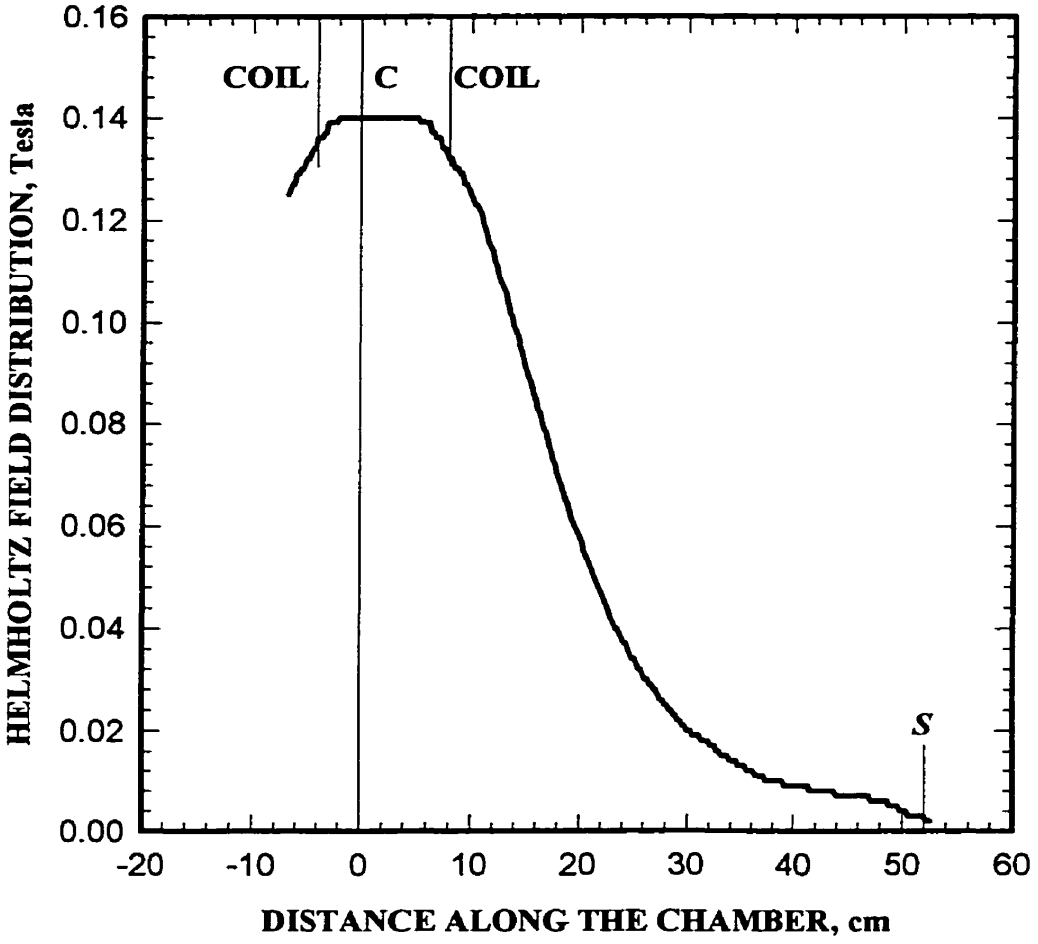

Figure (5-7) : Magnetic field distribution induced by Helmholtz coils along the chamber axis; C = cathode and S = substrate.

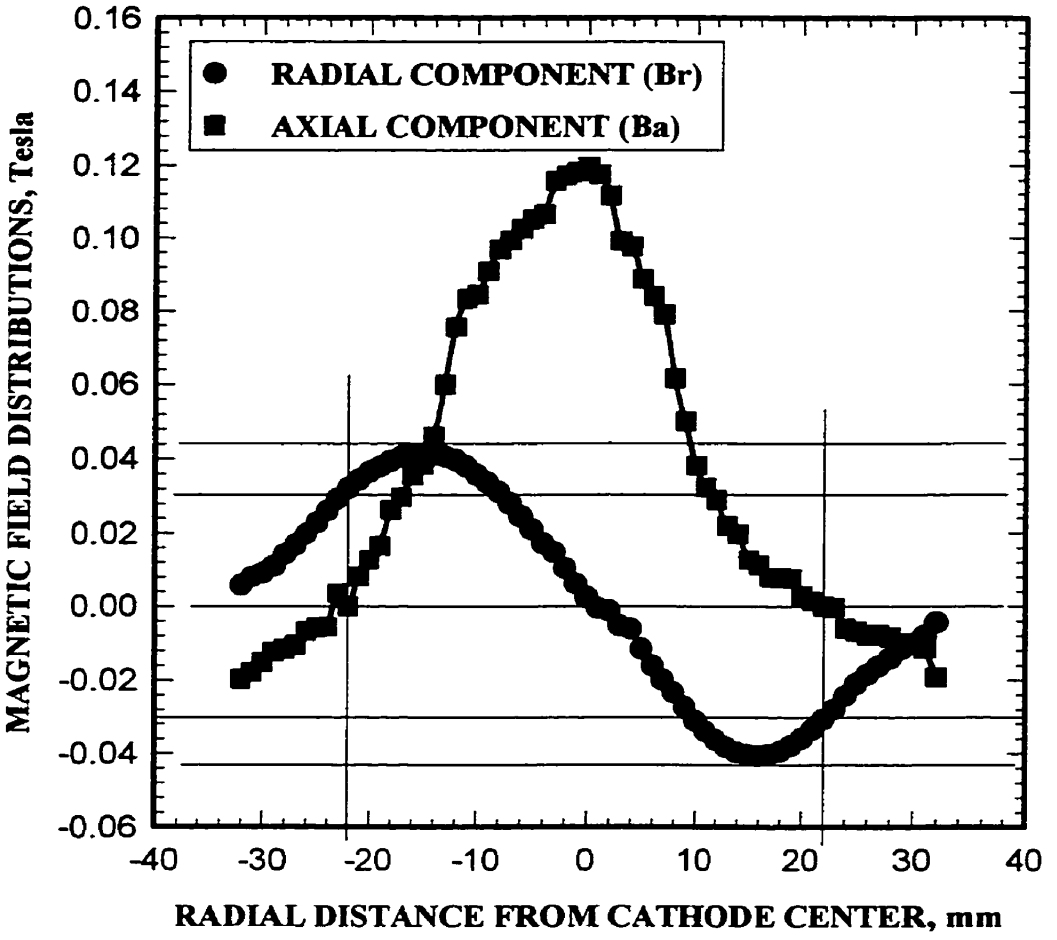

Figure (5-8) : Radial and axial magnetic field distributions induced by permanent magnets arrangement in the presence of Helmholtz field over the cathode surface.

5-3-2 : ARC SPOT VELOCITY

The spot velocity in the continuous system is measured optically by projecting the image of the arc spot onto an imaging plane containing one photodiode. The time required for the arc spot to pass in front of the photodiode two successive times is measured using an oscilloscope. The arc spot velocity is measured by dividing the circumference of the arc trace by this time. Placing the photodiode and the lens away from the pumping system is necessary to avoid the effect of the vibration and allow the arc trace image to pass over the photodiode.

The arc spot velocity is measured in the continuous mode for two cases, with Helmholtz field BH = 0.14 T (1400 Gauss) and without Helmholtz field BH = 0. For both cases constant radial magnetic field intensity Br = 0.03 T is applied over the cathode surface to rotate the arc spot. Figure 5-9 shows a comparison between the spot velocities in the pulse and continuous modes for different graphite types at constant radial magnetic field intensity (Br = 0.03 T). The spot velocity in the continuous mode is found to be lower than that in the pulse mode no matter if the arc is confined or not. In the continuous mode, the confinement of the plasma is found to increase the spot velocity. Confining the arc increases the plasma density over the cathode surface which enhances the probability of creating new emission sites and increases the spot velocity. More arc stability and voltage noise reduction are observed when Helmholtz field is used. In the absence of Helmholtz field the arc voltage was fluctuating between 0 V and 200 V, preventing the arc from running for extended periods. The chamber and windows around the periphery of the cathode were also getting very hot after a few seconds in the case of unconfined (diffused)

arc. Confining the arc using Helmholtz field avoids these problems and reduces the arc voltage fluctuation to voltage values between 35 V and 55 V. The reduction of the spot velocity in the continuous mode might be due to a change in the emission mechanism. As will be shown in the next section, the arc spot traces left on the cathode are very different in both situations. They are passing from individual and well separated cathode spots in the pulsed mode to a very uniform arc trace on which new emission sites are created directly on the side rim of previously existing craters. In both modes, pulse and continuous, the spot velocity shows a strong dependence on the graphite type. Figure 5-9 in fact indicates that, although the absolute velocity values are up to a factor of 60 smaller, the trends with varying cathode materials are in fact the same.

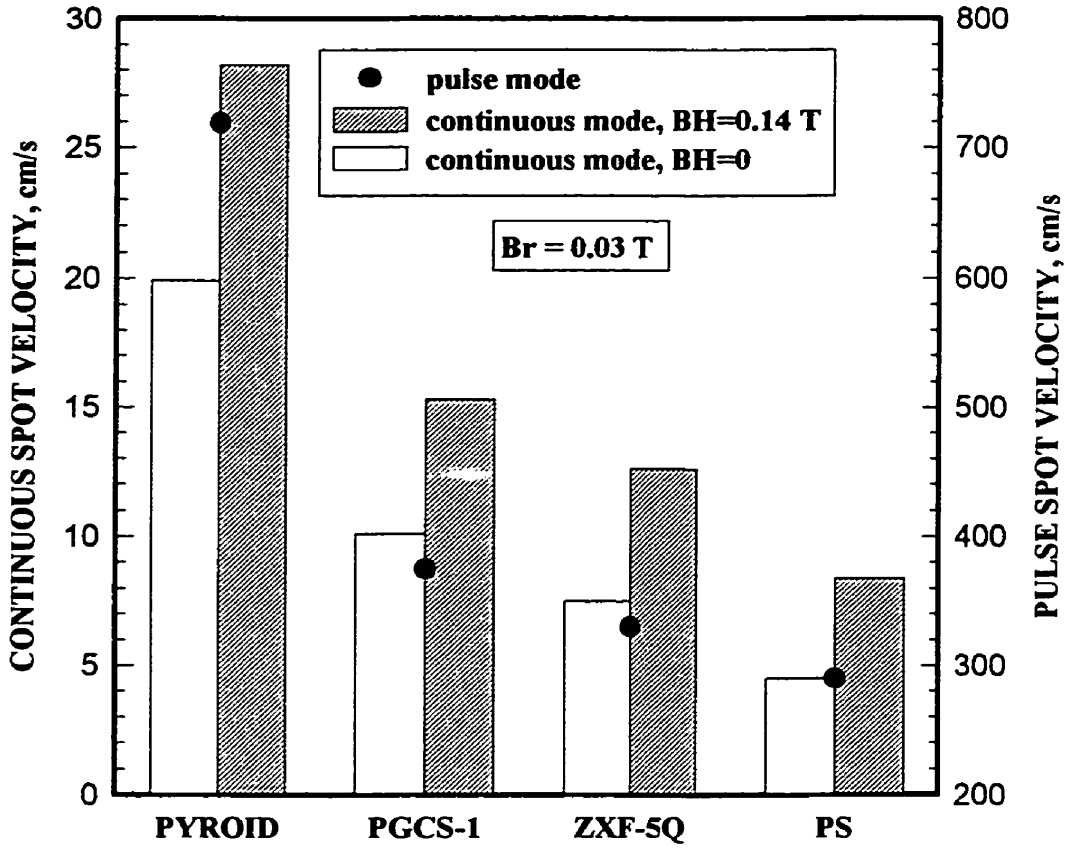

Figure (5-9) : Cathode spot velocity in the pulse (dots, right axis) and continuous modes (columns, left axis) for different graphite materials at constant radial magnetic field intensity of 0.03 T. The continuous mode velocity data are given for both no Helmholtz confining field and for an axial field value of 0.14 T. The arc current for all cases is I=70 A.

5-3-3 : ION CURRENT FLUX

The ion flux distribution was measured using a probe consisting of a central brass rod (1 cm in diameter) surrounded by six brass rings (2,3,4,5,6 and 7 cm outer diameter) as shown in Figure 5-10. Each ring was isolated from the other and from the central rod by a very thin Mylar sheet. The ion current was measured using a digital multimeter by measuring the voltage drop across a high power (5 watt) 1 ohm resistor connected with each ring independently. The probe was grounded and placed at a fixed distance away from the cathode with the center of the probe being in line with the center of the cathode. Knowing the value of the current as well as the surface area of each insulated ring on the probe, it was possible to calculate the current density assuming a uniform distribution of the current collected on the probe surface. Since each concentric ring was insulated, measurements of current density for different radial positions were made possible, these measurements being averaged over angles θ from 0 to 2π in cylindrical geometry.

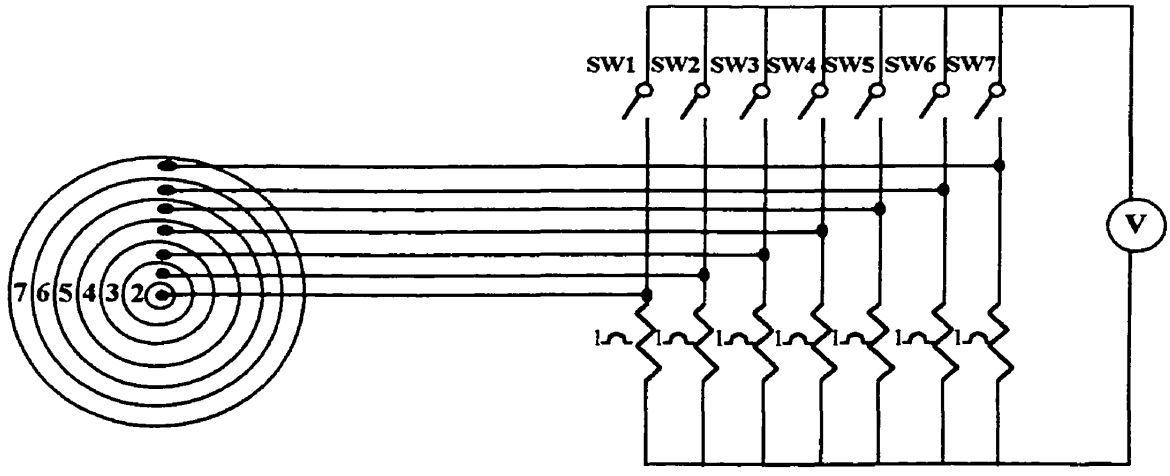

Figure (5-10) : Schematic for the ion current probe.

Figure 5-11 illustrates the effect of different types of graphite on the average ion current flux emitted from the cathode spot and reaching the 7 cm diameter probe located at an axial distance of 52 cm from the cathode with the presence of the Helmholtz field. The change in velocity of the cathode spot for the various graphite materials is also indicated in Figure 5-11 for constant radial magnetic field intensity of 0.03 Tesla. As for all other bar charts presented, the order of the materials on the figure follows that of Table 4-1. Figure 5-11 indicates that different types of graphite emit various average ion current densities under similar conditions. Cathodes showing higher spot velocities also emit higher ion current densities averaged over the 7 cm diameter probe. The system geometry, particularly the respective size of the probe used and the chamber tube (IT in Figure 5-2), did not allow the measurement of the ion flux at any distance less than 52 cm (the distance between the cathode and the end of the tube). Therefore, the ion current measurement at BH = 0 was not possible; at the 52 cm distance the ions were not able to reach the substrate in a measurable quantity without the use of the Helmholtz field. The 52 cm distance represents the typical cathode to substrate distance in this system. The axial magnetic field component induced by Helmholtz coils (BH) is equal to 0.14 T at the cathode position.

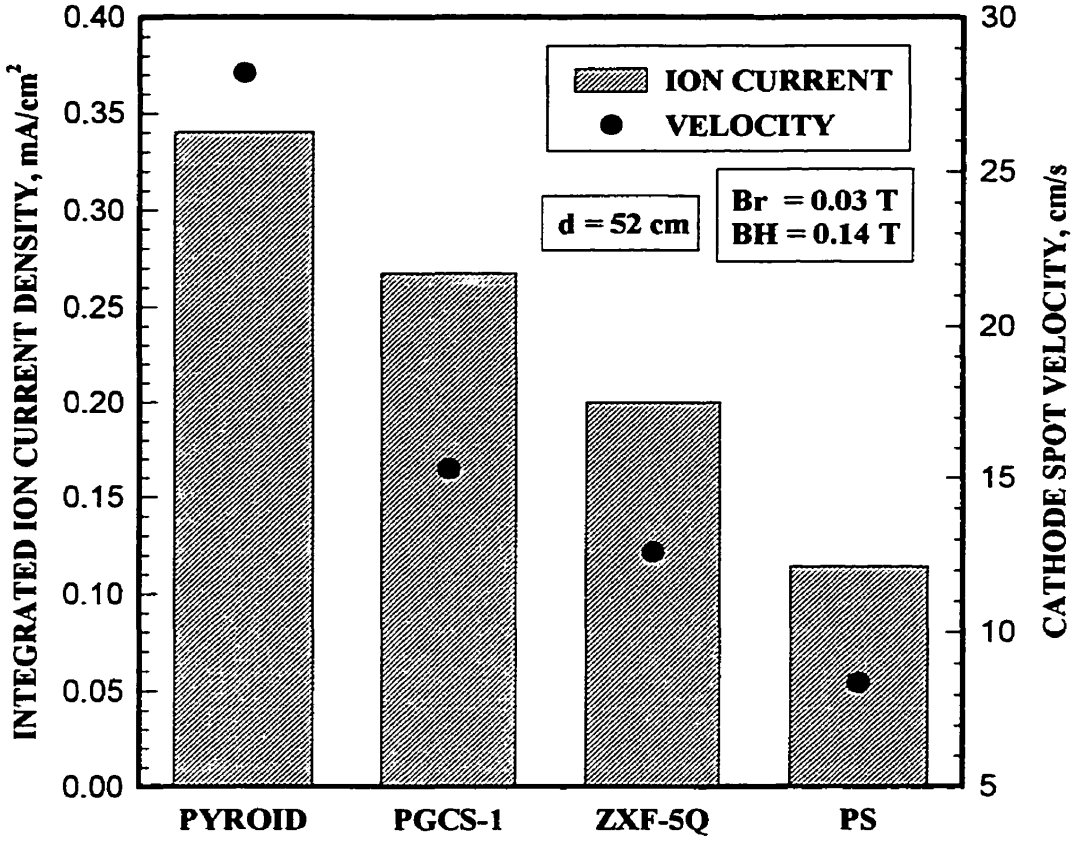

Figure (5-11) : Total ion flux collected (columns, left axis) over a probe of 7 cm diameter at 52 cm from the cathode, and spot velocity (dots, right axis) at radial constant magnetic field intensity of 0.03 T and 70 A arc current for four graphite materials. The Helmholtz axial confining field is set at 0.14 T.

The radial distribution of the ion current flux emitted from the cathode spot to a probe at a distance of 52 cm opposite to the cathode is shown in Figure 5-12 for different types of graphite. It is important to see the configuration of the cathode and probe (Figure 5-13) in order to explain these results. The arc trace is found to be always at a radial distance between 2.1 and 2.3 cm from the center of the cathode. The arc trace over the graphite cathode surface using a continuous arc mode is shown in Figure (5-14a) where it was mainly confined to the region of zero axial magnetic field component (Ba). This explains why the ion flux observed in Figure 5-12 is typically peaked for all materials at a radial distance corresponding to the arc rotation position, as shown in Figure 5-12. At any radial position, different graphite types again emit various ion fluxes. The most important result indicated by Figure 5-12 is that the types of graphite emitting higher ion current fluxes are also those corresponding to the materials showing higher spot velocities (Figure 5-9). The arc trace shown in Figure (5-14b), a close up of Figure (5-14a), indicates the difficulty of isolating the cathode spot or measuring the rim or size of any spot. It seems that the liquid (melted) layers are overlapping on each other and that a new cathode spot is initiated directly at the edge of an extinguishing one. Such a liquid phase was shown clearly in Figure (4-20b) using a low voltage (3 kV) high resolution field emission scanning electron microscope (FEGSEM) for the case of pulsed mode spots. Conditions prevailing in the continuous mode seem to indicate a much easier current emission from the spot and also a more important melted volume. Although spots typically overlap in Figure (5-14b), estimation of individual spot size can still be made from the morphology of the melted-like volume. One can roughly evaluate the spot diameter to vary between 60 to

100 μm. This can be compared to the spot size values of Figure 4-21 for pulsed mode discharges or the same material, leading to a mean size of 44 μm. The continuous mode with the increased plasma density above the cathode surface thus leads to mean spot sizes that are typically two times larger than the pulsed mode. For the arc current of 70 A used in these experiments, one can safely assume (as confirmed by visual observation during the run) only one single arc spot is burning. The continuous mode of operation hence implies an important reduction in the electric current density within the spot. Based on the description of retrograde motion given by Drouet (1985), one direct consequence of such a decrease current density is an expected decrease in the retrograde velocity of the arc spot in this mode of operation. The velocity decrease here goes from 290 cm/s in the pulsed mode down to 5 cm/s in the continuous mode (Figure 5-9). The larger spot size and expected reduction in the current density are consequences of an easier electron emission from the surface. These effects should correlate with a reduction of the plasma pressure in the cathode spot volume, such a reduction being highly favorable with regards to reducing the macro-particles emission.

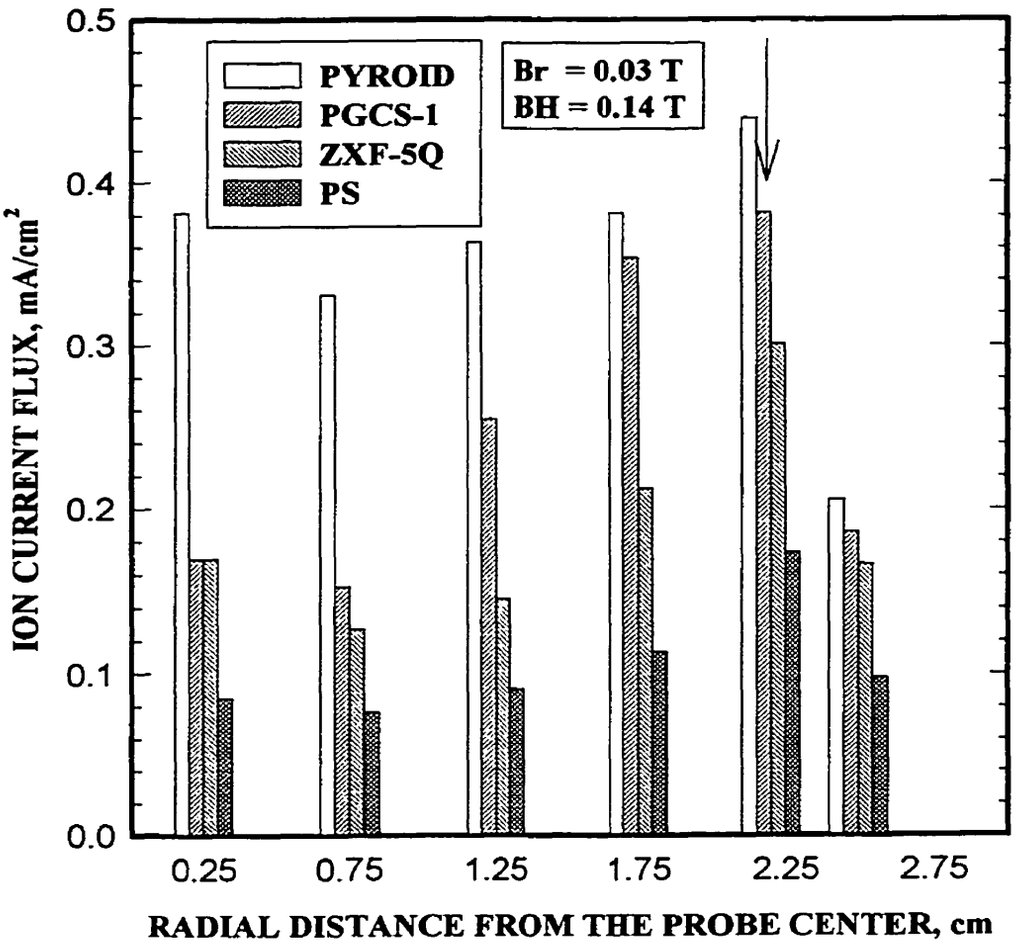

Figure (5-12) : Radial ion flux distribution for the different graphite types collected at a distance of 52 cm from the cathode, an arc current of 70 A, and same field values as in Figure 5-11. The arrow on top of the figure indicates the radial position of the arc rotation on the cathode.

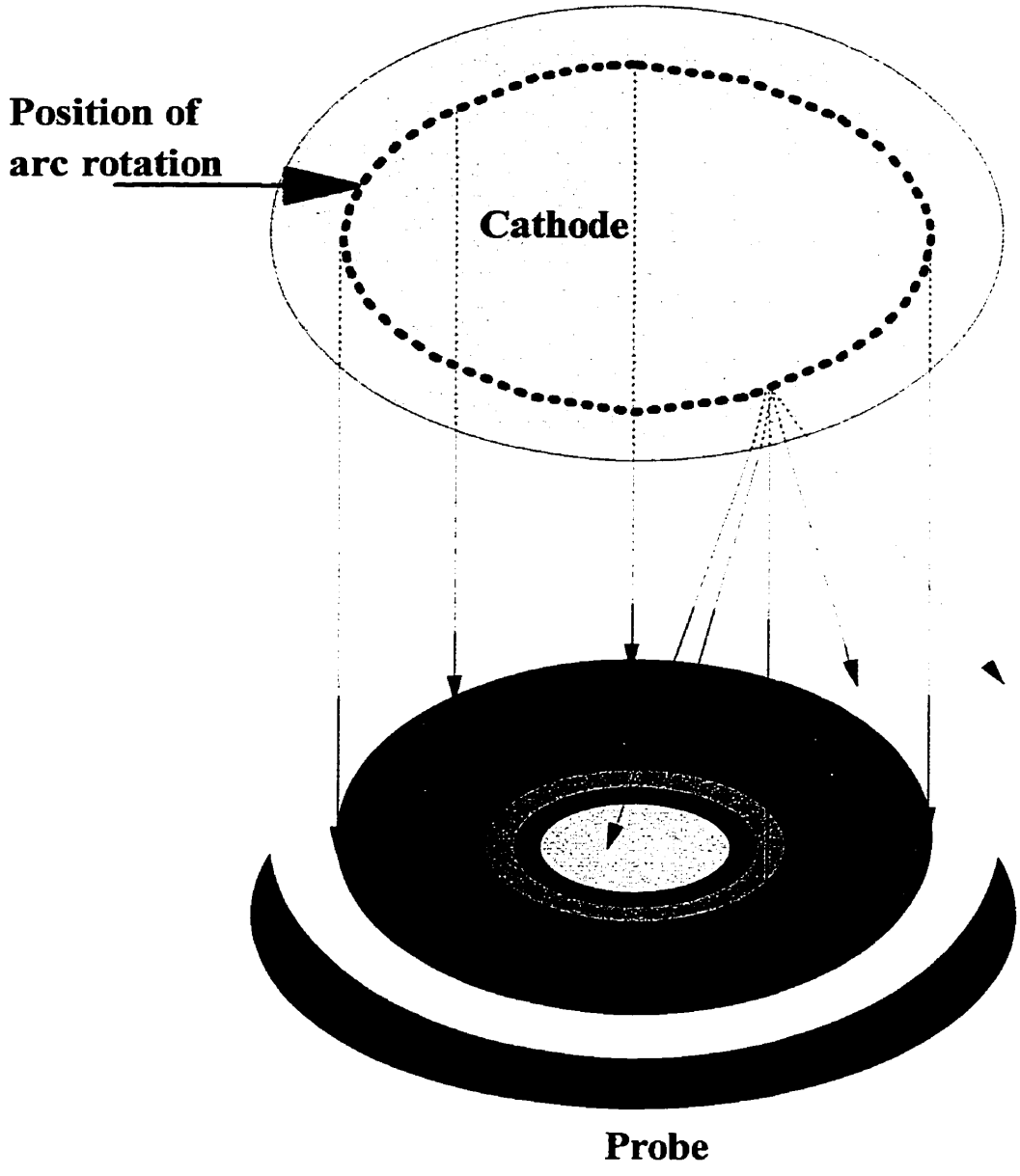

Figure (5-13) : Cathode and probe configuration.

A)

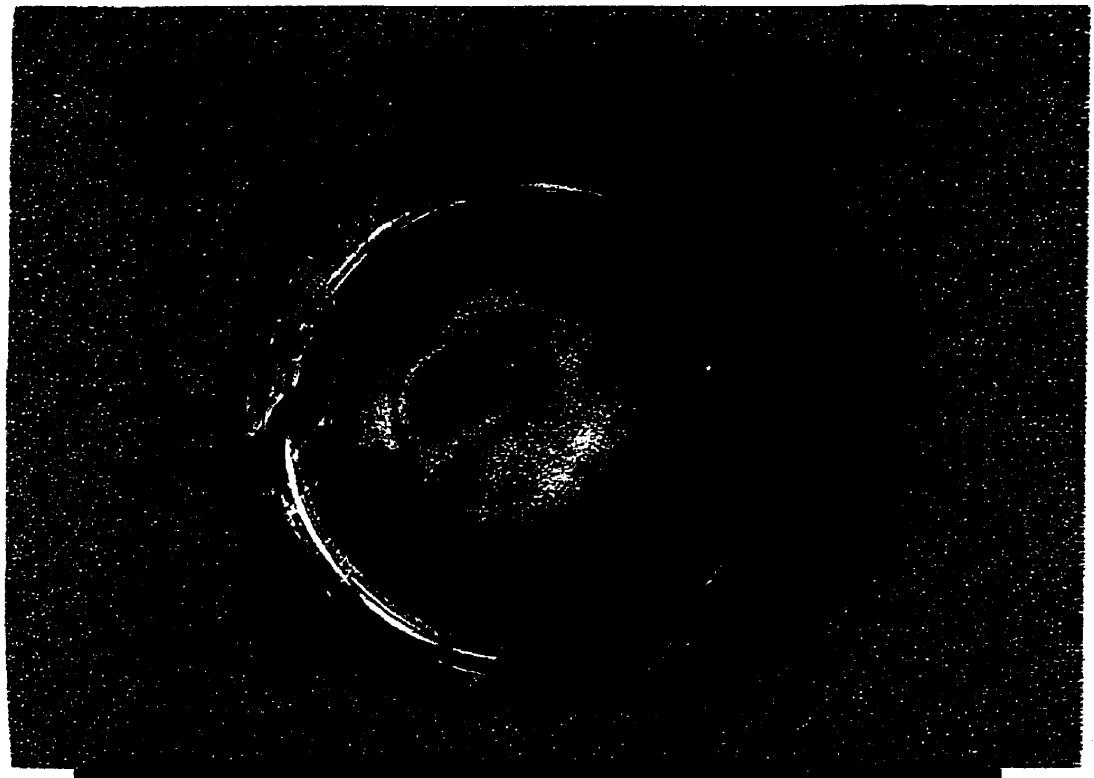

B)

Figure (5-14) : a) Arc spot trace over graphite cathode using a continuous arc mode for PS cathode; I = 70 A; Br = 0.03 T; BH = 0.14 T and t = 1.0 minute.

b) Close up of Figure (5-14a).

5-3-4 : ION ENERGY

The ion energy analyzer (IEA) also called orifice probe is shown in Figure 5-15 and used to determine various plasma parameters such as electron and ion temperatures T_e, T_i, number densities n_e and n_i, respectively, in addition to the space potential V_s. The analyzer is placed opposite to the cathode in place of the substrate at different distances from the cathode. It consists of a cylindrical stainless steel casing (3.81 cm in length and 2.54 cm in diameter). The casing contains one stainless steel foil (SF), four elctroformed-nikel grids (G1, G2, G3, G4), copper collector (C), stainless steel disks (SD), teflon insulators (I) and stainless steel centering rings (CR). The copper collector is vacuum coated with graphite to reduce electron secondary emission. This design is based on (Prokopenko et al 1974 and Reinke et al 1992).

A small orifice of 0.1 mm in diameter is drilled at the center of the stainless steel foil with a sharp-edge to avoid the collection of the current by the walls of the orifice. The orifice diameter is chosen to be smaller than the sheath thickness, so that the sheath over the orifice is not disturbed. For plasmas at low pressures, sheath thickness equals approximately 10 times Debye length (Franklin et al 1968), which leads to 1.1 mm approximately for our conditions. The pumping holes (PH) are used to reduce the need of complex differential pumping which would normally be employed to reduce the collisions in the analyzer. Ingram & Braithwaite (1988) also avoided the use of the differential pumping by reducing the depth of the analyzer to about 0.75 mm using Kapton sheet as a spacer between grids and copper-clad Kapton as the means of electrical connection to the grids. This makes the collisions within the analyzer less significant than collisions outside

because the space charge layer thickness (several millimeters) is larger than the shallowness of the analyzer.

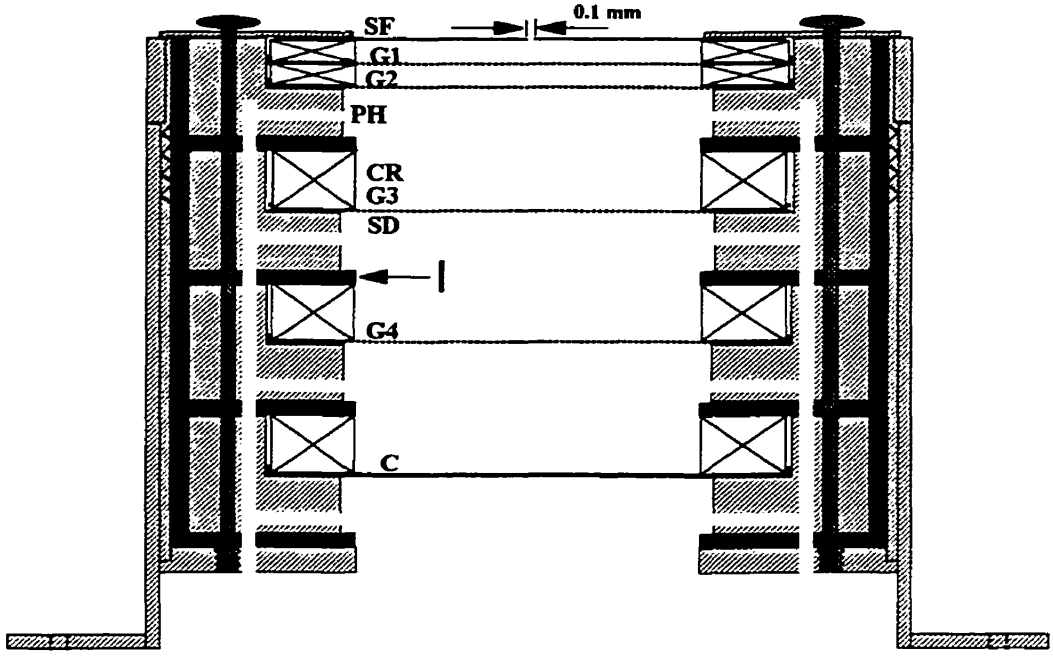

Figure (5-15) : Schematic for the ion energy analyzer (IEA).

The double grids G1 and G2 (1000 lines/in. each) are placed below the stainless steel foil, G1 being located 2 mm below the orifice. The idea behind the use of these two grids is to prevent the field penetration from the collector to the orifice. The use of these shielding grids help achieving flat saturation regions of constant current instead of having slopes to the ion and electron saturation regions. Grids distances are chosen to minimize both field penetration and space-charge effects (Green 1970 and Rusteberg et al 1995). It must be larger than half of the Debye length. The double grids are followed by grid G3

(100 lines/in.) to repel electrons or ions, depending on the biased potential to grid G3 (V_3 in Figure 5-16). Grid G4 (100 lines/in.) can be used to measure the fraction of the secondary electrons emitted from the collector surface by applying different bias between G4 and the collector C. The orifice plate is always at zero potential (grounded) to provide a reference for other potentials.

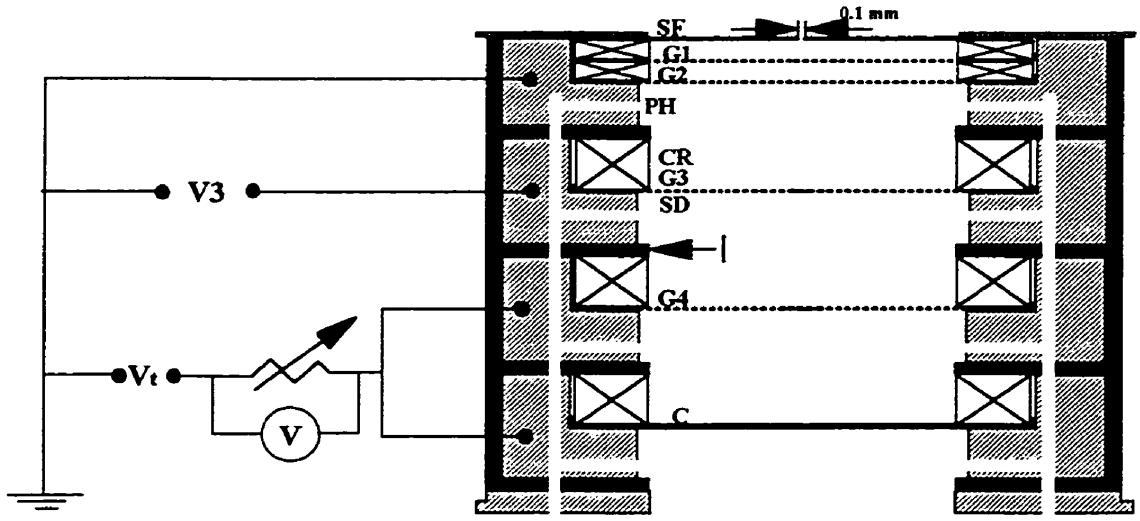

Figure (5-16) : Schematic of the electrical circuit that is used with the IEA.

The method used to determined the various plasma parameters is explained below based on the theoretical orifice probe current-voltage characteristics (Figure 5-17) and the associated equations (Prokopenko et al 1972). The equations are :

The total ion current collected by C and G4 in amperes is given by :

$I_i = I(V_t)$ 5-1

if $V_t \leq 0$ (accelerating case).

or $V_1 \geq V_t \geq 0$ (retarding case).

where V_1 is the full potential drop across the sheath ($V_1 = V_s - V_w$). V_s is the sheath potential and V_w is the orifice plate or wall potential ($V_w = 0$).

The ions of mass m_i have all gained a perpendicular velocity $\sqrt{\frac{2eV_1}{m_i}}$, which is superimposed on their random velocities. They are related for values of $V_t > 0$, but are still all collected until a voltage $V_t = V_1$ is reached. As in the case of the electrons, the ion current will then drop exponentially to zero. This ion current is given by :

$$I_i = I(V_1) exp(\frac{-e(V_t - V_1)}{k T_i}) \quad \text{.....} \quad 5\text{-}2$$

if $V_1 - V_t \geq 0$ (retarding case).

The electron current is given by :

$$I_e = -e n_e A_p exp(\frac{-eV_1}{k T_e}) \sqrt{(\frac{k T_e}{2\pi m_e})} \quad \text{.....} \quad 5\text{-}3$$

if $V_t \geq 0$ (accelerating case)

and

$$I_e = -e n_e A_p exp(\frac{-e(V_1 - V_t)}{k T_e}) \sqrt{(\frac{k T_e}{2\pi m_e})} \quad \text{.....} \quad 5\text{-}4$$

if $V_t \leq 0$ (retarding case)

The constants e and k refer to the magnitude of the electronic charge ($e = 1.6 \times 10^{-19}$ C) and Boltzmann's constant ($k = 1.38 \times 10^{-23}$ Joules /°C), respectively. The total ion current passing through the orifice is given by $I(V_1)$ while the voltage difference between the

collector and wall potential by V_t. The electron mass and number density, ion mass and orifice area are represented by m_e n_e, m_i and $A_p = 7.854 \times 10^{-3}$ mm^2, respectively.

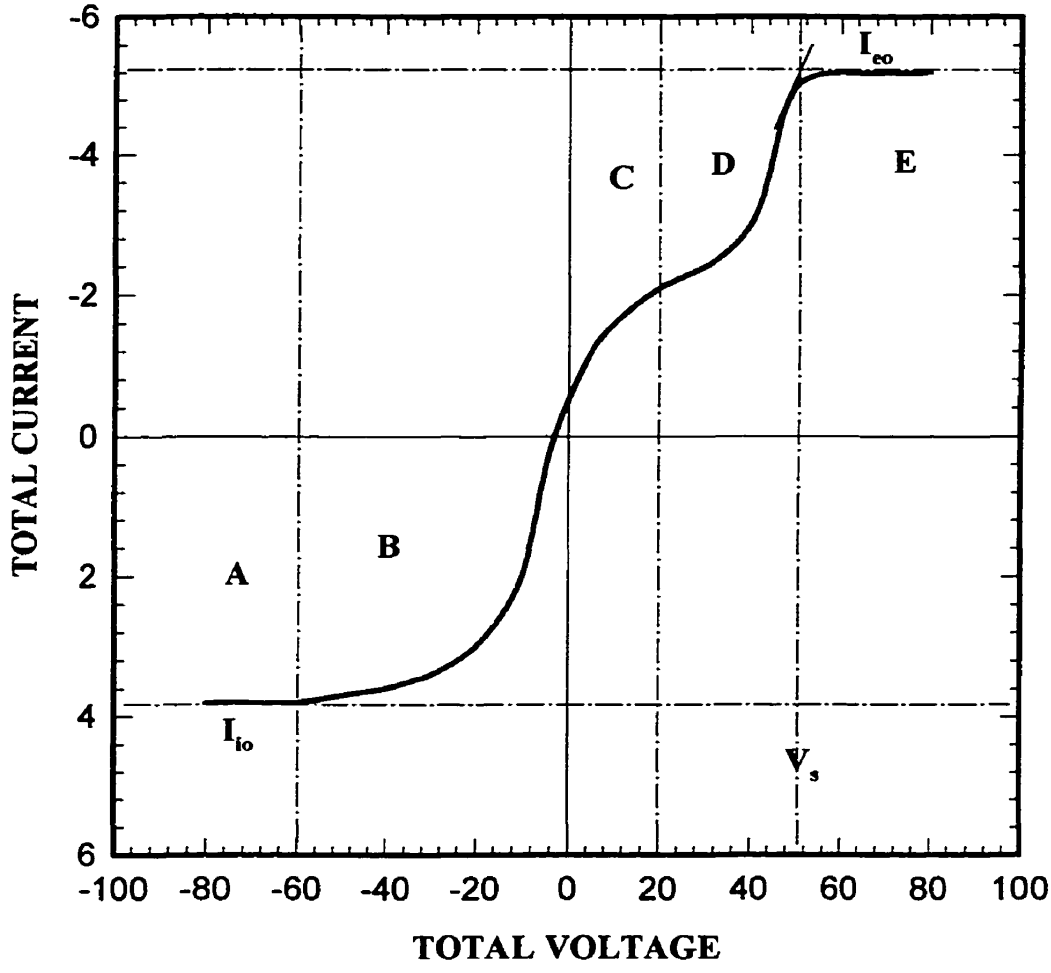

Figure (5-17) : Theoretical orifice probe characteristics for an infinite plane collector.

Five regions are recognized in Figure 5-17; A = ion saturation region; B = electron-retarding region; C = net saturation region; D = ion-retarding region and E = electron saturation region. The space potential (V_s) is determined as the abscissa of the intersection point of the extrapolated electron saturation current and the tangent of the exponentially increasing part of region D. Assuming that the plasma is sufficiently homogeneous and collisionless, the ion and electron temperatures can be extracted from the slope of a semilog plot in the retarding regions D and B, respectively. The slope is $\frac{d(\ln I)}{dV_i}=\frac{e}{kT}$ for both cases. The corresponding equations are equation 5-2 for ions and equation 5-4 for electrons. The quasineutrality of the singly ionized plasma requires that the ion and electron densities are equal (i.e., $z\, n_i = n_e$), where z is the charge state. Davis & Miller (1969) found that ion charges for carbon are predominantly z=+1 (96%) and z=+2 (4%). The determination of the electron current density can be done by substituting the values of the electron temperature (kT_e), the electron saturation current (I_{eo}) and $V_i = V_s - V_w$ in equation 5-3. The ion and electron saturation currents I_{io} and I_{eo}, respectively, and the sheath potential V_s can be obtained directly from Figure 5-17.

In this work, the current-voltage data are collected at arc current of 70 A and vacuum pressure of 10^{-3} Torr. In the case of arc confinement using Helmholtz field (BH = 0.14 T) the cathode-probe distance was equal to 52 cm, while it was equal to 9 cm when BH = 0. G3 is kept at zero voltage in all cases and the total current is collected from G4 and C at different voltages.

Figure 5-18 shows the current-voltage characteristics for two graphite types (**PYROID** and **ZXF-5Q**) at different conditions. Curves (a) and (b) indicate the total

current characteristics for **PYROID** and **ZXF-5Q** graphite types, respectively, using Helmholtz field (BH = 0.14 T) to see the effect of different graphite types with different surface properties on the energy and the number density of ions. Curve (c) shows the I-V characteristics for **ZXF-5Q** at BH = 0 (i.e., diffused arc) to be compared with curve (b). The semilog plots for the determination of ion and electron energies are illustrated in Figures 5-19 and 5-20, respectively. The results are summarized in Table 5-1. Under similar conditions different graphite materials emit varying ion number densities with different energies. The comparison between **ZXF-5Q** and **PYROID** graphite types under the same conditions indicates that ion energy and flux density are increasing for materials showing higher spot velocities. For the same graphite material (**ZXF-5Q**), ion number density and energy were also found to be increasing when the arc is confined. Results summarized in Table 5-1 indicate that 1) arc confinement increases the deposition rate due to the increase in ion number density emitted from the cathode; 2) the need for substrate biasing can be avoided due to the high ion energy that is achieved from the arc confinement and the choice of the graphite type. The effect of the magnetic field confinement on the plasma parameters are studied by (Sathrum & Coll 1992) for the flux impinging TiN films in modified arc evaporation source. Their results are described in Table 5-2. Our results (Table 5-1) are in agreement with the results shown in Table 5-2 in terms of the evolution of the electron temperatures as a function of the magnetic field. Electrons at higher magnetic field strengths are more than energetic enough to dissociate and ionize other species. The electron temperatures calculated in this work are for

electrons at 52 cm from the cathode. Electrons close to the cathode surface are expected to have much higher temperatures.

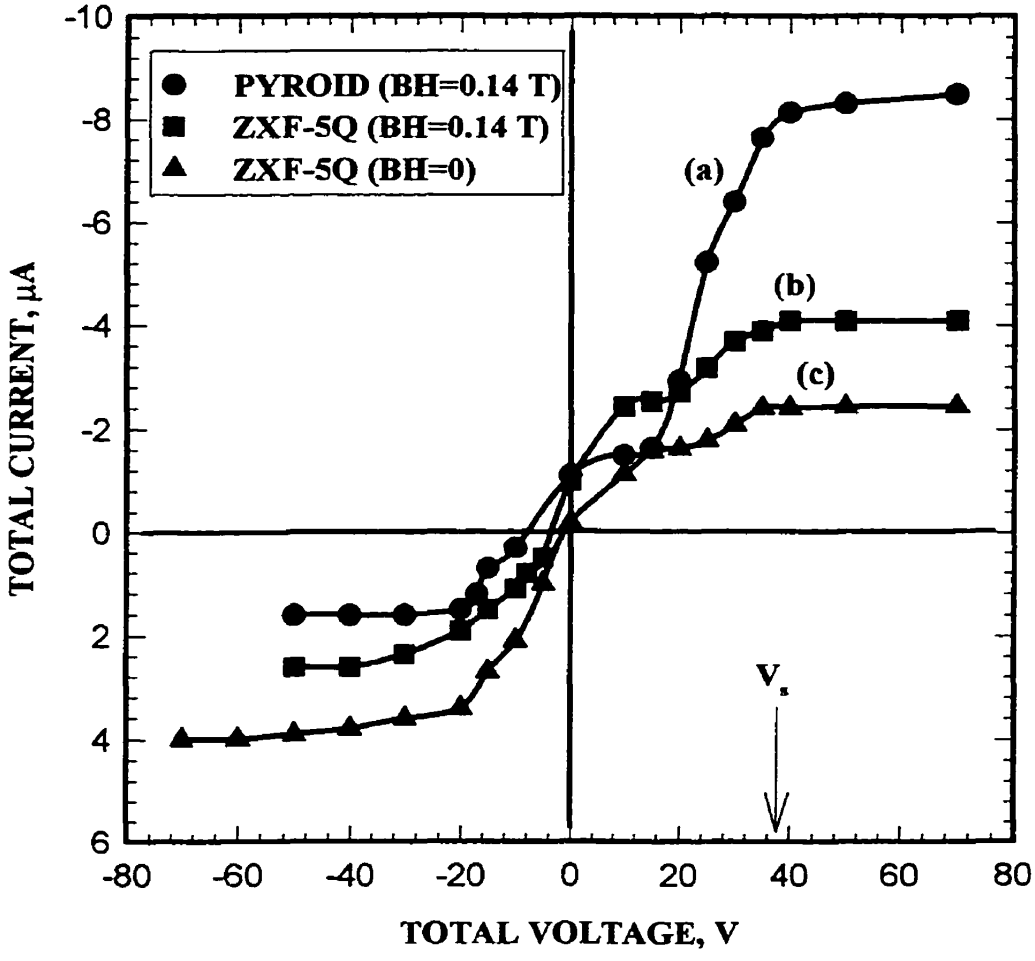

Figure (5-18) : Experimental total current-voltage characteristics curves for two graphite types at different conditions.

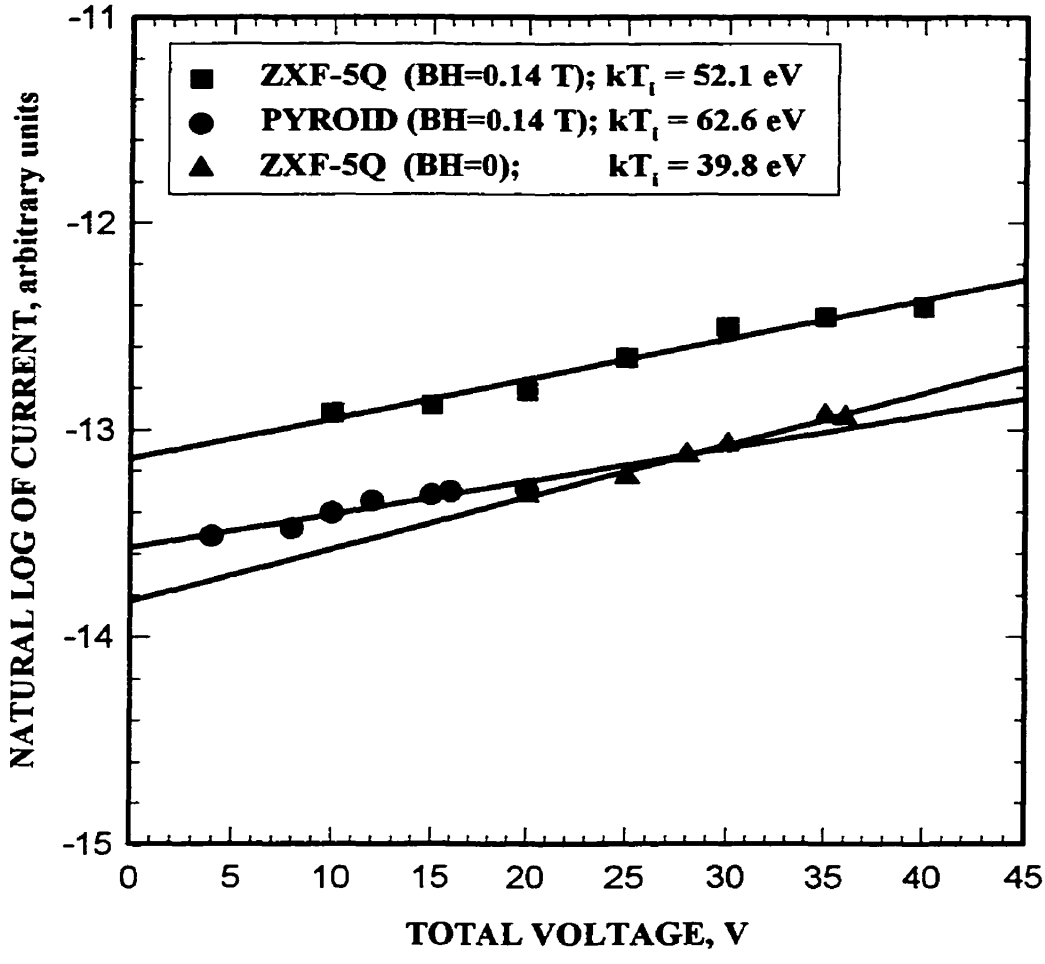

Figure (5-19) : A semilog plot of ion current (in arbitrary units) against retarding potentials for three different cases.

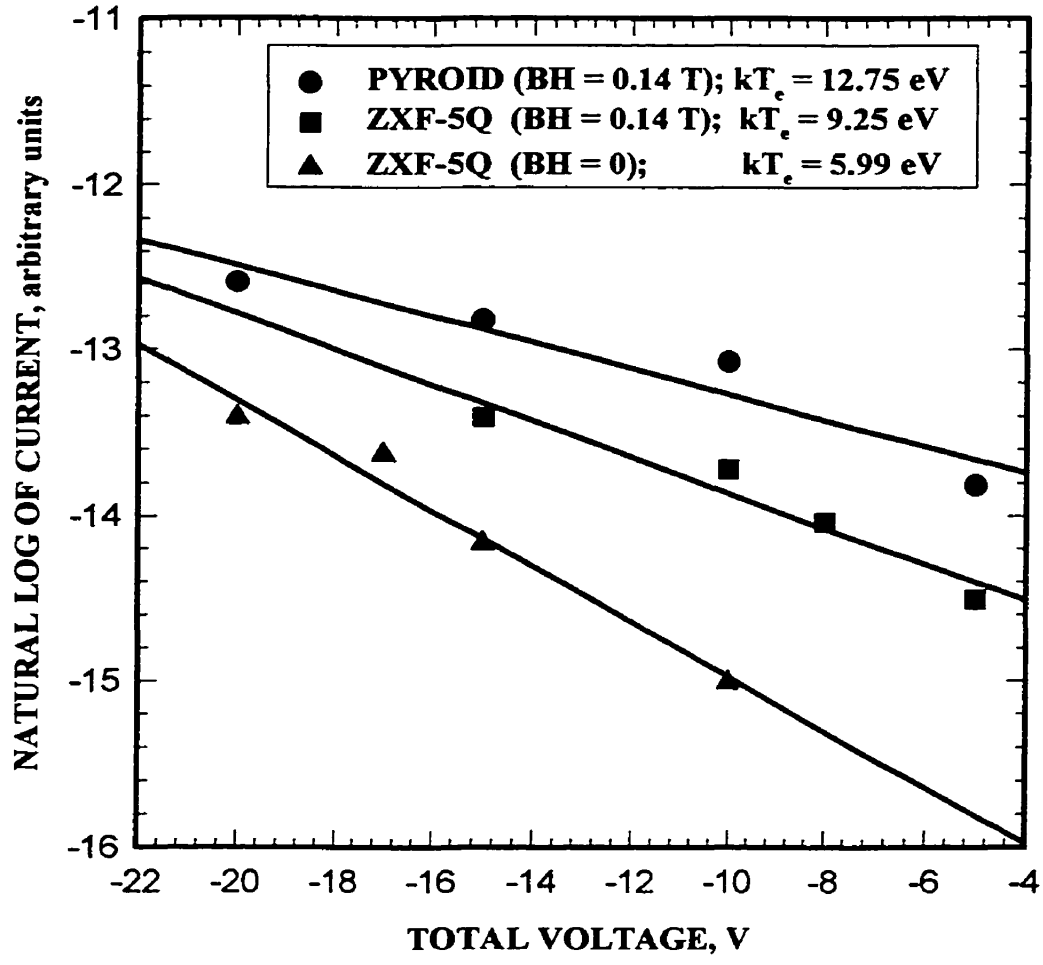

Figure (5-20) : A semilog plot of electron current (in arbitrary units) against retarding potentials for three different cases.

Table 5-1 : Ion Energy Analyzer (IEA) Results

Cathode type	BH (Tesla)	$k T_i$ (eV)	$k T_e$ (eV)	$n_i = n_e$ (m^{-3})	I_{io} (A)	I_{eo} (A)
PYROID	0.14	62.6	12.75	5.75×10^{14}	4.0×10^{-6}	8.5×10^{-6}
ZXF-5Q	0.14	52.1	9.25	1.05×10^{14}	2.6×10^{-6}	4.1×10^{-6}
ZXF-5Q	0	39.8	5.99	8.54×10^{12}	1.6×10^{-6}	2.5×10^{-6}

Table 5-2 : Electron Temperature kT_e, Plasma Density n and Floating Potential V_f vs. Magnetic Field Strength (Sathrum & Coll 1992).

Magnetic field (G)	kT_e (eV)	n ($\times 10^{10}$ cm^{-3})	$-V_f$ (V)
0	2.5 ± 1.5		1.0 ± 0.4
335	6.0 ± 1.5	0.80 ± 0.15	5.8 ± 0.4
670	10.0 ± 1.5	1.01 ± 0.26	8.9 ± 0.4
890	12.0 ± 1.5	1.48 ± 0.32	5.5 ± 0.4
1450	25.0 ± 2.0	1.66 ± 0.32	2.5 ± 0.4

5-3-5 : CATHODE EROSION RATE

In the continuous arc mode, cathode erosion rates and corresponding arc spot velocities at constant radial magnetic field intensity Br = 0.03 T is illustrated in Figure 5-21 for various types of graphite. The total mass loss normalized to the total electric charge passing through the cathode is found to be increasing for graphite types having higher spot velocities in both cases, with and without Helmholtz field. This is in agreement with Figure 4-17 evaluated using the pulsed arc mode. In the case of using Helmholtz field (BH = 0.14 T), the erosion rate is found to be lower than that without the magnetic field confinement (BH = 0). Erosion rate measurements are replicated more than three (3) times for each experiment. The arc duration time and current were constant and equal to 1.5 minutes and 70 A, respectively.

The increase in erosion rate for cathodes having higher spot velocities at constant radial magnetic field intensity is expected to be due to the increase in the ion emission assuming that the number of macro-particles is decreased with increasing spot velocity. In the case of BH = 0, the erosion rate was found to be higher than that at BH = 0.14 T due to the decrease in the arc spot velocity that leads to more macro-particles emission. This will be confirmed in the following sections.

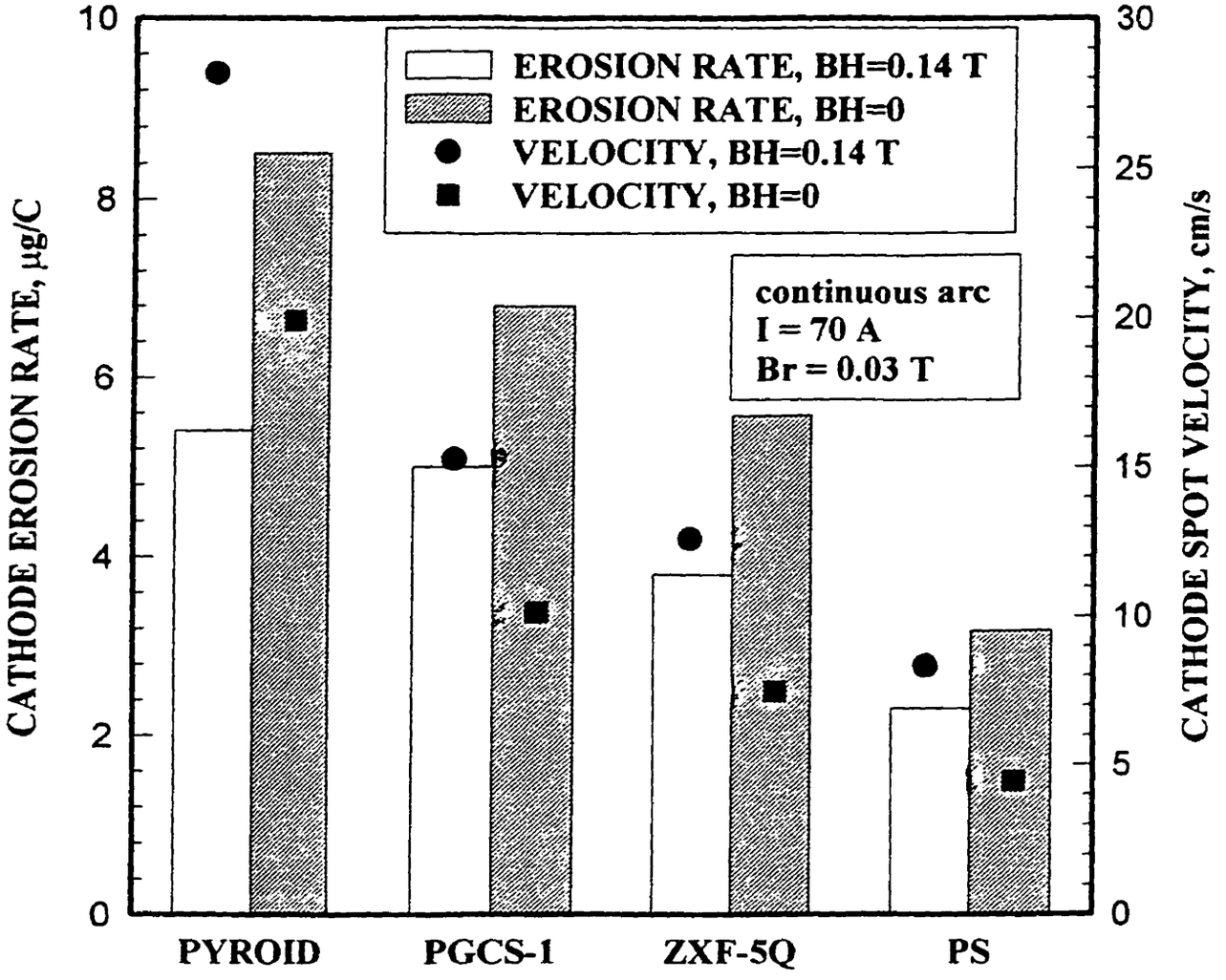

Figure (5-21) : Effect of the types of graphite in the continuous mode on erosion rate (columns, left axis) and spot velocity (dots, right axis) at constant radial magnetic field intensity of 0.03 T for two values of the axial confining magnetic field.

5-3-6 : PARTICLES NUMBER DENSITY

The particles number density observed on the substrates are measured by using an image analyzer software connected to the scanning electron microscope. The typical sequence of operations that an image processor might go through are as follows:

To get an image from a sample into the memory of the computer, an image acquisition hardware is attached to a scanning electron microscope (SEM), the image is digitized into a black and white image. The shades of black and white, called grey-levels, represent intensity information. Image acquisition alone is not really image processing, but if we average several frames together, image enhancement is being done. Averaging of successive frames of data enhances an image by decreasing the relative intensity of noise. Once an image has been acquired, the intensity levels stored for each of the pixels (single dots in the image) can be modified to improve the visual effect. In a washed-out picture, the information may still be there but the difference is too subtle to be perceived. Exaggeration of these differences can result in a vast improvement in picture quality. This technique is known as contrast stretching. Once a quality picture is obtained, the picture is stored. This stored image is however in a form which makes it difficult for the computer to distinguish an object from background. The term segmentation refers to the conversion of an image from grey level to binary. In a binary image, pixels corresponding to features of interest are either on or off. Segmentation requires a value judgement as to whether a pixel is part of the object or not. It should be apparent that errors may be made in the creation of a binary image. It may be necessary to join lines, fill holes, and disconnect separated objects. Binary filters or manual editing can accomplish this clean up. A binary image contains a compact description of what is object and what is background. Using

the binary image, the computer can generate a variety of sizing parameters including number of particles, areas, lengths, and widths, etc.

The number of particles in each sample is evaluated by analyzing five different locations on each (12.7 mm diameter) substrate, then taking the average of the number of particles from the five locations. The area of each location is 1681 μm^2. The substrates for all measurements are located in the direction perpendicular to the cathode surface, on the main axis of the discharge. The particle sizes were found to be in the ranges of 0.3 μm to 10 μm in diameter. The thickness of the deposited film depends strongly on both deposition time and arc current. It is therefore necessary to normalize the number of particles to the surface area of the films measured and to the electric charge passing through the cathode (i.e., deposition time x arc current). Also of practical importance, the data on particle density in the films are normalized to the coating thickness.

Figure 5-22 illustrates that cathodes showing higher spot velocities correlate with a smaller number density of particles in the deposited films, as expected in Part 2. This again indicates that various graphite material morphology will emit different quantities of particles towards the substrate under similar operating conditions. Comparing with Figure (1-7), one can notice the huge reduction in the number density of the emitted particles using a steered arc. The number density of particles shown in Figure 5-22 was measured at a 9 cm distance between cathode and substrate, 70 A arc current and 1.5 minutes arc duration time without arc confinement. The deposition at 9 cm distance between cathode and substrate, using Helmholtz coils (BH = 0.14 T) was not possible due to the high ion flux density and high energy which melted the substrate. Therefore, we are forced to keep

the substrate very far from the cathode when Helmholtz field is used. At a distance of 52 cm between the cathode and the substrate, with Br = 0.03 T and BH = 0.14 T, no particles were observed in the produced DLC films as shown by the absence of any feature in Figure 5-23a. This can be compared to Figure 5-23b corresponding to the **PYROID** sample in Figure 5-22. The thickness of the DLC film corresponding to Figure 5-23a is 634.4 Å, this results from an arc current of 70 A during 30 seconds deposition time. The diamond-like nature of these films is analyzed in section 5-3-8.

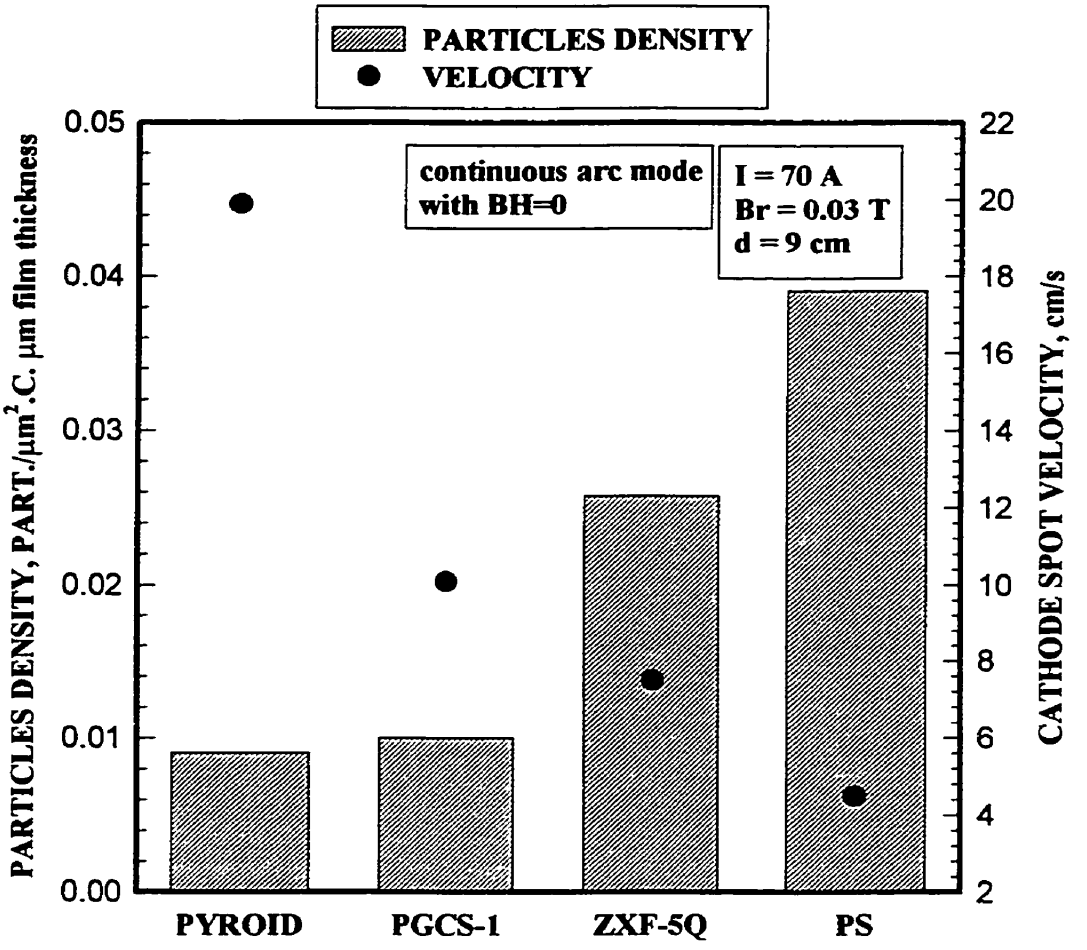

Figure (5-22) : Effect of the types of graphite on the number density of emitted particles (columns, left axis) normalized to the deposited film thickness over silicon wafer substrates located at a distance of d = 9 cm, arc time of t = 90 seconds and Br = 0.03 T in the continuous mode. The corresponding arc velocities for the same materials are also given (dots, right axis).

A)

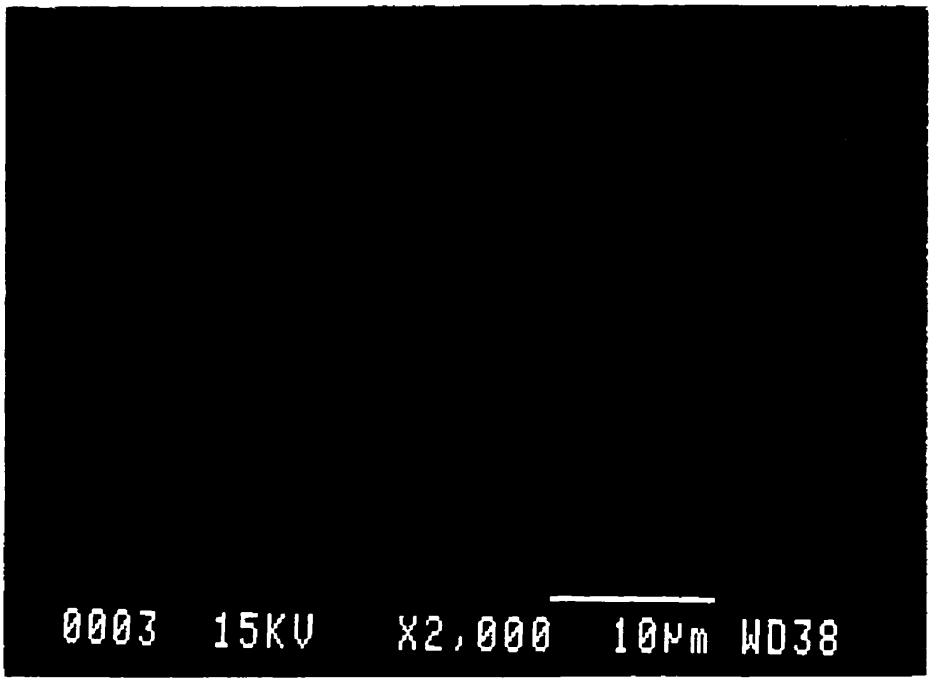

B)

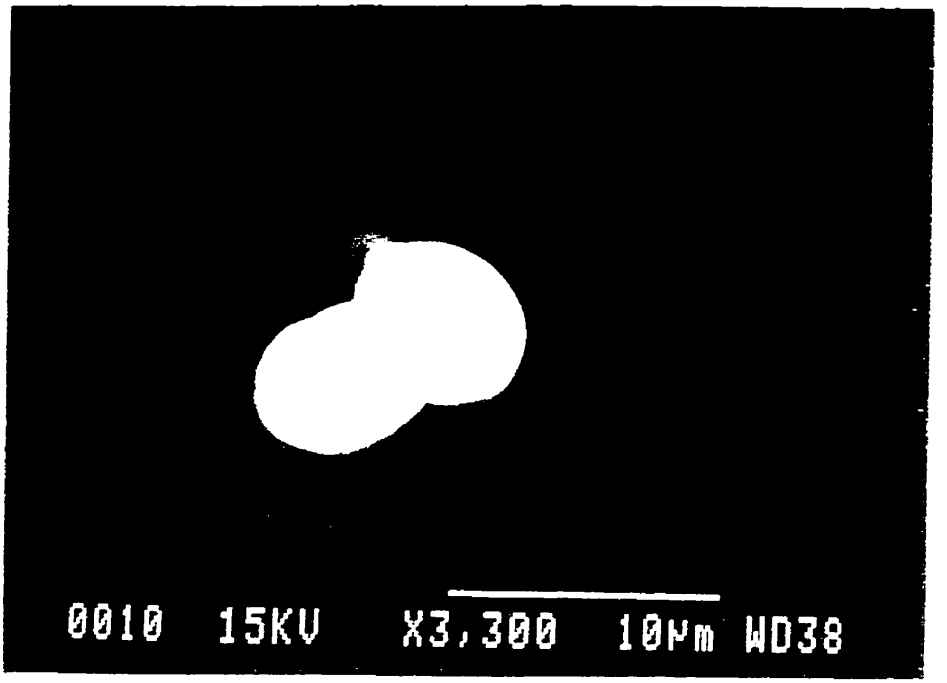

Figure (5-23) : a) SEM recording showing a DLC film free of particles produced at 52 cm distance between cathode and substrate; Br = 0.03 T and BH = 0.14 T.

b) Another SEM picture corresponding to the **PYROID** cathode on Figure 5-22.

5-3-7 : FILMS THICKNESS AND ROUGHNESS

The thickness and the roughness of the films, normalized to the total electric charge passing through the cathode, are both found to be decreasing when cathodes showing higher spot velocities are used, as shown in Figures 5-24 and 5-25, respectively. All data points of Figures 5-24 and 5-25 correspond to arc currents of 70 A and deposition times of 90 seconds. The use of a Helmholtz field to confine the plasma in front of the cathode was not used at the cathode to substrate distance of 9 cm due to the very high ion flux and energy that melted the substrates. At the same time, without Helmholtz field it was very difficult to have deposition and growth of a film for distances larger than 9 cm. Hence the two curves correspond to (d=9 cm, BH=0) and (d=45 cm, BH=0.14 T). The total thickness measured for one minute long experiment is typically in the range of 0.06 μm to 0.6 μm depending on cathode type, radial magnetic field intensity over the cathode surface and the Helmholtz field intensity on the arc. A major difference in the film characteristics is related to the fact that films deposited at 45 cm distance were essentially free of particles. The anode is designed to act as a shield for the particles and chunks that are emitted at low angles. In spite of the larger substrate-cathode distance, the film thickness for the confined arc is found to be larger than that in the case of no arc confinement. This is an indication of the enhancement of the ion flux emission using Helmholtz field. On the other hand, films deposited at cathode to substrate distance of 9 cm have a higher particle content and show higher roughness as shown in Figure 5-25. Although the increase in the spot velocity is found to increase the ion flux emission, it is also decreasing the macro-particles and chunks emission significantly. Therefore, the

decrease in the film thickness for cathodes showing higher spot velocities (Figure 5-24) may eventually be related to the reduction in the macro-particles and chunks. The higher energies of the ion flux produced for these cathodes may also possibly result in more important sputtering effects on the coating surface.

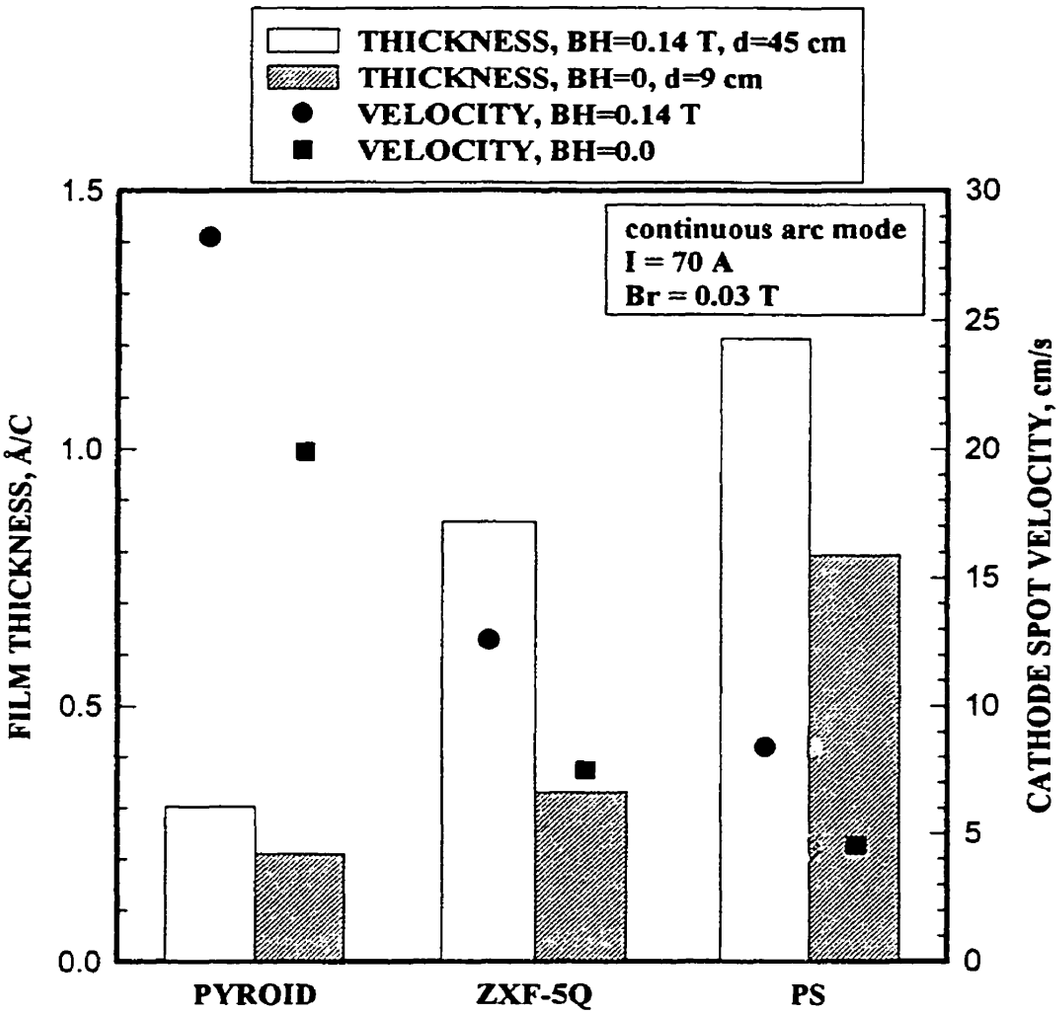

Figure (5-24) : Effect of the types of graphite on film thickness (columns, left axis) and spot velocity (dots, right axis) at constant magnetic field intensity over glass substrate for deposition times of 1.5 minutes.

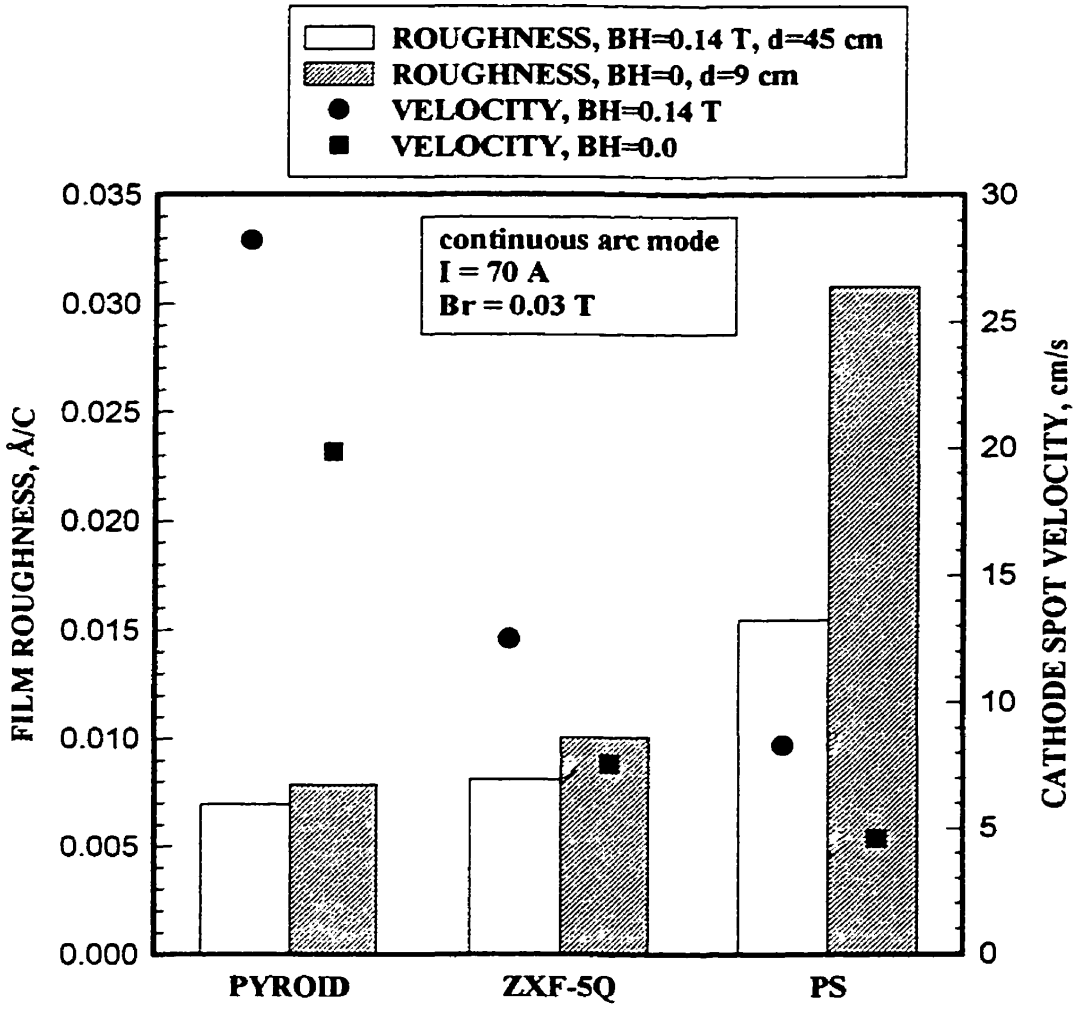

Figure (5-25) : Effect of the types of graphite on film roughness (columns, left axis) and spot velocity (dots, right axis) at constant magnetic field intensity over glass substrate for deposition times of 1.5 minutes.

5-3-8 : FILM STRUCTURE

The structure of the deposited particle-free carbon films are analyzed using infrared spectroscopy (IRS). The spectrum shown in Figure 5-26 presents very strong peaks around 2970 cm^{-1} to 2870 cm^{-1}. These peaks refer to the presence of diamond-like carbon (DLC) structure as described in section 3-4-1. The areas under each peak refer to the concentration of sp^3, sp^2 and sp^1 bonds. Qualitatively speaking, Figure 5-26 indicates that sp^3 bonds are predominant in this film. The smallest (weakest) sp^2 & sp^1 peaks make it difficult to convolute these peaks to get a quantitative ratios. Although neither hydrogen nor any other gas is added to the chamber, carbon-hydrogen bonds exist in the films. This may be due to the residual amount of hydrogen in the vacuum chamber and/or from water vapour induced contamination.

The structure of different films deposited on different substrate types, glass, silicon wafers, (Ti 90/ Al 6/ V 4) and (Fe/ Cr 18/ Ni 8/ Mo 3) alloys were investigated. The structures of all the films were similar and consist of diamond-like carbon (DLC). There is no observable changes in the spectra obtained by analyzing the films on different substrates. All of them show the same characteristic peaks appearing in Figure 5-26.

The adhesion of the produced DLC film was tested by wiping the film strongly by a cloth wetted with acetone several times. No damages is observed on the film surface. It sustained its brownish color, transparency and adhesion. It was not possible to test the hardness of these films in the present study.

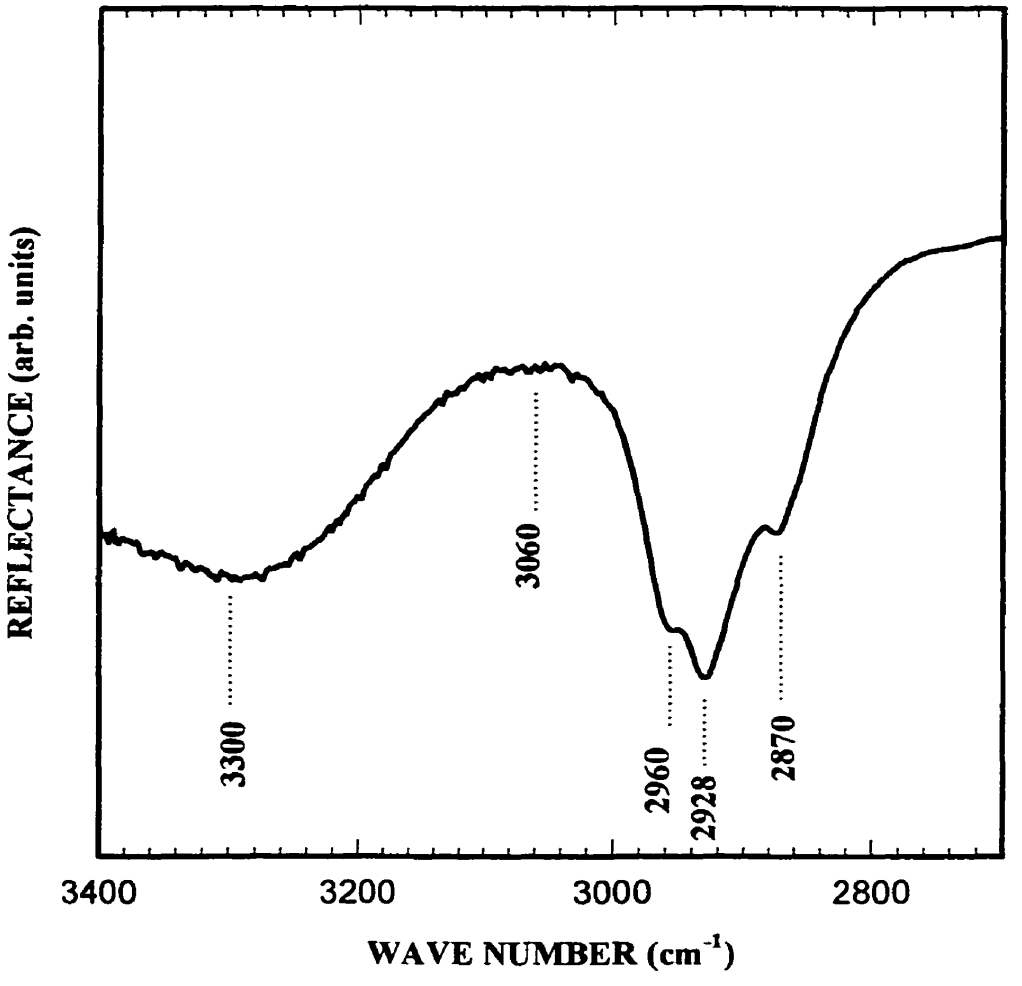

Figure (5-26) : Infrared spectrum for diamond-like carbon film deposited on glass substrate.

5-4 : DISCUSSION

Structural considerations of the graphite materials used are shown here to be very important and strongly affecting the actual behavior of the cathode spot. The control of the heat load input to a given site of the electrode is found to be very important in view of macro-particles reduction. Therefore, the effort was focused in this work at the design of the vacuum arc ion plating system working in a continuous arc mode with forced movement of the arc spot to distribute the heat load on the cathode surface. The transverse magnetic field on the electrode surface was generated using permanent magnets behind the cathode, and the arc plasma was confined in front of the cathode using a pair of coils around the electrodes arranged in a Helmholtz geometry. This configuration was used to rotate the arc spot over the cathode surface and increase the arc stability. As a result, the residence time of the spot at any given location on the electrode was decreased when compared to typical AIP systems used so far in industry showing random arc movement with no magnetic field control for graphite systems. Decreasing the residence time of the arc spot on a given site of the cathode results in a reduced heat load on that site. As a consequence, the macro-particles emission of the arc-ion plating source for DLC films was shown to be reduced. Another factor favoring a reduction of the emitted macro-particles and of irregularly shaped particles (chunks) is the improvement of arc stability induced by the axial magnetic field from the Helmholtz coils. Arc stability removes the problem of regular arc extinction/re-ignition on the graphite cathode. Many studies indicated this extinction/re-ignition process is the source of an intense macro-particle emission. In fact, typical AIP systems use a shutter to hide the substrate during the early

ignition stage. AIP system on graphite are typically using mechanical trigger electrode actuated by a current zero in the arc circuit. These systems are continuously actuated during the deposition process, leading to another strong source of macro-particle emission. With the magnetic configuration designed in this project, the arc was shown to be stable and could be run over long times without the need for re-ignition. It was typically shut off manually after a preset deposition time.

The objective behind the use of the Helmholtz field being to create higher plasma density on the cathode surface, it hence promotes the probability to create new emission sites and increases the arc stability. One motivation behind this choice is related to the technical difficulty to attain high radial (parallel to the erosion surface) magnetic field intensities to bring the arc into rotation. The high field intensities and velocities attained in the pulsed experiments were difficult to implement because of the cooling requirements and the geometry of cathodes in the continuous mode. As stated above, the presence of the higher plasma density over the cathode spot also helps to sustain the arc running for longer times without self extinguishing. Good confinement of the plasma using Helmholtz coils prevents the strong ion flux from leaving toward the walls surrounding the cathode (passive border) and the vacuum chamber, and prevents stray arcing. The shift from free expansion to confined arc plasma hence reduces the strong heating of the chamber walls around the cathode. The need for high cooling rates to the chamber walls is avoided in this way and the possibility of keeping the arc running for longer times is achieved. Confining the arc also increases the deposition rate significantly through the reduction in the ion

losses. The number density and energy of emitted ions are shown to be higher when the arc is confined.

The increase in the magnetic field induced by the Helmholtz coils leads to a significant increase in the plasma fluxes through the anode aperture, which makes the deposition possible at substrates located at far distances from the cathode. On the other hand, this increases the possibility of separating the plasma column from the anode and the risk of extinguishing the arc. Therefore, a compromise between arc current and Helmholtz magnetic field strength is required in the geometry used here.

As shown in Figure 1-8, it was very difficult to move the arc over the graphite surface using the same field intensities as used with metallic electrodes. With no imposed magnetic field to rotate the arc, the movement over metallic electrode is found to be random as shown in Figure 1-10. On the other hand, practically no random movement is observed over graphite cathodes in similar conditions (Figure 1-9). By choosing a proper graphite type and applying an appropriate radial magnetic field intensity, it was possible to force the arc to rotate in the retrograde direction uniformly over the graphite cathode surface (Figure 5-14a). The rotation of the cathode spot occurs along a path (typically circular, in fact following quite exactly the magnets arrangement behind the cathode) where the perpendicular magnetic field component to the cathode surface is zero. The ignition point is neither at the center of the cathode nor at the position of zero axial field component but in between as shown in Figure 5-14a. Under the effect of the radial magnetic field intensity the arc spot is forced to move rapidly to the position of the zero axial magnetic field intensity and follows the direction of the radial component. After

running the arc for long times, a narrow circular (ring) erosion groove is observed due to the repeated motion on the same arc trace. The arc trace in the continuous mode is clearly distinctive but the spot features are not. In the pulse mode, it was easy and clear to observe an isolated cathode spot and measure its size and rim width. This is different in the continuous arc mode where all the spots were attached to each other and forming a chain (Figure 5-14b).

Using the criteria of Ba = 0 to define the position of arc rotation, one may hence design varying magnetic field geometries that would generate a uniform cathode erosion over the entire cathode surface by changing the position of the zero axial field component. This behavior prevents the arc to rotate over the same track for long periods and reduces the heat load input to a given site on the cathode surface.

Graphite cathodes typically work in a thermionic emission mode. In vacuum the emission process at the cathode should also move towards thermionic emission if the cathode local temperature becomes high enough at low arc mobility. When forcing the arc to move on a cold cathode, the discharge mode is forced to shift towards thermo-field (T-F) type 1 emission (see section 1-1-3). A good indication of the thermo-field nature of the steered cathode arc attachment on graphite are the erosion trace patterns observed in Figure 4-15 showing the tree like structure. This structure of rapid ignition/extinction of localized arc spots is very similar to metallic electrodes and typical of the thermo-field emission regime. Therefore a shift from thermionic to T-F emission may be occurring due to the difficulties to reach temperatures for thermionic emission imposed by smaller residence times. Other indications of graphite spot behavior that is now being pushed to

operate similarly to metallic electrodes are shown in Figure (4-18). Large spots diameters (type 2) are observed at the lower spot velocities, with a shift towards smaller spots (type 1) at higher velocities, both types being present in intermediate situations. This observation is very similar to the case of metallic electrodes without/with surface contamination. It has been shown for example that a pure metallic electrode such as titanium yields larger mean cathode spot size and lower spot mobility (Kim 1995). Contaminated electrode such as titanium with a TiN layer yields much smaller spot sizes, higher arc mobility and also much smaller macro-droplet emission from the reduction in surface melting. It seems that the operating mode induced here at high transverse magnetic field over the various graphite structures is reproducing this trend. The surface impurities/contaminations being replaced in the case of graphite by effects linked to surface irregularities such as porosity. The trend is however for graphite an increased arc mobility and decreased macro-particle emission corresponding with a reduction in surface irregularities. The enhanced plasma density above the cathode surface induced by the Helmholtz field in the continuous mode can be viewed here to go in a similar direction as a contaminated layer on a metallic electrode. The increase in plasma density results in stronger surface electric fields and easier emission.

Graphite cathodes are porous materials and have a high boiling point temperature. This porosity may cause a strong temperature gradient through the cathode material adjacent to the spot. There exist therefore a high probability that the arc will find a preferred location and simply remain there. The erosion rate is thus expected to be higher than that for non-porous graphite cathodes. Porosity may also cause thermal shock effects

inducing a mechanical removal of the material on the cathode surface. Using cathodes with smaller pore size were found to be favorable in reducing the particles emission.

The observed deposition rate in the absence of a Helmholtz confining field was a strong function of cathode to substrate distance. Essentially no deposition was observed on the substrate if it was placed at a distance larger than 9 cm from the cathode. The deposition rate increased as the Helmholtz magnetic field increased, and at a close distance the flux emitted was too strong in this design and resulted in the melting of the substrate. "Close distance" in this case corresponded to 9 cm or less, i.e., the maximum distance for deposition without the Helmholtz confining field.

From Figure 5-11 the ion current flux emitted from the cathode is seen to be increasing for cathodes showing higher spot velocities. At the same time, Figure 4-8 indicates that various graphite material types show different cathode spot velocities at fixed operating conditions (especially the applied magnetic field and arc current). Therefore, the good choice of the graphite cathode type showing high spot velocity should also result in a stronger ion flux emitted towards the substrate. This is confirmed in Figure 5-12 where the ion fluxes emitted from different graphite types are observed to vary at any fixed radial position in accordance to the arc velocity induced by the differences in their surface properties. Also the ion number densities for **PYROID** and **ZXF-5Q** graphite types described in Table 5-1 form another confirmation for the increase of the ion flux emission using cathodes showing higher spot velocity at similar conditions.

Figure 5-22 shows that lower number density of particles can be emitted from the cathode if the arc spot velocity is increased. The increase in the arc spot velocity can be

achieved by increasing the radial magnetic field intensity (Br) over the cathode surface and/or using graphite types with smaller pore size, electrical resistivity or higher density and grain size. Combining the results of Figures 4-8, 5-11 and 5-22 together, one can notice the possibility of producing films from graphite cathodes at higher ion deposition rate and lower macro-particles emission. Films produced at 52 cm from the cathode in the presence of Helmholtz confining field were free of detectable particles and show DLC structure (Figure 5-26).

Figure 5-18 shows the total current-voltage characteristics measured for two graphite types at different conditions using the ion energy analyzer (IEA) shown in Figure 5-15. For potential V_t sufficiently negative, all the current collected by C and G4 may be considered to be essentially due to ions (ion saturation region). As the total potential increases, more and more electrons are able to overcome the retarding potential drop. At sufficiently high V_t, no ions are collected and all the electrons passing through the orifice are reaching the collector (electron saturation region). The ion and electron saturation regions are both fairly flat indicating that the field penetration through the orifice is avoided by using the earthed double grids G1 and G2. This is also an indication of the usefulness of using the pumping holes to reduce the collisions within the probe. From the results summarized in Table 5-1, the measured carbon ion energy and flux density were found to be varying for different graphite types. Also for the same graphite material the ion flux density and energy were higher when the arc plasma is confined. An ion energy of E_i = 52 eV was measured for **ZXF-5Q** graphite material (BH = 0.14 T and Br = 0.03 T). This ion energy is found to be very high compared to the typical ion energies of 30 eV

found in such system (Davis & Miller 1969 and Kutzner & Miller 1989). The reason behind such high energy value is possibly due to the confinement of the arc using Helmholtz field. This confinement may prevent the loss of highly energized ions, leading to an increased average ion energy. The increased average ion energy may also be the result of the "smoother" regime in the cathode spot. The strong decrease in macro-particle emission should lead to 1) an increase of the fraction of ionized species in the arc plasma, the particle in-flight evaporation contribution being eliminated, but also 2) the elimination of the low energy ion component coming possibly from the neutral vapor of macro-particle or spot origin that is ionized. The trend towards an increase mean ion energy is hence not surprising. This high energy is still within the energy limit of 20 eV to 60 eV required for the production of diamond-like films. What is extremely interesting however is that this average energy now falls in the optimal energy range for DLC deposition in terms of film quality (Strel'nitskii et al 1978). Using Helmholtz field confinement allows us to eliminate biasing the substrate to accelerate the ions and increase their bombardment energy. Some control of the ion energy can even possibly be done by controlling the current passing through the coils. Such a reduction in the complexity of the deposition system is particularly interesting for industrial applications and more particularly when the substrates to coat are electrically insulative.

PYROID graphite shows the highest velocity due to its highest density, lowest electrical resistivity and lowest pore size. All data in this thesis indicate this material should be preferred to attain a stable carbon ion source for AIP with low or no macro-particle emission. It is however very expensive (it's price is about seven times the price of

PGCS-1 or **ZXF-5Q**) and also exhibits maximum anisotropy. Anisotropy of the crystalline structure directly results in a very strongly anisotropic electrical resistivity distribution within the material (see Table 4-1). The exact effects of such a distribution is out of the scope of this work, one can however speculate on an increase of the net electrical and thermal conductivity of the cathode surface around the spot. Such an evolution is pushing the graphite material towards properties similar to those of metallic electrodes. This trend is observed over essentially all the arc characteristics studied, the **PYROID** graphite is in fact approaching metallic electrode behavior with regards to arc spot mobility. **PGCS-1** is an isotropic material and shows the second highest velocity due to the high density, grain size and low electrical resistivity, it however has a very large pore size. This is increasing the chances of particle emission, it was found that the increase in the cathode pore size leads to the increase in the cathode spot size. As the cathode spot size increases, sustaining the arc becomes more difficult and the reignition of the arc is also very difficult. Repeated reignition has a detrimental effect on deposition because an impulse of macro-particles and chunks are emitted from the cathode at each ignition event. **ZXF-5Q** is isotropic and shows a relatively high arc spot velocity, has low pore size (0.2 μm), large grain size (1 μm), high density (1.8 g/cm^3) and low electrical resistivity (1650 μ.ohm.cm). These surface properties produce a small spot size on the cathode surface and decrease the chance of having to reignite the arc many times. Consequently, the number of emitted particles or chunks are decreased. In addition, it has a relatively low price. This last type of material would hence probably be the first choice for industrial AIP deposition system

considering the large cost difference of the source but the relatively small resulting changes in the deposited film properties.

5-5 : CONCLUSIONS

It is clear that rotating the arc spot over graphite surface is much more difficult compared to metallic electrodes under the same conditions. The rotation of the arc spot over graphite surfaces was achieved using permanent magnets behind the cathode. The arc was found to be rotating in a circular pattern at the radius where the perpendicular magnetic field component is equal to zero. Increasing the radial component results in an increase in the spot velocity. Different types of graphite showed different cathode spot behavior and emitted different quantities of particles and ions with various energies. The ion flux is peaked in the perpendicular direction to the cathode surface and the arc trace. The rotation of the arc spot over the graphite surface generates a more uniform erosion and better use of the cathode material, reduces the emission of particles and chunks and prevents any local overheating by spot anchoring. Although the effective emission mode at the cathode was not studied in this work, a shift of the arc emission regime from thermionic to thermo-field mode seem to be achieved by inducing rotation of the arc spot, confinement of the arc plasma and cooling of the cathode. Arc spot characteristics such as spot mobility and size confirm this trend. The control of the plasma flux, ion current and ion energy were possible through the change in the axial magnetic field component induced by Helmholtz coils. As a result of using a tangential field to the cathode to induce arc rotation and a confining field to increase plasma density at the cathode surface, the

cathode spot velocity, the ion energy and flux emissions are enhanced, while the number of particles emitted from the cathode spot is simultaneously decreased. The roughness and thickness of the films normalized to the total electric charge passing through the cathode were found to decrease for cathodes showing higher spot velocities. Diamond-like thin films free of particles were produced in this work using graphite in a continuous arc ion plating system without using any filtering technique.

GENERAL CONCLUSIONS

The effect of graphite surface properties on arc spot movement is investigated for eleven graphite types. Graphite cathodes having low pore size, low electrical resistivity, high grain size, and high density are found to show high spot velocity at constant external magnetic field intensity.

A given magnetic field intensity is required for each type of graphite cathodes in order to achieve the same spot velocity. In this study, these magnetic field values are determined for eleven types of graphite cathodes and the evolution of arc mobility is evaluated as a function of various surface characteristic parameters.

The arc spot is rotated over the graphite cathode surface in the typical retrograde direction using radial magnetic field component induced by permanent magnets fixed behind the cathode. The plasma is also confined using axial magnetic field component induced by Helmholtz coils.

The combined magnetic fields are employed to produce uniform DLC films, free of particles. The high ion energy bombardment needed for DLC formation was achieved by this magnetic configuration without the need for any substrate biasing.

Film thickness and roughness normalized to the total electric charge passing through the cathode are found to be decreasing with the increase in the cathode spot velocity due to the reduction in the macro-particles and chunks emission.

Cathodes having small pore size show high spot velocity, less particles emission and smaller cathode spot size. This makes the arc running for longer periods before self

extinguishing, reducing in this way another macro-particle emission mechanism linked to the mechanical triggering sequence.

CONTRIBUTIONS

Study the effect of the surface properties for various (eleven) graphite types on the arc spot behaviour. This investigation will direct the attention of the researchers to the importance of considering each graphite characteristic individually as a different material showing specific arc properties.

Different erosion rate values are measured for the various types of graphite under varying external magnetic field intensities. This is shown to be related to the change in the surface properties of the various graphite materials. In the literature, the erosion rate for carbon was given previously with a unique value of 17 μg/C (Kimblin 1973).

The maximum arc current per spot was found to be changing for the various graphite material types, the literature data indicating again a unique value equal to 200 A/spot (Kimblin 1973).

The smooth rotation of the arc spot over graphite cathode in a continuous mode in a way similar to metallic electrode was achieved through proper material selection and magnetic field configuration.

The control of the particle emission from graphite cathodes through arc spot rotation and confinement of the discharge instead of filtering the emitted ion beam is a new contribution to the field of AIP.

Such a technique of macro-particle control at the source and optimization of the ion energy could strongly increase the industrial applicability of the AIP.

REFERENCES

- M.S.A. Agarwal and R. Holmes, " Arcing voltage of the metal vapour vacuum arc," J. Phys. D: Appl. Phys., Vol. 17, pp. 757-767 (1984).
- S. Aisenberg, " Properties and applications of diamond-like carbon films," J. Vac. Sci. Technol. A, Vol. 2, No. 2, pp. 369-371 (1984).
- S. Aisenberg and R. Chabot, " Ion-beam deposition of thin films of diamondlike carbon," J. Appl. Phys., Vol. 42, No. 7, pp. 2953-2958 (1971).
- S. Aisenberg and R. Chabot, " Physics of ion plating and ion beam deposition," J. Vac. Sci. Technol., Vol. 10, No. 1, pp. 104-107 (1973).
- S. Aisenberg and M. Stein, " The use of ion-beam deposited diamond-like carbon for improved optical-elements for high powered lasers," Proc. of 12th sym. on optical materials for high power lasers, ed. Harold E. Bennett et al (1982).
- I.I. Aksenov, V.G. Belous, V.G. Padalka and V.M. Khoroshikh, " Transport of plasma streams in a curvilinear plasma-optics system," Sov. J. Plasma Phys., Vol. 4, No. 4, pp. 425-428 (1978).
- I.I. Aksenov, S.I. Vakula, V.G. Padalka, V.E. Strel'nitskii and V.M. Khoroshikh, " High-efficiency source of pure carbon plasma," Sov. Phys. Tech. Phys. Vol. 25, No. 9, pp. 1164-1166 (1980).
- S. Anders and B. Jüttner, " Influence of residual gases on cathode spot behavior," IEEE Trans. Plasma Sci., Vol. 19, No. 5, pp. 705-712 (1991).
- L.P. Andersson, " A review of recent work on hard i-C films," Thin Solid Films, Vol. 86, pp. 193-200 (1981).

- J.C. Angus, " Empirical categorization and naming of diamond-like carbon films," Thin Solid Films, Vol. 142, pp. 145-151 (1986).
- B.A. Banks and S.K. Rutledge, " Ion beam sputter-deposited diamond-like films," J. Vac. Sci. Technol., Vol. 21, No. 3, pp. 807-815 (1982).
- S. Berg and L.P. Andersson, " Diamond-like carbon films produced in a butane plasma," Thin Solid Films, Vol. 58, pp. 117-120 (1979).
- B. Bhushan, A.J. Kellock, N-H Cho and J.W. Ager III, " Characterization of chemical bonding and physical characteristics of diamond-like amorphous carbon and diamond films," J. Matter. Res., Vol. 7, No. 2, pp. 404-410 (1992).
- R.L. Boxman and S. Goldsmith, " The interaction between plasma and macroparticles in a multi-cathode-spot vacuum arc," J. Appl. Phys. Vol. 52, pp. 151-161 (1981).
- B.F. Coll, P. Sathrum, R. Aharonov and M.A. Tamaor, " Diamond-like carbon films synthesized by cathodic arc evaporation," Thin Solid Films, Vol. 209, pp. 165-173 (1992).
- J.J. Cuomo, J.P. Doyle, J. Bruley and J.C. Liu, " Ion-beam sputtered diamond-like carbon with densities of 2.9 g/cm^3," J. Vac. Sci. Technol. A, Vol. 9, No. 4, pp. 2210-2215 (1991).
- J.J. Cuomo, D.L. Pappas, J. Bruley, J.P. Doyle and K.L. Saenger " Vapor deposition processes for amorphous carbon films with sp^3 fractions approaching diamond," J. Appl. Phys., Vol. 70, pp. 1706 (1991).
- R.F. Curl and R.F. Smalley, " Probing C60," Science, Vol. 242, pp. 1017-1022 (1988).

- J.E. Daalder, " Components of cathode erosion in vacuum arcs," J. Phys. D: Appl. Phys., Vol. 9, pp. 2379-2395 (1976).
- J.E. Daalder, " Random walk of cathode arc spots in vacuum," J. Phys. D:Appl. Phys., Vol. 16, pp. 17-27 (1983).
- J.E. Daalder, " Cathodic erosion of metal vapor arcs in vacuum," Ph.D. thesis, van de Technische Hogeschool, Eindhoven (1978)
- G. Davies and T. Evans, " Graphitization of diamond at zero pressure and at a high pressure," Proc. R. Soc. London A, Vol. 328, pp. 413-427 (1972).
- W.D. Davis and H.C. Miller, "Analysis of the electrode products emitted by dc arcs in a vacuum ambient," J. Appl. Phys., Vol. 40, No. 5, pp. 2212-2221 (1969).
- R. O. Dillon, J. A. Woollam and V. Katkanant, " Use of Raman scattering to investigate disorder and crystallite formation in as-deposited and annealed carbon films," Phys. Rev. Vol. B29, No. 6, pp. 3482-3489 (1984).
- B. Dischler, A. Bubenzer and P. Koidl, " Hard carbon coatings with low optical absorption," Appl. Phys. Lett. Vol. 42, No. 8, pp. 636-638 (1983).
- B.E. Djakov and R. Holmes, " Cathode spot division in vacuum arcs with solid metal cathodes," J. Phys. D: Appl. Phys., Vol. 4, pp. 504-509 (1971).
- M. Douyon de Azevedo, " Etude du depot par arc dans le vide de couches minces de carbone sous pression reduite d'hydrogene," Master Thesis, McGill University (1990).
- M. Douyon de Azevedo and J.-L. Meunier, " Ion flux intensity measurements on carbon cathode spot plasma interacting with low pressure hydrogen," in Proc. 14th. Int. Symp. on Disch. and Electr. Insul. In Vacuum (Santa Fe, NM), pp. 255-259 (1990).

- M.G. Drouet, " The physics of the retrograde motion of the electric arc," IEEE Trans. Plasma Sci., Vol. PS-13, No. 5, pp. 235-241 (1985).

- S. Falabella and D.M. Sanders, " Comparison of two filtered cathodic arc sources," J. Vac. Sci. Technol. A, Vol. 10, No. 2, pp. 394-397 (1992).

- D.Y. Fang, " Cathode spot velocity of vacuum arcs," J. Phys. D:Appl. Phys., Vol. 15, pp. 833-844 (1982).

- J.L. Franklin, S.A. Studniarz and P.K. Ghosh, " Translational energy distribution of electrons and positive ions in the plasma of microwave and high-frequency discharges of He, Ne and Ar," J. Appl. Phys. Vol. 39, No. 4, pp. 2052-2061 (1968).

- Y.H. Fu, " The influence of cathode surface microstructure on DC vacuum arcs," J. Phys. D: Appl. Phys. Vol. 22, pp. 94-102 (1989).

- D.R. Gaskell, " Introduction to Metallurgical thermodynamics," McGraw-Hill, New York (1981).

- T.S. Green, "Space charge effects in plasma particle analyzers," Plasma Phys., Vol. 12, pp. 877-883 (1970).

- A. Grill, V. Patel and B.S. Meyerson, " Temperature and bias effect on the physical and tribological properties of diamond-like carbon," J. Electrochem. Soc., Vol. 138, No. 8, pp. 2362-2366 (1991).

- M.H. Grimsditch and A.K. Ramdas, " Brillouin scattering in diamond," Phys. Rev. Vol. B11, No. 8, pp. 3139-3148 (1975).

- L. Holland and S.M. Ojha, " The growth of carbon films with random atomic structure from ion impact damage in a hydrocarbon plasma," Thin Solid Films, Vol. 58, pp. 107-116 (1979).

- S.G. Ingram and N. St. J. Braithwaite, " Ion and electron energy analysis at a surface in an RF discharge," J. Phys. D: Appl. Phys. Vol. 21, pp. 1496-1503 (1988).

- V.A. Ivanov, B. Jüttner and H. Pursh, Proceedings of the 11th International Symposium on Discharge and Electrical Insulation in vacuum, Berlin, pp. 157-160 (1984).

- F. Jansen, M. Machonkin, S. Kaplan and S. Hark, " The effects of hydrogenation on the properties of ion beam sputter deposited amorphous carbon," J. Vac. Sci. Technol. A, Vol. 3, No. 3, pp. 605-609 (1985).

- P.C. Johnson, " The cathodic arc plasma deposition of thin films," Physics of thin films, Vol. 14, pp. 130-199 (1989).

- B. Jüttner, " On the plasma density of metal vapor arcs," J. Phys. D: Appl. Phys. Vol. 18, pp. 2221- 2231 (1985).

- M. Kandah, "Droplets Generation Mechanisms by Graphite Cathodes in the Vacuum Arc Deposition technique," M.Eng. Thesis, McGill University (1993).

- M. Kandah and J.-L. Meunier, " Study of micro-droplets generation from vacuum arcs on graphite cathodes," J. Vac. Sci. Technol. A, Vol. 13, No. 5, pp. 2444-2450 (1995).

- I.G. Kesaev, " Laws governing the cathode drop and the threshold currents in an arc discharge on pure metals," Sov. Phys.-Tech. Phys. Vol. 9, No. 8, pp. 1146-1154 (1965).

- G. Kim, " The effects of low pressure nitrogen on titanium cathode sources in TiN arc ion plating," Ph.D. Thesis, McGill University (1995).

- C.W. Kimblin, " Erosion and ionization in the cathode spot regions of vacuum arcs," J. Appl. Phys., Vol. 44, No. 7, pp. 3074-3081 (1973).

- D.S. Knight and W.B. White, " Characterization of diamond films by Raman spectroscopy," J. Mater. Res., Vol. 4, No. 2, pp. 385-393 (1989).
- A.W. Koch, A.W. Nornberg and R. Behrisch, " Investigation of vacuum arcs on graphite cathodes," J. Nucl. Mat., Vol. 122 & 123, pp. 1437-1439 (1984).
- J. Kutzner and C. Miller, " Ion flux from the cathode region of a vacuum arc," IEEE Trans. Plasma Sci., Vol. PS-17, No. 5, pp. 688-694 (1989).
- R. Lossy, D.L. Pappas, R.A. Roy, J.J. Cuomo and V.M. Sura, " Filtered arc deposition of amorphous diamond," Appl. Phys. Lett., Vol. 61, No. 2, pp. 171-173 (1992).
- A.N. Luzin, Report to the fourth All-Union Conference on the Interactions of Atomic Particles with Soilds [in Russian], Part II, Khar'kov (1976).
- M. Mack, " Surface technology-wear protection," verlag moderne industrie AG & Co. Germany (1990).
- L. Martinu, " High energy density technologies in materials science," F. Garbassi and E. Occhiello (eds.), Kluwer Academic Publishers, pp. 77-87 (1990).
- D.M. Mattox, " Fundamentals of ion plating," J. Vac. Sci. Technol., Vol. 10, No. 1, pp. 47-52 (1973).
- D.R. McKenzie, "Tetrahedral bonding in amorphous carbon," Rep. Prog. Phys., Vol. 59, pp. 1611-1664 (1996).
- D.R. McKenzie, D. Muller, B.A. Pailthorpe, Z.H. Wang, E. Kravtchinskaia, D. Segal, P.B. Lukins, P.D. Swift, P.J. Martin, G. Amaratunga, P.H. Gaskell and A. Saeed, "Properties of tetrahedral amorphous carbon prepared by vacuum arc deposition," Diamond and Related Materials, Vol. 1, pp. 51-59 (1991).

- R. Messier, A.R. Badzian, T. Badzian, K.E. Spencer, P. Bachmann and R. Roy, " From diamond-like carbon to diamond coatings," Thin Solid Films, Vol. 153, pp. 1-9 (1987).
- B. Meyerson and F.W. Smith, " Electric and optical properties of hydrogenated amorphous carbon films," J. Non-cryst. Solid, Vol. 35-36, pp. 435-440 (1980).
- Y. Namba, J. Wei, T. Mohri and E.A. Heidapour, " Large grain size thin films of carbon with diamond structure," J. Vac. Sci. Technol. A, Vol. 7, No. 1, pp. 36-39 (1989).
- D.J. Page, " The Industrial Graphite Engineering Handbook," **UCAR** Carbon Company Inc. pp. 5C.03 (1991).
- V. Palshin, E.I. Meletis, S. Ves, S. Logothetidis, " Characterization of ion-beam-deposited diamond-like carbon films," Thin Solid Films, Vol. 270, pp. 165-172 (1995).
- D.L. Pappas, K.L. Saenger, J. Bruley, W. Krakow, J.J. Cuomo, T. Gu and R.W. Collins, " Pulsed laser deposition of diamond-like carbon films," J. Appl. Phys., Vol. 71, No. 11, pp. 5675-5684 (1992).
- S.M.L. Prokopenko, L.G. Laframboise and J.M. Goodings, " Evaluation of an orifice probe for plasma diagnostics," J. Phys. D: Appl. Phys., Vol. 5, pp. 2152-2160 (1972).
- S.M.L. Prokopenko, L.G. Laframboise and J.M. Goodings, " Orifice probe for plasma diagnostics: II. Multi-parameter analysis," J. Phys. D: Appl. Phys., Vol. 7, pp. 355-362 (1974).
- V.I. Rakhovskii, " Experimental study of the dynamics of cathode spots development," IEEE Trans. Plasma Sci., Vol. PS-4, No. 2, pp. 81-102 (1976).

- P. Reinke, S. Schelz, W. Jacob and W. Möller, " Influence of a direct current bias on the energy of ions from an electron cyclotron resonance plasma," J. Vac. Sci. Technol. A Vol. 10, No. 3, pp. 434-438 (1992).
- W.C. Roman, " Some observations on the forward and retrograde motion of electric arcs in transverse magnetic fields," Proc. 6th Int. Conf. Ionized Gases, Vol. 2, pp. 287-294 (1963).
- B. Rother, J. Siegel, I. Mühling, H. Fritzdch and K. Breuer, " Cathodic arc deposition of diamond-like carbon: effect of bias voltage and deposition angle," Materials Science and Engineering, Vol. A140, pp. 780-783 (1991).
- C. Rusteberg, M. Lindmayer, B. Jüttner and H. Pursch, " On the ion energy distribution of high current arcs in vacuum," IEEE Trans. Plasma Sci. Vol. 23, No. 6, pp. 909-914 (1995).
- D.M. Sanders, D.B. Boercker and S. Falabella, " Coating technology based on the vacuum arc- a review," IEEE Trans. Plasma Sci. Vol. 18, No. 6, pp. 883-893 (1990).
- P. Sathrum and B.F. Coll, " Plasma and deposition enhancement by modified arc evaporation source," Surf. Coat. Technol., Vol. 50, pp. 103-109 (1992).
- N. Savvides, " Four-fold to three-fold transition in diamond-like amorphous carbon films: A study of optical and electrical properties," J. Appl. Phys., Vol. 58, No. 1, pp. 518-521 (1985).
- S. Shalev, L.R. Boxman and S. Goldsmith, " Macroparticle dynamics during multi-cathode-spot vacuum arcs," IEEE Trans. Plasma Sci. Vol. PS-14, No. 1, pp. 59-62 (1986).
- C. Shichang, F. Dejun, X. Zhisan, Z. Hui and P. Xianzheng, " Investigation on diamond-like carbon films : structure, properties and doping effect," Nuclear Instruments and Methods in Physics Research, Vol. B39, pp. 692-695 (1989).

- E.G. Spencer, P.H. Schmidt, D.C. Joy and F.J. Sansalone, " Ion-beam deposited polycrystalline diamond-like films," Appl. Phys. Lett., Vol. 29, No. 2, pp. 118-120 (1976).
- J. Storer, J.E. Galvin and I.G. Brown, " Transport of vacuum arc plasma through straight and curved magnetic ducts," J. Appl. Phys., Vol. 66, No. 11, pp. 5245-5250 (1989).
- V.E. Strel'nitskii, V.G. Padalka and S.I. Vakula, " Properties of the diamond-like carbon film produced by the condensation of a plasma stream with an rf potential," Sov. Phys., Tech. Phys., Vol. 23, No. 2, pp. 222-224 (1978).
- H-C. Tsai and D.B. Bogy, " Characterization of diamond-like carbon films and their application as overcoats on thin films media for magnetic recording," J. Vac. Sci. Technol., Vol. 5, No. 6, pp. 3287-3312 (1987).
- F. Tuinstra and J.L. Koenig, " Raman Spectrum of graphite," J. Chem. Phys. Vol. 53, No. 3, pp. 1126-1130 (1970).
- D.T. Tuma, C.L. Chen and D.K. Davies, " Erosion products from the cathode spot region of a copper vacuum arc," J. Appl. Phys., Vol. 49, No. 7, pp. 3821-3831 (1978).
- T. Utsumi, " Measurements of cathode spot temperature in vacuum arcs," Appl. Phys. Lett., Vol. 18, No. 6, pp. 218-220 (1971).
- T. Utsumi and J.H. English, " Study of electrode products emitted by vacuum arcs in form of molten metal particles," J. Appl. Phys., Vol. 46, pp. 126-131 (1975).
- C. Weissmantel, " Ion beam deposition of special film structures," J. Vac. Sci. Technol., Vol. 18, No. 2, pp. 179-185 (1981).

- F. Xiong, Y.Y. Wang, V. Leppert and R.P.H. Chang, " Pulsed laser deposition of amorphous diamond-like carbon films with ArF (193) excimer laser," J. Mater. Res., Vol. 8, No. 9, pp. 2265-2272 (1993).
- J.W. Zou, K. Schmidt, K. Reichelt and B. Dischler, " The properties of a-C:H films deposited by plasma decomposition of C_2H_2," J. Appl. Phys. Vol. 67, No. 1, pp. 487-494 (1990).
- S.S. Zumdahl, " Chemical principles," D.C. Heath and Company, Lexington, Massachusetts, Toronto, pp. 780-781 (1995).